

PETRO VIETNAM

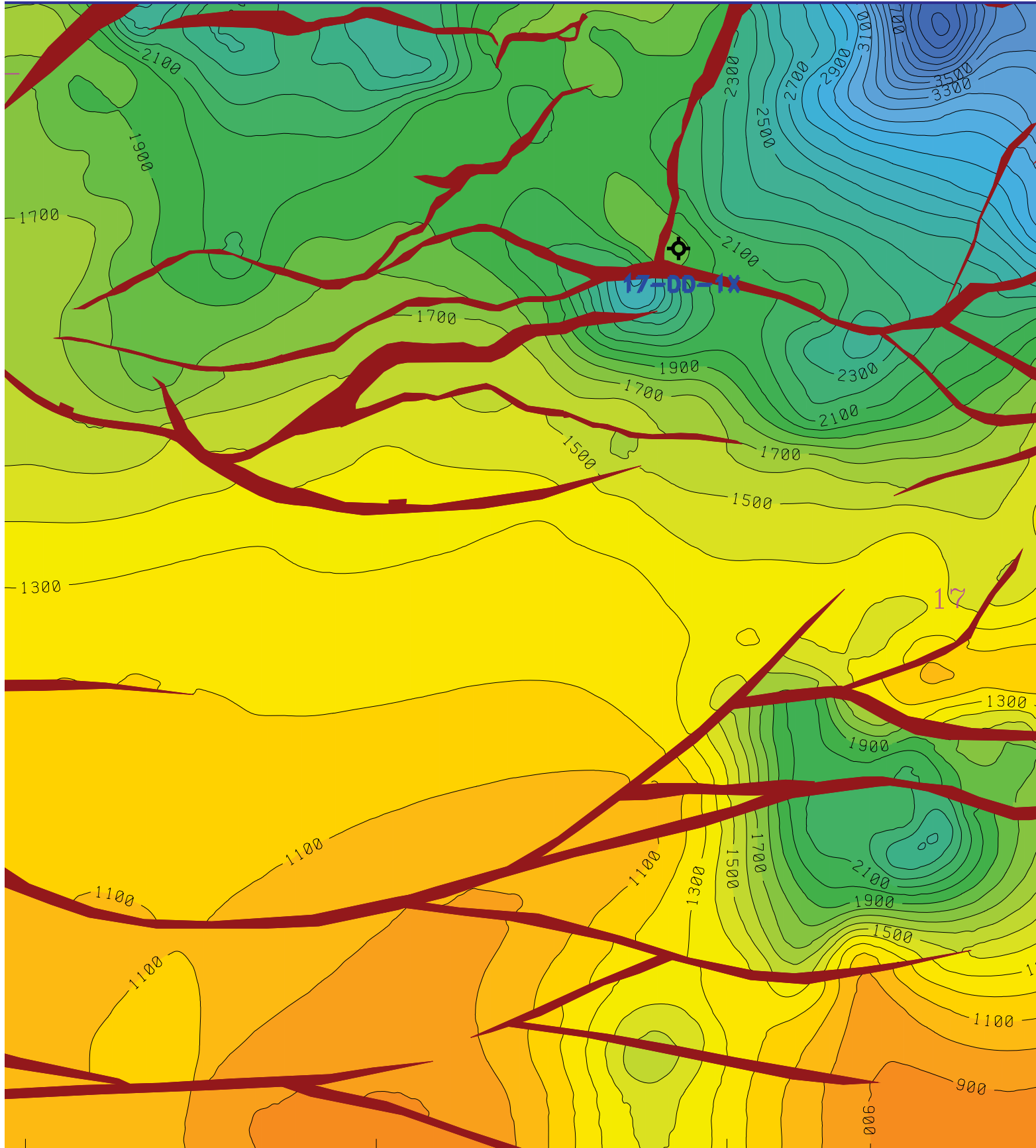
SCIENCE, TECHNOLOGY & INNOVATION

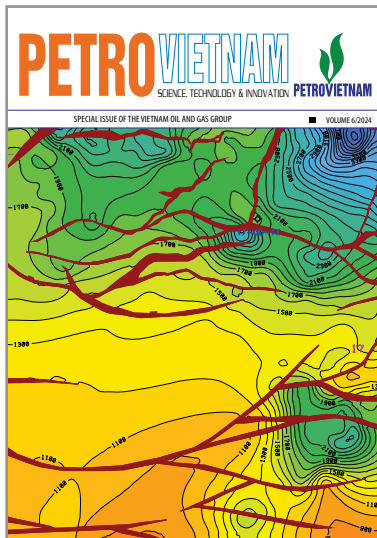


PETROVIETNAM

SPECIAL ISSUE OF THE VIETNAM OIL AND GAS GROUP

VOLUME 6/2024





EDITOR-IN-CHIEF

Dr. Le Xuan Huyen

DEPUTY EDITOR-IN-CHIEF

Dr. Le Manh Hung

MSc. Le Ngoc Son

EDITORIAL BOARD

Dr. Trinh Xuan Cuong

Dr. Nguyen Anh Duc

MSc. Vu Dao Minh

M.A. Tran Thai Ninh

MSc. Duong Manh Son

Assoc. Prof. Dr. Le Van Sy

M.A. Bui Minh Tien

MSc. Nguyen Van Tuan

MANAGEMENT BOARD

MSc. Le Van Khoa

M.A. Nguyen Thi Viet Ha

MSc. Nguyen Trung Dat

IMPLEMENTATION

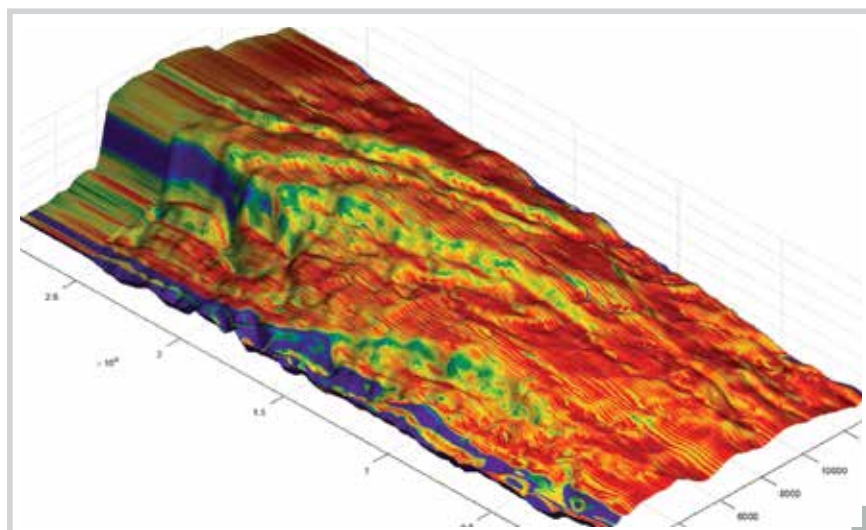
Vietnam Petroleum Institute

CONTACT ADDRESS

Floor 16th, VPI Tower, Trung Kinh street, Yen Hoa ward, Cau Giay district, Hanoi

Tel: 024-37727108 | 0982288671 * Fax: 024-37844156 * Email: tcdk@pvn.vn

Photo: Top basement time structure map of Cuu Long basin



PETROLEUM - SCIENCE, TECHNOLOGY AND INNOVATION



4. Simulation of 3D seismic illumination and its application in seismic acquisition survey design: Dual-source configuration (Flip-Flop)

14. Lessons learned in high-pressure high-temperature well completion in Vietnam

22. Study on applied technologies to propose solutions for enhancing hydraulic fracturing efficiency in tight sandstone reservoirs of the Cuu Long basin

31. Evaluation of the applicability of subsea wellheads running by jack up rig for oil and gas exploration projects in shallow water, offshore Vietnam

39. Production and optimisation of a well by hybrid artificial activation

47. Paraffin treatment of crude oil produced from the Central of Rong and Nam Rong - Doi Moi fields during transportation through uninsulated subsea pipelines

54. Research and application of high-performance drilling fluid systems in Vietsovetro Joint Venture

65. Quantitative Assessment of a Novel Method for Fluid Thermodynamic Test Simulation in Multicomponent Systems

82. Developing superhydrophobic/ superoleophilic polyurethane sponge based on Fe₃O₄ particles for oil - water separation



88. Governance in ESG of oil and gas sector

In 2024, the Vietnam Oil and Gas Group (Petrovietnam) achieved impressive production and business results despite global economic fluctuations and energy market volatility. Petrovietnam set a new record in total revenue, surpassing 1 quadrillion VND (approximately 9% of the country's total GDP), representing a 36% growth compared to the pre-Covid period levels. The Group contributed 165 trillion VND to the state budget, nearly 9% of the country's total budget revenue, marking a 52% rise from the pre-Covid period. The consolidated profit exceeded 2.3 billion USD. Notably, with 3 new oil and gas discoveries, Petrovietnam has increased its reserves by 15.2 million tons of oil equivalent. For the first time, the Group provided technical services for offshore renewable energy export projects, developed value chain linkages within its ecosystem, and promoted innovation to develop new products.

In alignment with Conclusion No. 76-KL/TW dated April 24, 2024, and Resolution No. 38/NQ-CP dated August 20, 2024, Petrovietnam is actively shaping its strategic development roadmap towards 2030, with a vision to 2050. This includes comprehensive solutions to transform into a national industrial-energy group, enhancing operational efficiency in traditional energy sectors, implementing carbon capture, utilization and storage (CCUS), and participating in new and renewable energy value chains. These efforts emphasize offshore and coastal wind power, hydrogen, ammonia, LNG import and trading supply chain, and energy equipment manufacturing, etc., with a focus on large-scale, strategic projects that create significant impact and high efficiency.

In this special issue, Petrovietnam is proud to present a selection of significant research papers that highlight key advancements and solutions in the oil and gas industry. The issue features studies on the simulation of 3D seismic illumination and its application in designing seismic acquisition surveys with dual-source configuration. It also includes an evaluation of the applicability of subsea wellheads deployed by jack-up rigs for oil and gas exploration in shallow waters, offshore Vietnam. In production, notable papers discuss the lessons learned in high-pressure, high-temperature well completions in Vietnam, present the research findings and application of high-performance drilling fluid systems, delve in innovative solutions for optimizing well production by hybrid artificial activation, and technologies to enhance hydraulic fracturing efficiency in tight sandstone reservoirs of the Cuu Long basin. Finally, the journal addresses governance in ESG practices in the oil and gas sector, reflecting Vietnamese petroleum industry's commitment to sustainable development.

Entering 2025, Petrovietnam concentrates on restructuring efforts in line with Resolution No. 18-NQ/TW dated October 25, 2017, which emphasizes continuing to innovate and streamline the organizational structure of the political system to ensure efficiency, effectiveness, and agility. Petrovietnam is committed to improving governance efficiency, targeting a growth of over 10%.

Focusing on science, technology, and innovation, the Editorial Board is confident that Petrovietnam Special Issue will remain a vital platform, providing expert and scientific perspectives along with solutions in management, governance, and technology. These contributions aim to establish a strong foundation for Petrovietnam's transition from traditional energy to green and sustainable development.

EDITOR-IN-CHIEF
Vice President of Petrovietnam

Dr. Le Xuan Huyen

SIMULATION OF 3D SEISMIC ILLUMINATION AND ITS APPLICATION IN SEISMIC ACQUISITION SURVEY DESIGN - DUAL-SOURCE CONFIGURATION (FLIP-FLOP)

Ta Quang Minh, Pham The Hoang Ha, Nguyen Minh Quang, Nguyen Danh Lam, Bui Le Thu

Vietnam Petroleum Institute

Email: minh tq@vpi.pvn.vn

<https://doi.org/10.47800/PVSI.2024.06-01>

Summary

An ideal seismic survey should produce an even seismic illumination on the subsurface horizons and adequately illuminate faults. Thus, in seismic acquisition survey design, simulated seismic illumination is usually among the first steps to perform. In this paper the authors discuss how to perform a 3D seismic illumination simulation on a model of the subsurface environment using the Ray tracing technology. The results of the seismic illumination process using the Ray-Tracing method (ray propagation model) for the study area generate various illumination-related maps to help assessing and optimizing the effectiveness of any particular seismic survey configuration. The paper also applied this technology to models and real-field data with a dual-source (flip-flop) configuration, producing various illumination map results to illustrate the effectiveness.

Key words: Survey design, seismic illumination, wave propagation, simulation.

1. Introduction

Seismic surveys are the first stage of oil and gas exploration process, helping to identify potential hydrocarbon accumulation zones. Currently, seismic survey designs are mostly done by foreign contractors using foreign commercial software. Seismic illumination simulation [1] is a key part of seismic acquisition survey design. The goal is to ensure an even seismic illumination on the target area, so that any seismic amplitude anomalies can accurately reflect lithology/fluid anomalies in the geology. Optimizing the design minimizes signal quality issues in poorly illuminated areas like fault shadows or under salt domes. However, in practice, in areas with complex velocity fields or geological structures, wavefields become distorted, reducing illumination intensity and coverage. Seismic illumination maps can help predict anomalies and adjust acquisition designs accordingly. Currently, seismic illumination design and simulation are done using commercial software, which comes with licensing costs. Since a similar software in Vietnam is not yet available, the seismic processing team

at the Vietnam Petroleum Institute (VPI) has carried out research and try to develop the seismic illumination technology, which will allow us to manage and control the process independently and design more complex acquisition geometries.

Illumination maps are built based on the results of the seismic illumination process using the Ray-tracing [2], a method that simulates how seismic waves propagate through complex geological structures. It provides crucial information, such as hit map, incident angle, max offset ... to evaluate and optimize the design of seismic acquisition configurations. The research results as well as the testing of 3D seismic illumination technology will be presented in detail in this paper.

2. Theoretical basis

Seismic waves propagate according to the wave equation, which is simplified into the ray equation (indicating the directions in which rays travel) and the transport equation (describing the variation of amplitude along the ray [3]). From these simple elements, an overall illumination map is constructed. To simulate seismic waves illuminating seismic objects, the Ray-tracing method is used, which is the core method employed in seismic illumination technology.



Date of receipt: 24/10/2024.

Date of review and editing: 24/10 - 5/12/2024.

Date of approval: 5/12/2024.

2.1. The Ray-tracing method

The Ray-tracing equation, also known as the eikonal equation, is a differential equation that describes the path of seismic wave rays as they propagate through a medium with slowly spatial varying velocity and reflection properties of surfaces. In other words, this equation simulates the propagation process of seismic waves in complex structures. It can be expressed as [2]:

$$[\nabla T]^2 - \frac{1}{v(\vec{x})^2} = 0 \tag{1}$$

Where:

T: Is the wave travel time;

∇T : Is the gradient of the wave travel time (the change in wave travel time with respect to position);

v: Is the seismic wave velocity.

The eikonal equation can be transformed into a system of stage-space equations:

$$\frac{d\vec{x}}{dt} = v^2(\vec{x})\vec{p} \tag{2}$$

$$\frac{d\vec{p}}{dt} = - \frac{\nabla v(\vec{x})}{v(\vec{x})} \tag{3}$$

Where \vec{p} is the slowness vector, representing the direction and magnitude of the ray velocity at the reference point; dt is the time step used to calculate the ray path.

Equations (2) and (3) can be numerically solved using the Runge-Kutta method (RK4) [4]. This is a classical method used to solve differential equations. Therefore, it is applied in seismic raytracing to solve the first-order system of equations (2) and (3), thereby determining the path of seismic wave rays in a velocity-varying medium.

Figure 1 illustrates how ray-tracing is performed in velocity field by this method [5]. The field is discretized into samples for computational simulation. In this field, the ray trajectory is estimated repeatedly after every fixed time interval or step. At the end of each step, the current position of a tracing ray is updated and the values of the velocity and ray parameters at the nearest sample to this position are used to define the next position of the ray.

An important characteristic in seismic wave simulation is that the wave will be reflected at horizon surfaces before returning to the receiver. Additionally, the reflected wave shown in Figure 1 can travel in various ways and may even bend before hitting the reflection boundary, as illustrated in Figure 2 (turning ray). This occurs due to total internal reflection at shallower interfaces (when the angle of incidence is greater than the critical angle). This phenomenon can affect the construction of the illumination map, particularly in areas with velocity anomalies.

2.2. The dual-source configuration (flip-flop shooting)

Flip-flop shooting is a widely used technique in seismic surveys that alternates

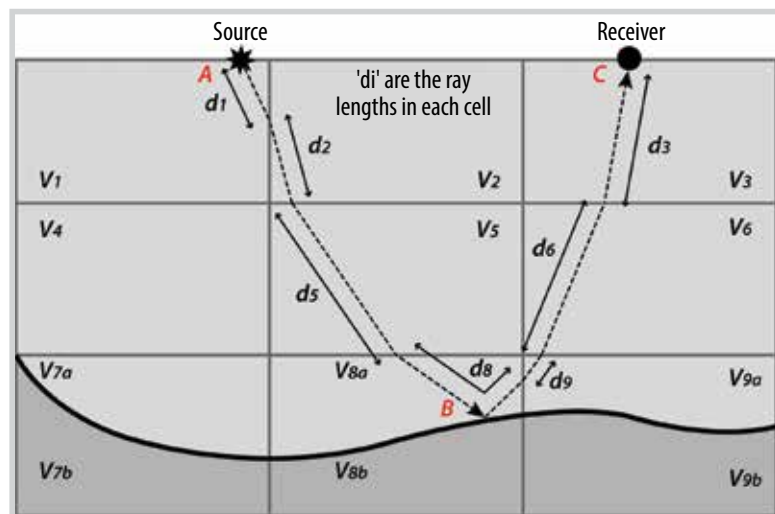


Figure 1. Ray-tracing in the velocity field.

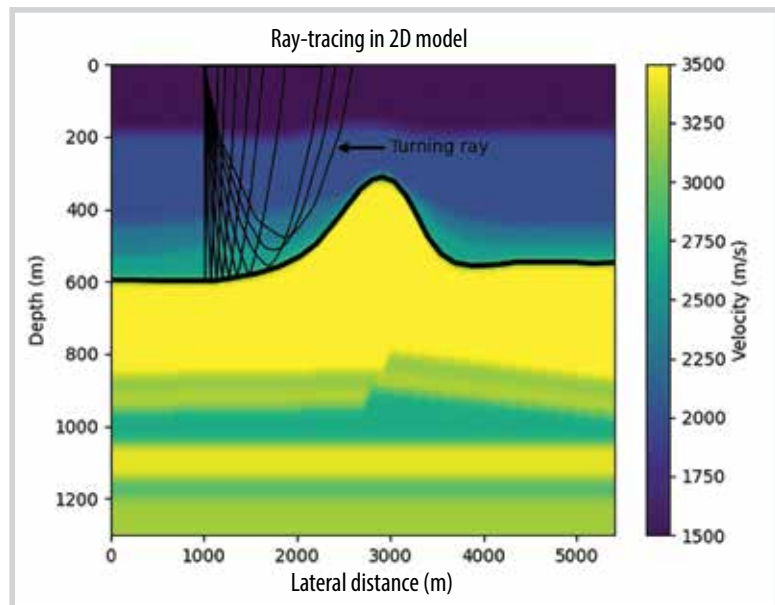


Figure 2. Ray-tracing Runge-Kutta with a single reflector.

between two seismic sources. While one source is being recharged, the other is actively acquiring data. This dual-source configuration enhances seismic coverage and resolution by increasing the number of subsurface inlines, thereby improving the overall data quality. Figure 3a shows the acquisition geometry. Figure 3b shows a map view of the trajectory of the shots used in this study.

2.3. The results - counting the hits

As the seismic acquisition vessel travel through the area, typically planned by a route optimization software such as SURVOPT, the acquisition configuration were simulated to regularly deploy a source, ray-trace the seismic wave to the target horizons and reflect the ray back to the receiver arrays. For those rays that arrive to the receiver array, the ray’s corresponding hit to the subsurface horizon were counted and tally at the end of the vessel run. Thus, a hit map can be generated which can be used to assess:

- Which region of the subsurface receive more or less hits.
- Whether the illumination is even.
- Ability of the particular survey configuration to shine on a particular fault, i.e. the ability to provide enough strength of the seismic wave on the fault.

Since the history of the travel rays were traced, a number of other useful indices can be tallied such as:

- Offsets - The distance between the receiver that receives the traced ray and the originated source.
- Azimuth: Source-receiver’s azimuth.
- Incident angle: The angle that the seismic wave arrive to a particular surface
- Travel time: The time that the seismic wave travels along the ray from the source to the receiver.

From these indices, corresponding maps can be generated (section 4).

3. Experiments in 3D synthetic model

Ray tracing and seismic illumination experiments on various 3D synthetic model were conducted to assess the performance of the method.

3.1. 3D single ray simulation

3D synthetic model experiments were conducted to assess the performance of the ray-tracing method, as

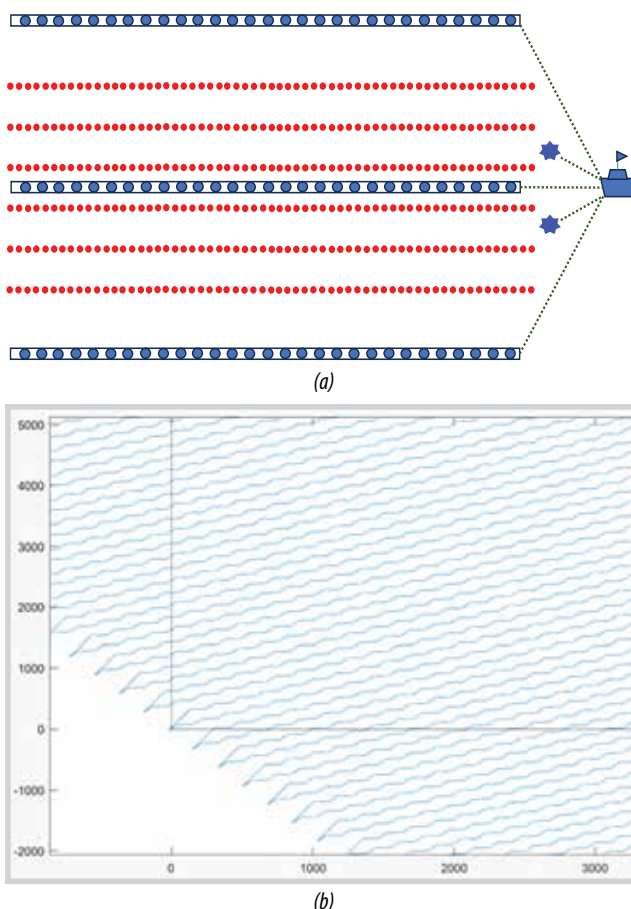


Figure 3. (a) Acquisition geometry with flip-flop shooting, (b) Trajectory of the shots in flip-flop shooting.

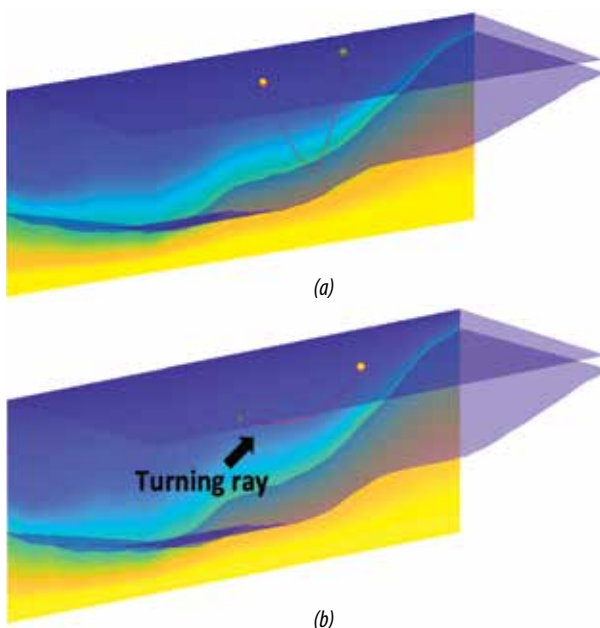


Figure 4. Ray-tracing in 3D synthetic model: (a) ray reflects at the horizon, (b) turning ray.

shown in Figure 4. The results align with the expected behavior of wave rays in an inhomogeneous medium. Both reflection and turning rays were successfully simulated (Figure 4b).

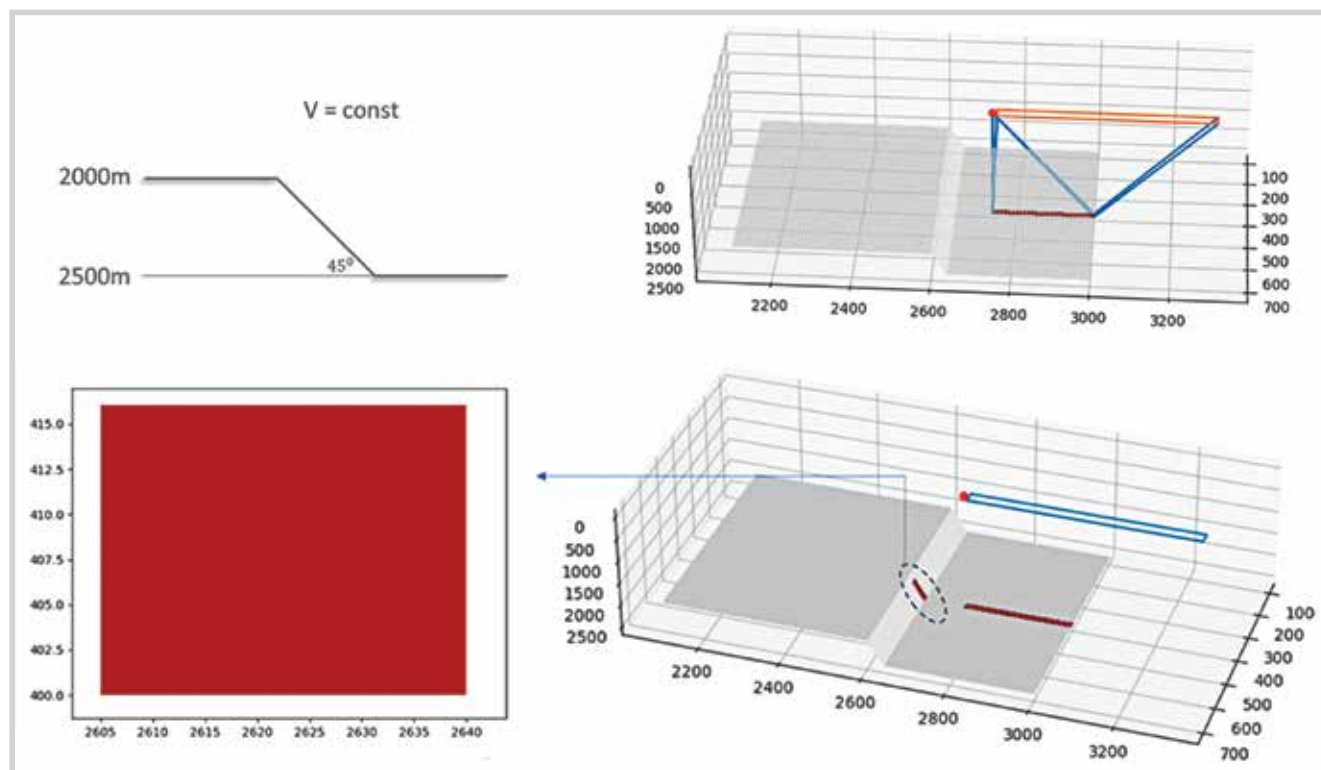


Figure 5. Ray-tracing in an isotropic velocity model.

3.2. 3D single shot simulation in a constant velocity model

Note that if the velocity is a constant, the horizon is a plane, and the source/receiver configuration is known then the number of hit to a grid point in the horizon can be calculated beforehand. To validate the method's accuracy for seismic illumination, a single-shot illumination experiment was conducted in a simple 3D dipping horizon model (constant velocity model and 45° horizon to simulate a fault) and the results were compared with theoretical calculations (Figure 5). The acquisition configuration is demonstrated in Table 1.

The illuminated area on the 45° horizon, is depicted in Figure 5. As shown in Table 2, the theoretically illuminated area, which is 34.5 grid cells, while the simulated illumination area spans 35 grid cells (with an error of less than 1 grid cell due to the discretization of the model). That implies an excellent match. Similar experiments on various models show the reliability of our illumination software.

3.3. 3D single shot simulation in a spatially-varying velocity model and a real horizon with comparison to the result from a commercial software

Another single-shot illumination experiment was conducted in a spatial varying velocity model and

Table 1. Acquisition configuration for single shot simulation in a constant velocity model

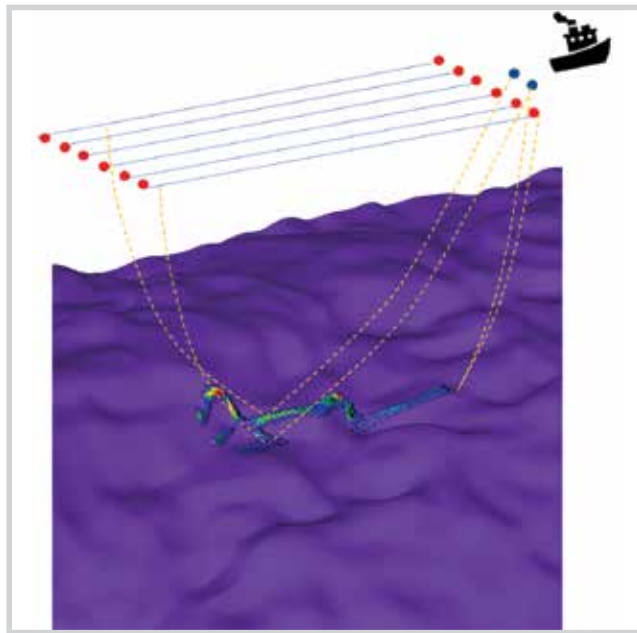
Source distance (m)	25
Source depth (m)	6
Number of cables	8
Cable distance (m)	50
Cable depth	15
Number of receivers/cable	281
Receiver interval (m)	25
Minimum offset (m)	150

Table 2. Comparison of illuminated area on the 45° horizon

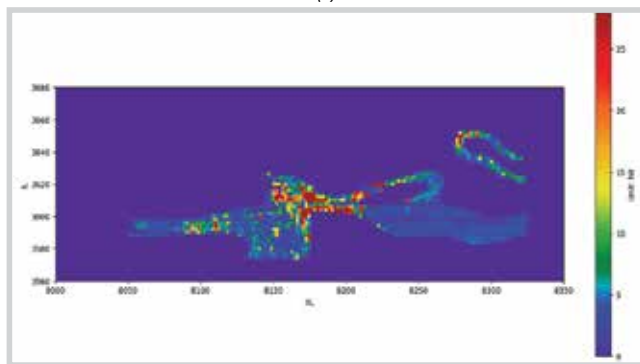
Theoretical illuminated area	34.5 grid cells
Simulated illuminated area	35 grid cells

compared with results from a leading commercial seismic illumination software. Figure 6 demonstrates a high degree of consistency between the hitmap of the single-shot illumination produced by the VPI software (Figure 6b) and that from commercial software (Figure 6c). This confirms that the VPI software can be reliably used for multiple-shot testing, providing a viable alternative for large-scale seismic illumination experiments.

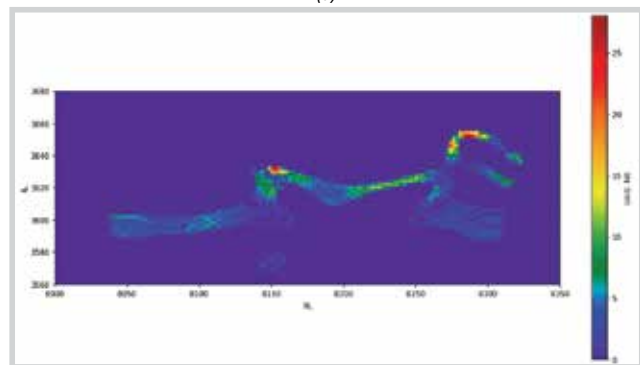
A single-shot illumination experiment was also conducted near a complex geological structure, specifically a large fault, to further assess the method's reliability. Figure 7 shows the illuminated part of the horizon (red grids) near the fault.



(a)



(b)



(c)

Figure 6. (a) Single-shot illumination in 3D model with spatially-varying velocity model and a real horizon. Illumination hitmap of single-shot illumination produced by (b) VPI software, (c) commercial software.

4. Field application

In this study, a set of illumination maps are constructed by using VPI software and compared with those created by a foreign contractor for an operational block in the Malay-Tho Chu basin. The seismic acquisition configuration was chosen to align with that used by the foreign contractor

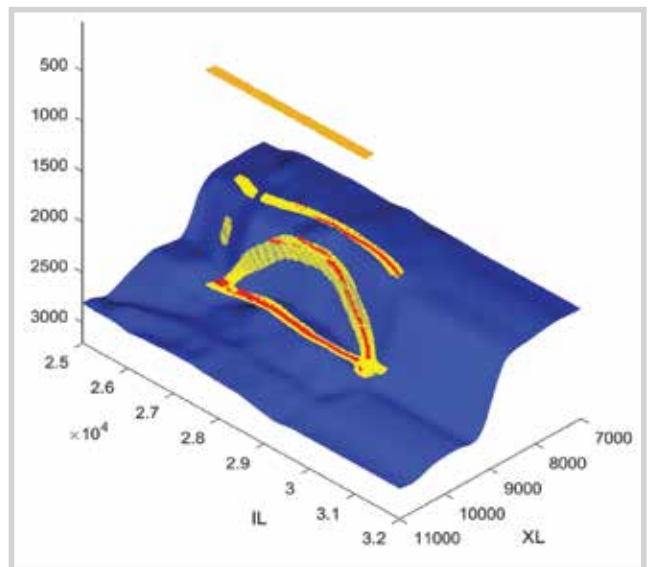


Figure 7. Illuminated part of complex horizon (fault).

Table 3. Seismic acquisition configuration for studied block

Parameter	Value
Number of cables	8
Cable distance (m)	50
Receiver interval (m)	12.5
Cable depth (m)	10
Cable length (m)	7,000
Minimum offset (m)	100
Numbers of explosive sources	2 (flip-flop)
Explosive interval (m)	18.75
Source depth (m)	6
Distance between 2 sail line (m)	175

to facilitate a direct comparison of the results (Table 3). The suitable selection of data acquisition parameters in 3D seismic surveys has a significant impact on the quality of the data collected [6].

Experience in building models for ray-tracing indicates that horizons and attribute blocks must be adequately smoothed to prevent anomalies that may arise during the ray tracing process. This smoothing is particularly important when simulated seismic waves encounter rough or angular surfaces of boundary layers, or when wave paths become overly complex due to abrupt changes in attribute values (such as V_p and Rho). Figure 8 illustrates the results of a ray-tracing test conducted on the horizon X in studied block, highlighting the differences before and after the smoothing process.

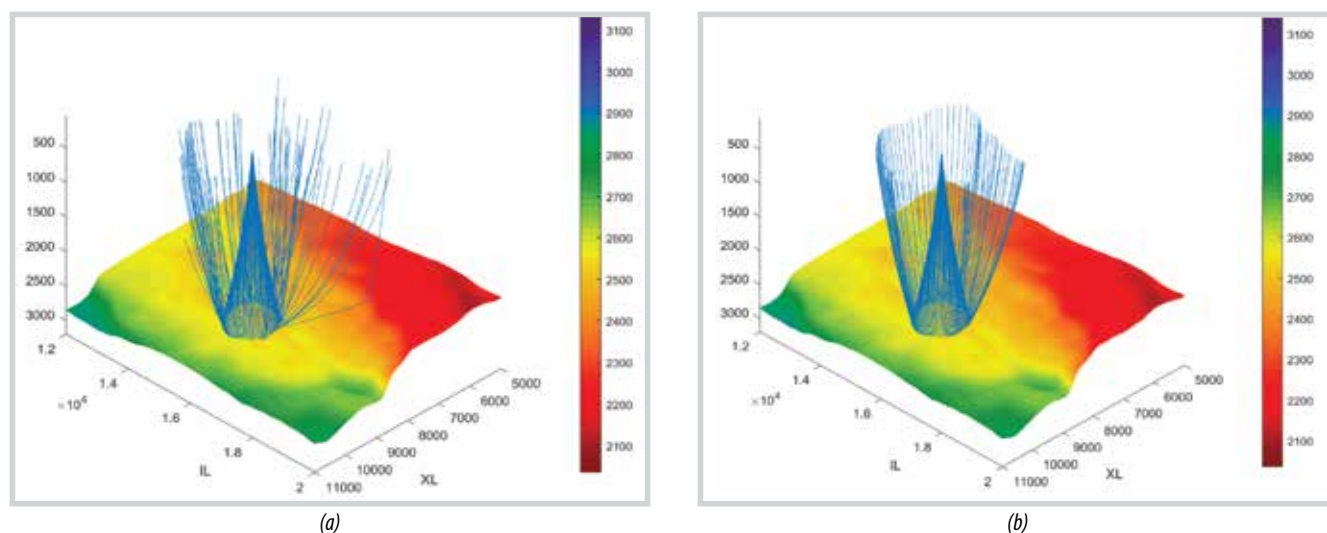


Figure 8. The ray-tracing results on horizon X: (a) before and (b) after smoothing with a filter length of 20 sample points.

Table 4. Definition of output maps

No.	Map	Definition
1	Hit map	Map of Horizon's grid points with the value of each grid point proportional to the Number of Sources and Receivers that the wave can reach that particular grid point and returning to the receiver array.
2	Max.angle map	Map of Horizon's grid points with the value of each grid point proportional to the maximum incident angle of the rays that a source can reach this grid point and the reflection ray returns to the receiver array.
3	Max.offset map	Map of Horizon's grid points with the value of each grid point proportional to the maximum offset of all receivers that receive the reflection ray from the particular grid point.
4	Max.travel time map	Map of Horizon's grid points with the value of each grid point proportional to the maximum travel time of any rays that can reach that particular point and return to the receiver array.
5	SMA map	Map of Horizon's grid points with the value of each grid point proportional to the Simulated Migration Amplitude [7].

In the final step, illumination maps will be generated by performing ray-tracing within the established model using the selected configuration. The process requires a mildly smoothed illuminated horizon and an input velocity model, which is also smoothed.

The creation of illumination maps involves aggregating the number of reflected rays that reached receiver array at each point on the horizon, along with key parameters (offset, incident angle, travel time...). For each source-receiver pair, the wave ray is simulated as it reflects off the horizon and returns to the receiver. By summing the reflections at each horizon point, a hitmap is produced, showing the intensity of illumination for a given acquisition setup. Besides the hit map, a set of output maps are also built in illumination process as shown in Table 4.

To enable comparison, the illumination results generated using VPI software will be labeled as VPI, while those obtained from the foreign contractor will be designated as FC. Figure 9 presents the hitmap of horizon X, located in the Malay-Tho Chu basin, allowing for a

direct comparison of the illumination patterns produced by both methods. Some key observations can be made as follows:

- The FC results show lower resolution but good illumination of larger faults. However, smaller faults are not clearly distinguished from the surrounding areas.
- The VPI results, with higher resolution, reveal variations in brightness according to the fault size, offering clearer differentiation between large and small faults.

Figure 10 demonstrates other output illumination maps by using VPI software. The following observations can be made from these results:

- The maximum offset values are relatively uniform across the horizon surface, except at locations where faults are present. This observation aligns with the hitmap results, as areas with flat terrain exhibit similar brightness, even though they are located at different depths.
- The maximum travel time map shows no clear variation with the depth of the horizon; however, it is noted that the shallow terrain in the northern region has

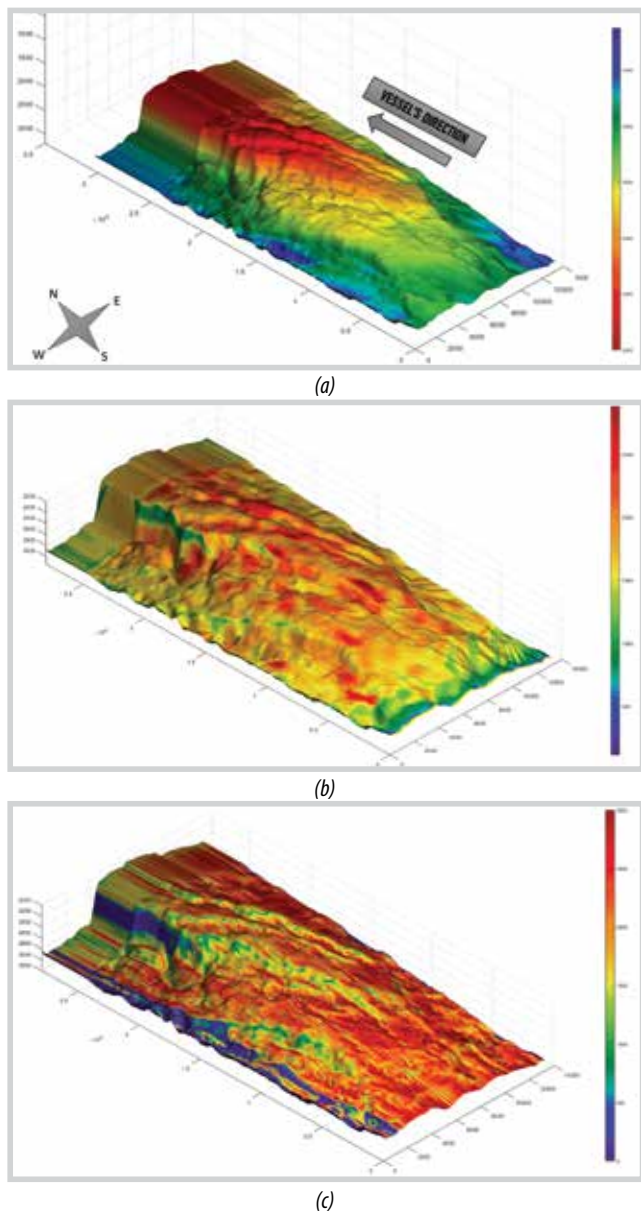


Figure 9. (a) Depth map of horizon X, (b) FC hitmap, (c) VPI hitmap.

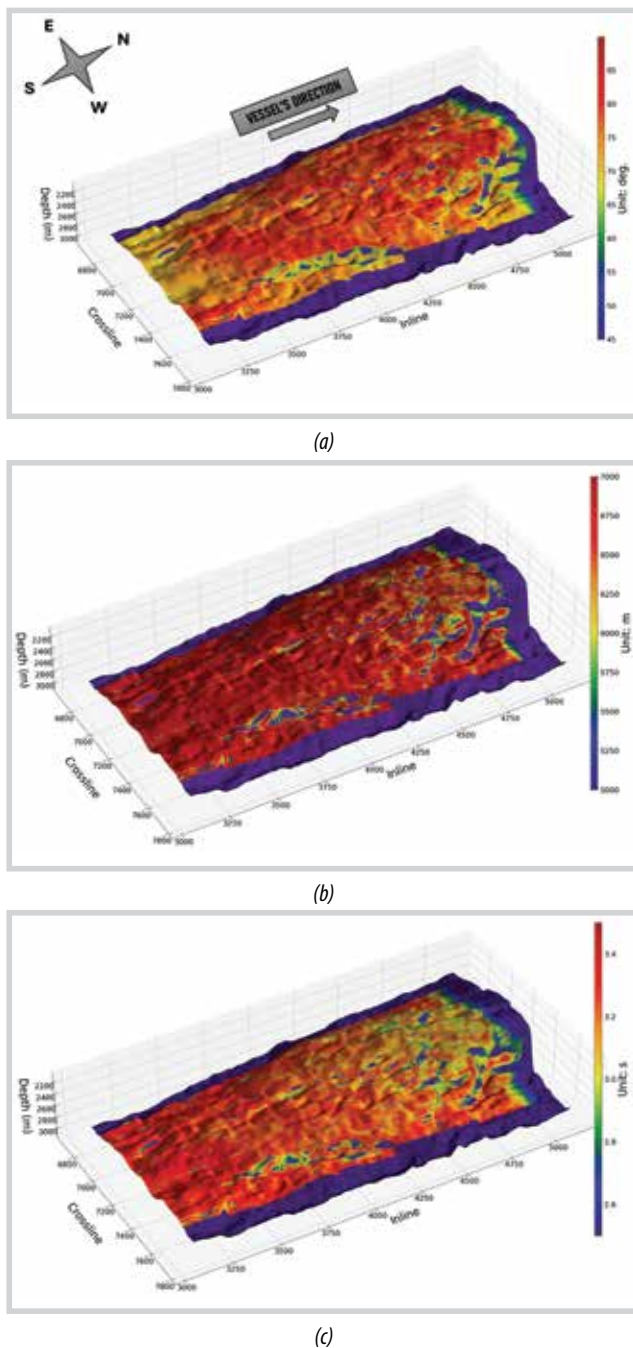


Figure 10. (a) Max. angle map (b) Max. offset map (c) Max. travel time map.

smaller travel time values compared to the deeper areas in the southern and southwestern regions.

- The maximum incident angle map clearly varies with the depth of the horizon and is consistent with theoretical expectations, as the shallow area exhibits larger incident angles compared to the deeper region.

Combining with the Kirchhoff migration equation [8], a simulated migration amplitude map can be constructed to predict the effect of illumination on the final migrated seismic cube. An evenly illuminated SMA map means that

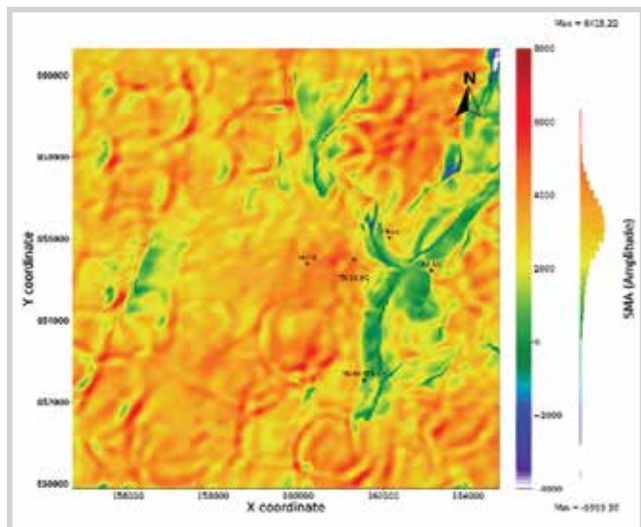
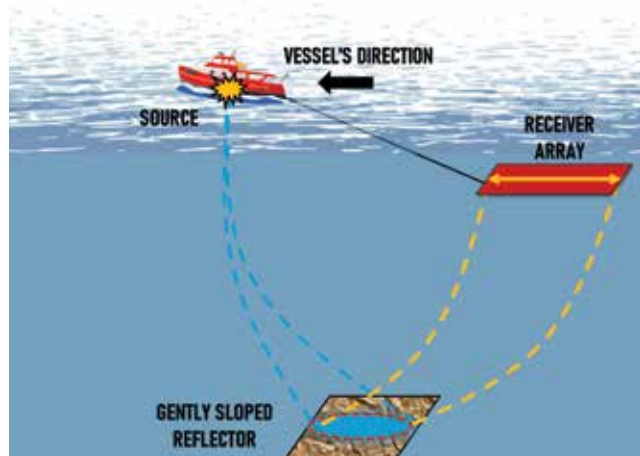
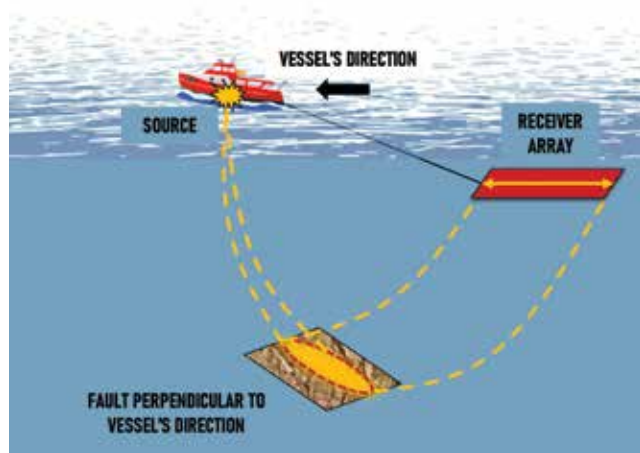


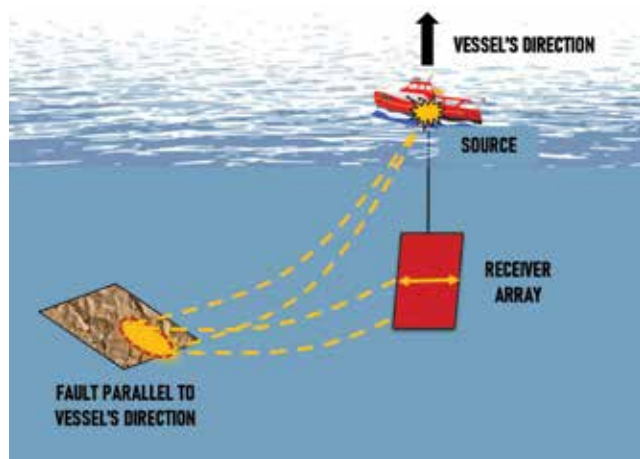
Figure 11. SMA map of a small region.



(a)



(b)



(c)

Figure 12. Different reflector topographies.

any seismic anomaly extracted from the future seismic cube is due to the change in the actual lithology and fluid of the target geology, not an artifact of the illumination. In this study, an SMA map for a small region was constructed as part of the analysis (Figure 11).

5. Discussion

The design of a seismic survey plays a critical role in determining the quality and accuracy of illumination results. Factors such as source-receiver geometry, source spacing, and acquisition aperture directly affect the ability to image subsurface structures. Poorly designed surveys can lead to incomplete coverage, reduced resolution, and significant shadow zones, particularly in complex geological settings. Conversely, optimized survey designs enhance the illumination of key target areas, ensuring higher resolution and more accurate imaging of subsurface features.

- Effect of vessel's direction relative to horizon's dip direction

In practice, the size of the receiver array is constrained by the number of cables and the length of each cable. Additionally, spatial sampling of signals is limited by the spacing between the cables and the receivers on each cable. Consequently, different topographies, which influence the propagation of reflected seismic waves, will yield varying illumination results. Reflector topographies categorized into three primary types (Figure 12):

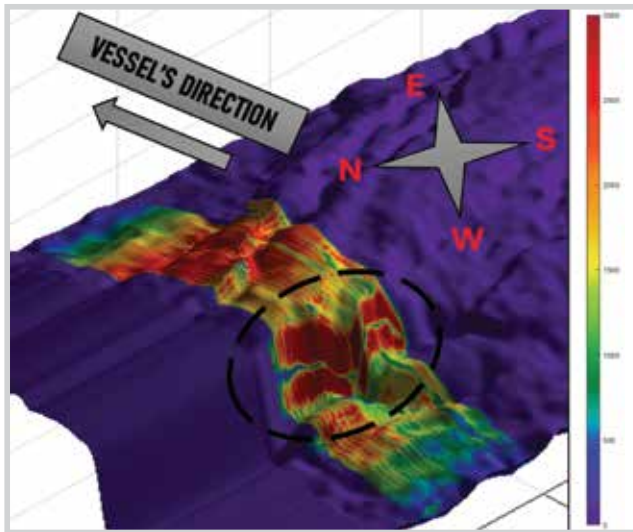
- Gently sloped reflectors;
- Faults perpendicular to the vessel's direction;
- Faults parallel to the vessel's direction.

A gently sloped reflector represents the most favorable topography for illumination (Figure 12a). This topography simplifies the calculations and design of the receiver system, facilitating optimal illumination conditions. As a result, it enhances the accuracy of planning and data collection in seismic surveys.

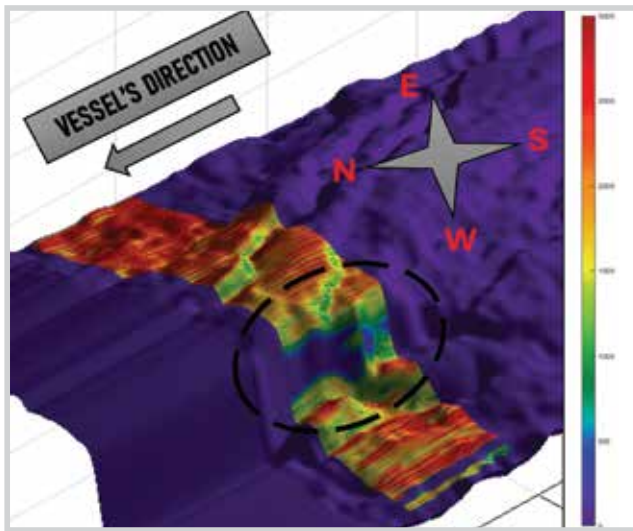
In case of a fault, it is necessary to consider influence of the vessel's direction relative to the horizon's dip direction. The effectiveness of illumination can vary significantly depending on the interaction between seismic wave propagation and reflector orientation.

When the vessel's direction is perpendicular to the faults (Figure 12b), seismic waves can effectively illuminate the fault, producing clearer and more coherent reflections. This alignment enhances the likelihood of capturing direct wave paths, thereby improving the quality of the seismic data.

In contrast, when the vessel's direction is parallel to the faults (Figure 12), the illumination may be less



(a)



(b)

Figure 13. Hitmap of a fault in two case: (a) fault perpendicular to the vessel's direction, (b) fault parallel to the vessel's direction.

effective. The seismic waves may encounter more complex reflection patterns and potential shadow zones, leading to weaker signals and less distinct reflections from the dipped horizon.

Figure 13 shows the hitmaps of a big fault illuminated by 2 different vessel's directions. The fault is better illuminated when the vessel's direction is perpendicular to the fault (Figure 13).

- Impact of depth

Flat reflective surfaces positioned at varying depths will generally experience similar illumination under ideal conditions, assuming there are no velocity anomalies or obstacles in the wave field's path. However, in practice, reflective surfaces frequently exhibit continuous depth variations and can display abrupt changes in areas affected

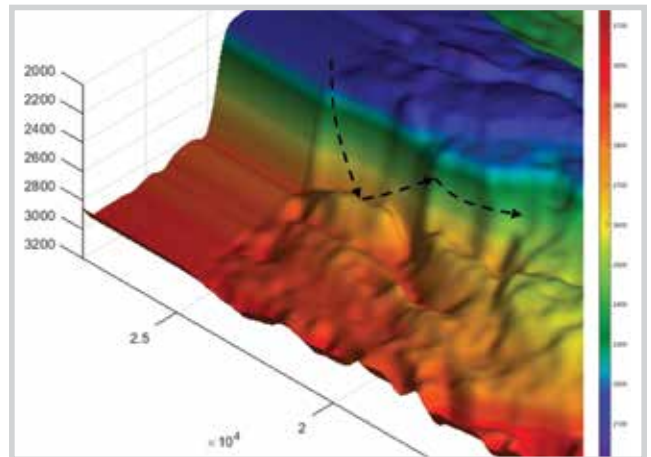
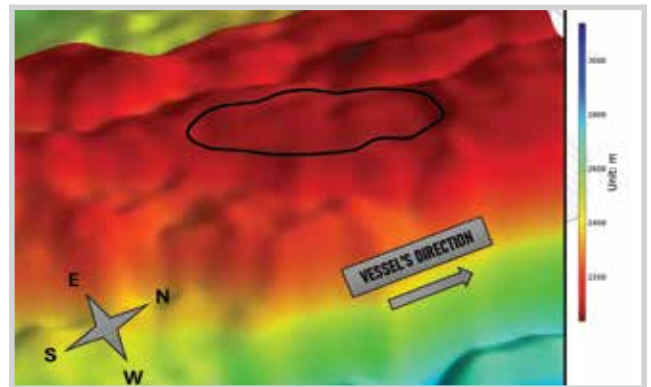
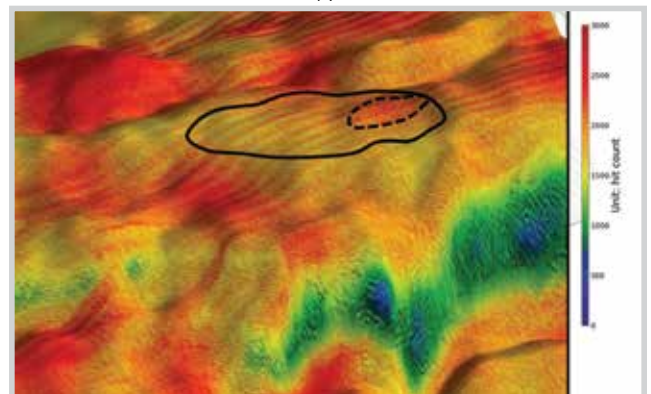


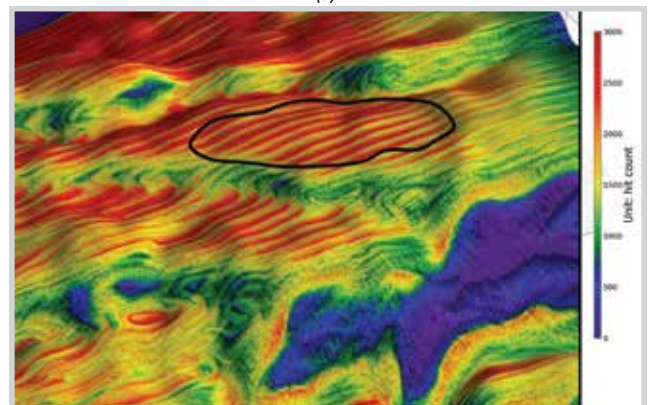
Figure 14. Big fault obstructs the signal's return to the surface.



(a)



(b)



(c)

Figure 15. (a) Depth map of horizon X, (b) FC hitmap, (c) VPI hitmap.

by faulting. Consequently, regions located at greater depths are often less effectively illuminated, as higher terrain can obstruct the signal's return to the surface. This effect is especially pronounced in proximity to big faults, where the complex topography further complicates wave propagation and reflection (Figure 14).

- Comparison on shallow flat zone

Figure 15 is a zoomed-in version of Figure 9, focusing on the solid black outlined area that represents the flattest and shallowest part of Horizon X. Within this region, the FC results reveal an unusually bright area, indicated by the dashed black line. The nearby large fault is illuminated weakly in both results, reflecting the impact of the vessel's direction relative to the horizon's dip direction. This observation underscores the influence of acquisition geometry on illumination quality.

6. Computational workload analysis

In addition to the algorithms used in seismic illumination technology, the application of parallel programming also plays a crucial role in this research. For studied horizon, the terrain's complexity and significant depth posed challenges in terms of calculation time. To illuminate the entire area of 350 km² with the current acquisition configuration, 112,500 shots need to be carried out. If only one CPU is used, the total computation time for all the shots would be huge.

For that reason, parallel programming has been applied, utilizing a total of 600 CPUs (50 nodes x 12 CPUs/node). As a result, the time required to create an illumination map for horizon X has been reduced to just over 4 days.

7. Conclusion

As presented in this paper, 3D seismic illumination is an important step needed to be performed before the actual roll-out of a seismic survey. This step provides a critical information regarding the amount and quality of seismic illumination that can reach any subsurface region, i.e. a more uniform illumination implies the future acquired seismic data can truly reflect the changes in lithology and fluid, regions that lacks illumination, such as under a fault, should require attention from survey design to seismic processing to balance out the results.

Theoretical research and technology development for the 3D seismic illumination method has been presented. The results on model data have shown the sensibility and

accuracy of the developed technology. Application to the field data with the flip-flop acquisition configuration has shown promising results that at least comparable to results from a foreign contractor. Technology optimization such as parallel computing has been mentioned too.

In addition to the research and development, mastering seismic illumination technology also serves as the basis for simulating more complex configuration (such as three-source configuration) or arbitrary vessel trajectories. Developing this technology independently at the VPI allows for reduced reliance on commercial software, lowers implementation costs, allows more control of the process and enhances the capability for future support and quality control of survey design.

References

- [1] Glenn Bear, Chih-Ping Lu, Richard Lu, Dennis Willen, and Ian Watson, "The construction of subsurface illumination and amplitude maps via ray tracing", *The Leading Edge*, 1999. DOI: 10.1190/1.1438700.
- [2] G.F. Margrave, "Raytracing for inhomogeneous media", *Numerical methods of exploration geology with algorithms in MATLAB*, 2003.
- [3] John E. Vidale, "Finite-difference calculation of traveltimes in three dimensions", *Geophysics*, Volume 55, Issue 5, pp. 521 - 526, 1990. DOI: 10.1190/1.1442863.
- [4] William H. Press, Saul A. Teukolsky, William T. Vetterling and Brian P. Flannery, *Numerical Recipes: The art of scientific computing*, 3rd edition. Cambridge University Press, 2007.
- [5] Pham The Hoang Ha, Doan Huy Hien, Ta Quang Minh, Mai Thi Lua, and Nguyen Hoang Anh, "Some results of seismic travel-time reflection tomography study", *Petrovietnam Journal*, Volume 10, pp. 4 - 16, 2021.
- [6] D. Dondurur, "2.5 data acquisition parameters", *Acquisition and processing of marine seismic data*. Elsevier, 2018, pp. 112 - 131.
- [7] Renaud Laurain, Vetle Vinje and Christian Strand, "Simulated migration amplitude for improving amplitude estimates in seismic illumination studies", *The Leading Edge*, Volume 23, Issue 3, 2004. DOI: 10.1190/1.1690896.
- [8] William A. Schneider, "Integral formulation for migration in two and three dimensions", *Geophysics*, Volume 13, Issue 1, pp. 19 - 76, 1978.

LESSONS LEARNED IN HIGH-PRESSURE HIGH-TEMPERATURE WELL COMPLETION IN VIETNAM

Nguyen Minh Quy¹, Le Vu Quan¹, Ngo Huu Hai², Dang Anh Tuan², Nguyen Pham Huy Cuong³

¹Vietnam Petroleum Institute (VPI)

²Vietnam Petroleum Association (VPA)

³Bien Dong Petroleum Operating Company (Bien Dong POC)

Email: quanlv@vpi.pvn.vn

<https://doi.org/10.47800/PVSI.2024.06-02>

Summary

Well completion operation in high-pressure and high-temperature (HPHT) conditions is a big challenge for both operators and service companies. These encompass all aspects in well construction and production operation such as drilling, completion, workover, IOR/EOR application, specialized equipment, etc. Effective risk management, cost control, deployment of skilled human resources for HPHT wells require managers and operators to approach in a way different from that used in conventional environment. The lessons learned from well completion operations in HPHT conditions, summarized from construction practices at gas fields in Nam Con Son basin offshore Vietnam, provide valuable insights and serve as a noteworthy reference for the design and execution of HPHT well completions in the future.

Key words: High-pressure and high-temperature (HPHT), well completion, IOR/EOR, Nam Con Son basin.

1. Introduction

In recent years, the definition of “high-pressure high-temperature” (HPHT) wells has varied across companies and oil and gas associations. The American Petroleum Institute (API) classifies HPHT wells based on its guidelines for specialized HPHT equipment. According to API standards, a well is classified as high-temperature if the static temperature at the total depth exceeds 350°F (approximately 177°C), and as high-pressure if the shut-in surface pressure exceeds 15,000 psi (approximately 103 MPa). Wells exhibiting one or both criteria are categorized as HPHT wells. Meanwhile, the Society of Petroleum Engineers (SPE), the International Association of Drilling Contractors (IADC), and several multinational oil companies (such as Schlumberger) use a slightly different thresholds, setting high-temperature at 300°F (around 149°C) and high-pressure at 10,000 psi (around 69 MPa), as shown in Figure 1.

In Vietnam’s oil and gas operations, although there are no official regulations for HPHT classification,

Petrovietnam and oil and gas contractors have adopted HPHT standards based on the definitions provided by SPE and IADC, with certain adjustments to accommodate local conditions. A well with a bottom-hole temperature exceeding 149°C and bottom-hole pressure below 10,000 psi is still classified HPHT if it is drilled an abnormal pressure formation having a minimum average pressure gradient of 2.43 psi/ft and an expected maximum formation pressure equivalent to approximately 15.4 ppg EMW. In recent years, several HPHT fields/discoveries have been brought into production and development in Nam

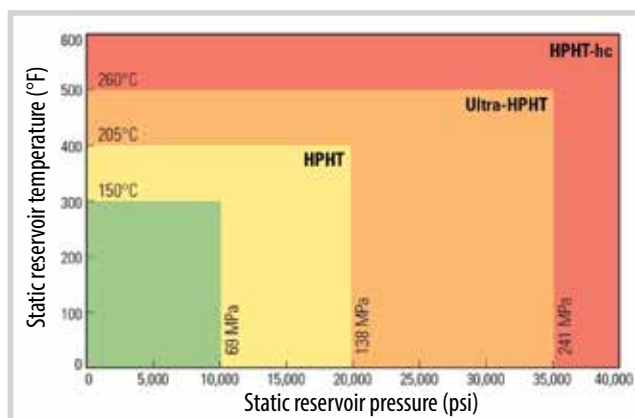


Figure 1. HPHT thresholds [1].



Date of receipt: 24/10/2024.

Date of review and editing: 24/10 - 23/12/2024.

Date of approval: 23/12/2024.

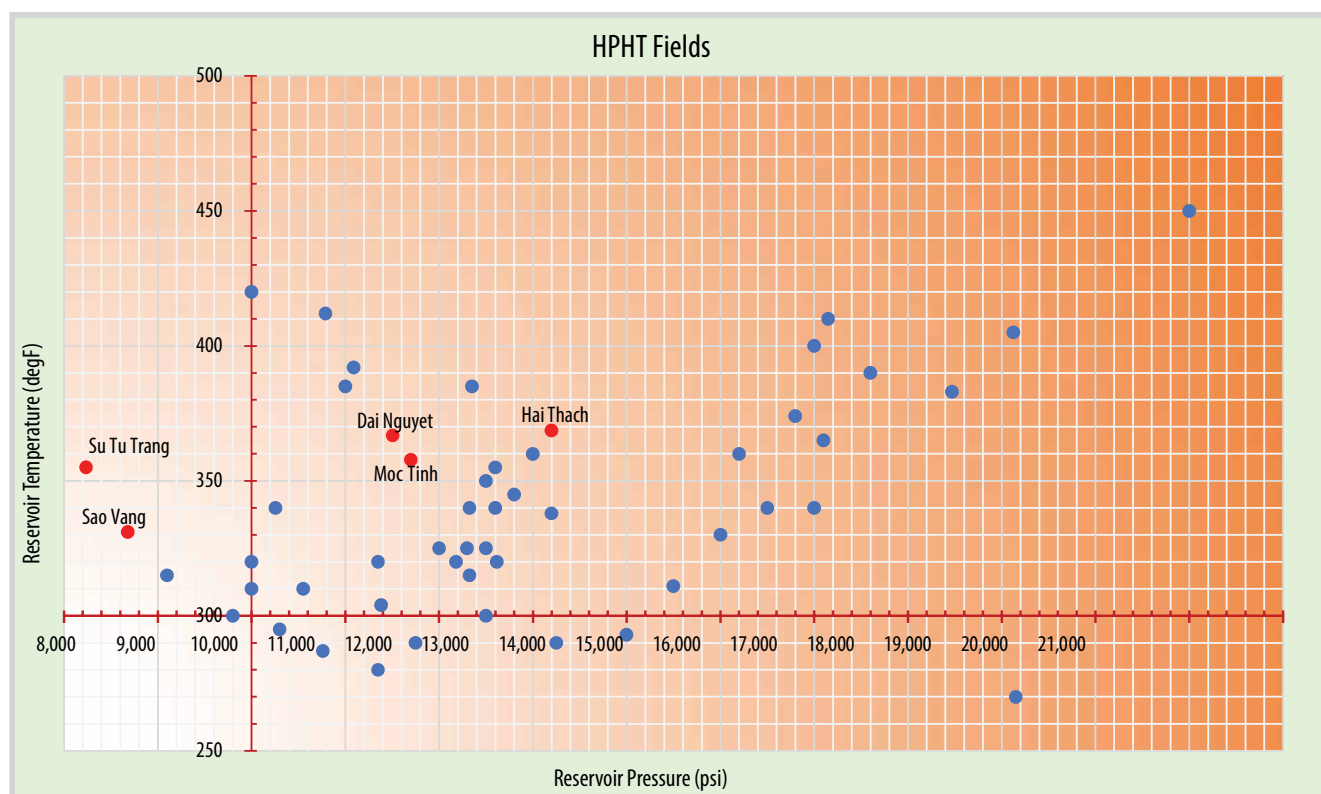


Figure 2. HPHT field examples worldwide and Vietnam [2].

Con Son basin (Figure 2). Effective and safe well completion operations have played a significant role in ensuring the stable and secure production at the A and B fields, as well as in maintaining the on-schedule other field developments in the Nam Con Son.

During the production process, several wells in the A and B fields have encountered issues such as condensate buildup near the wellbore and liquid accumulation at the bottom of the well. To address these issues, various remedial solutions have been studied and proposed, which include circulating production combined with periodic gas injection into the well and installing velocity strings to regulate the upward flow rate of the well’s production stream. Nonetheless, the implementation of these solutions has faced challenges due to the HPHT characteristics of the reservoir and the complexities of the well completion structures. The lessons learned from well completion operations at the A and B fields will serve as valuable references applicable to other HPHT formations in the future.

2. Issues during completion operation in the A field wells

- There are seven wells drilled on the A platform, including four wells (A-1P/3P/4P/7P) targeting the Upper Miocene B (UMB) 15-20, two wells targeting the Upper Miocene A (UMA) 10-20 and well A-2X for appraising deep reservoirs. The drilling campaign in the A field was divided into two phases: Phase

1 conducted in the early stage of the project with four wells A-1P/3P/6P and A-2X; and Phase 2, carried out in the late stage of the project, began after the completion of drilling nine wells in the B field then the rig was moved back to the A field to drill the remaining three wells A-4P/5P/7P before the project closure. During the interval between Phase 1 and Phase 2, some off-line interventions were taken place in the A platform, including perforation, zonal isolation, and addressing equipment failure.

During Phase 1, the completion operations mainly focused on deployment of the upper completion string. In this early stage of the project, several incidents occurred, and most of lessons learned and recommendations were documented in this stage.

+ The completion of A-1P encountered a failure of the wellbore clean-up tools during the inflow test with base oil, conducted in preparation for displacing underbalanced completion brine. The completion tool cleaner (CTC) was prematurely sheared due to excessive compression during the inflow test which resulted in pulling out the damaged equipment and subsequently deploying a retrievable test tool system (RTTS) packer. The well was then successfully

inflow-tested and displaced to potassium formate. During the displacement from drilling mud to completion brine, the circulation system revealed its limitation. Specifically, the return system utilized a shared flow path for both drilling mud and completion brine, leading to increased operational time consumption. To fix this issue, the circulation was modified. The completion process also encountered equipment failures due to both human error (packer backing out due to inattention, lubricator valve (LV) fittings stuck inside operating ports) and design limitation (the SB pulling tool being unable to release from the fishing neck, the RPT running tool failing to hold off the shear screws). Eventually, the completion string was successfully deployed, and well was secured before handed over to production. Then the rig was skidded to the next well.

+ The completion of A-3P got an issue with the positive test of the 5½" liner lap, which failed at 7,200 psi during a 7,500 psi test. An easy shut-off valve (EZSV) bridge plug was set on the liner shoe and a tieback packer was installed on the 5½" liner lap but the test was still unsuccessful at 7,200 psi. Despite this, the well still proved good inflow test over 5 hours, and the completion brine was displaced while maintaining well integrity throughout the completion phase. The completion string was successfully deployed and set without any other major issues.

+ The completion of A-6P was taken place after a 20-day suspension for drilling and casing the 22" section of well A-2X. The prolonged suspension with drilling mud left in the well caused barite sag, leading to difficulties in deploying the wellbore clean-up string. It took about 2 days to clean the barite sag and condition the mud in the hole. Following these operations, the completion was successfully deployed, and the well was securely handed over to production.

- The completion of A-2X experienced a failure during the positive test of the 5½" liner lap at 6,400 psi then it was unable to hold 3,200 psi. After several attempts to address the issue, the gas circulation increased to 11% before reducing to zero after several bottom-ups. The well was then successfully inflow-tested for five hours and displaced to brine. However, during the inflow test, the completion tool cleaner circulation sub was sheared out due to high compression stress. As a result, the wellbore clean-up string had to be stripped out to replace the failure equipment with backup tools.

In Phase 2, after the drilling rig moved from B field to A field, the operation included completion and perforation for the last three wells of the project (A-4P/5P/7P). These wells were drilled into UMB 15-20 (A-4P/7P) and UMA 10-20 (A-5P).

+ The completion of A-5P encountered multiple issues involving the segment bond tool (SBT), logging tool and PBL (Multi Activation Bypass) sub during the wellbore clean-ups. Excessive cement at the 5½" liner shoe required activation of the PBL sub to increase the pump rate while milling the cement by a 4⅛" mill tooth bit. The PBL sub was deactivated and maintained integrity during the subsequent positive and negative tests. However, during the displacement of the well into brine, the pill train returned to the surface at early stroke, indicating a leak in the PBL sub. An onshore investigation showed a washout at one (1) port side of PBL and the absence of two O-rings.

+ The A-7P well was the last well drilled in the A field and of the project. It had the issue with the 5½" liner shoe as the plug was over-displaced, leading to the failure of the positive test at 3,170 psi. To fix it, an EZSV bridge plug was set right above the landing collar, and a subsequent positive test was successfully conducted at 3,200 psi. The well was then inflow-tested with base oil as normal, and the completion string was deployed successfully in completion brine. The well was secured and handed over to production.

3. Issues during completion operation in the B field wells

There are nine wells drilled on B platforms including five wells (B-1P/4P/5P/6P/9PST) targeting the LMH reservoirs which are classified as HPHT and four wells (B-2P/3P/7P/8P) targeting the UMA and Middle Miocene flank (MMF) reservoirs, exhibiting pressures and temperatures similar to those in the A field. These wells were spudded after the drilling rig moved from the A platform to the B. Some wells were perforated under simultaneous operations (SIMOPS) conditions, allowing intervention equipment access below the rig floor while drilling adjacent wells. Upon completing the last well (B-9PST), the drilling rig was moved back to the A platform to drill the remaining three wells in the A field before the project concluded.

- The B-3P well was the first well drilled on the B platform, targeting MMF30 reservoir. Its completion phase smoothly proceeded as normal operation conducted in the A field when the well was tested and displaced

into brine. However, during the dummy run, the tubing hanger (TBHG) was unable to land correctly. The blowout preventer (BOP) was nipped down and the multi-bowl was split to investigate the upper section inside. It was found that the landing shoulder of the isolation test tool (used to test BOP) rolled up, preventing the spacer of TBHG from landing properly. The edges were fined and all obstructions were cleared to allow TBHG landing correctly. The operation was resumed to deploy upper completion without any further incident.

- The B-1P well was drilled into the LMH reservoirs to appraise the deep targets in LMH 45A-45B-46. In the completion, the TBHG was again unable to land properly during dummy run, this time due to high elevation of the 10" bridging hanger. This was the first well in the project (followed by B-4P) to use the bridging hanger, necessitated by the damage of wicker on the 10" casing hanger (CSHG). The bridging hanger does not have a locking ring to secure it in-place during pressure test, causing it to move upward approximately 1". The multi-bowl again was split to confirm the high elevation of bridging hanger, and

shims were adjusted on the TBHG spacer. The operation was resumed, and completion string was deployed in the hole. Upon landing the X-mas tree, the TBHG was found too deep for the VG-52 seal ring. Anyhow, the Xmas tree was successfully tested with its secondary seal on the TBHG neck, ensuring the well was safe for perforation.

- The rig was then skidded from B-2P to B-1P after finish drilling the 13 5/8" section to perform the second perforation in the LMH 20-25-30 reservoirs of well B-1P. The LMH 45A-45B were abandoned by setting an EZSV bridge plug and topping it with a 50 m cement plug. EZSV bridge plug was stuck in the 5 1/2" liner at 3,904 m (desired setting depth of 4,078 m). After several unsuccessful attempts to move the bridge plug, it was decided to set at stuck point. The e-line tool string was successfully retrieved to the surface without damage. The bridge plug passed an 8,000-psi pressure test and an inflow-test with a surface pressure of 436 psi. A 40 m cement plug was spotted on top of the bridge plug. Then, the well was perforated in the LMH 20-25-30 reservoirs and handed over to production. The rig was then skidded back to B-2P to drill the 10" section.

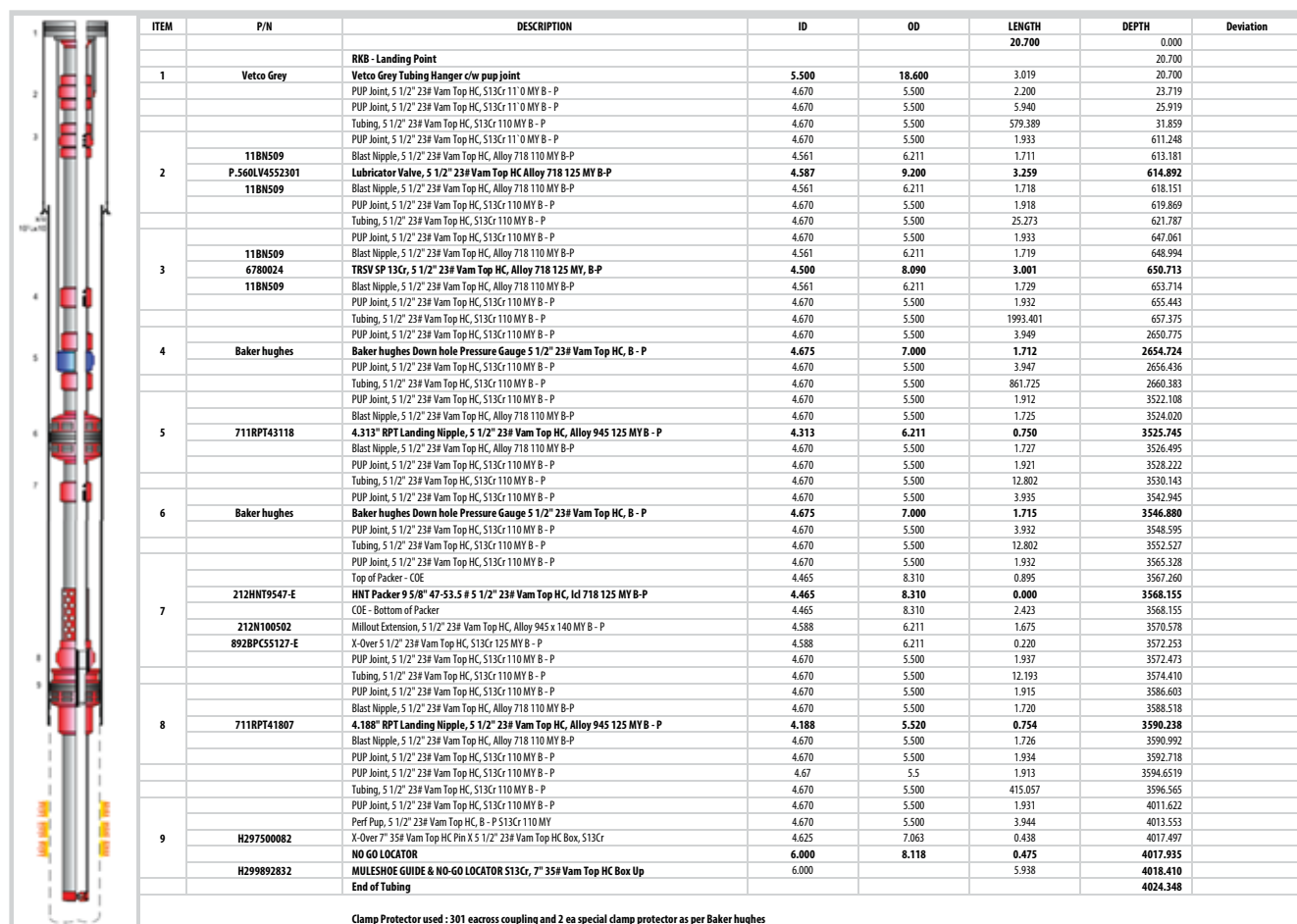


Figure 3. B-8P well completion schematic.

- The B-2P well was drilled, completed, and perforated into UMA 40, MMF5-10 reservoirs. The operation went as planned with the perforation using 1.75" coiled tubing to deploy 170 m of 2 7/8" high nitrogen steel (HNS) guns. After finishing the 22" casing in the B-5P well, the memory production logging tool (MPLT) string was deployed into the B-2P well. The MPLT operation was executed successfully without any tool failure, and well was then handed over to production. During production phase, the down hole gauge (DHG) lost signal; troubleshooting confirmed a complete failure of the electronics.

- The B-5PST well was side-tracked from the original well plan due to the issue encountered while drilling through the targets. During the completion phase, the well was successfully tested and displaced to completion brine. Then, the 10" SBT was logged as normal, however, the tools were found broken at the bow springs at surface. The well was subsequently cleaned with two clean-up trips: the first using an 8 3/8" flat bottom junk mill, and the second using a 4 1/8" mill tooth bit, without any obstruction encountered in both runs. An investigation indicated a complacency during rig-up and rig-down of wire-line tools by air tugger. The lesson learned was to use wireline with load cell for rig-up/down the tools to avoid similar incidents. The SBT run on the 5 1/2" liner was omitted due to the concern of remaining junk in the hole. The completion string was then deployed with any further incident.

- The B-6P well was completed with a deviation from the plan which omitted the cement bond log in production liner. The well was then perforated in the LMH 20-30 with 1.75" coiled tubing and 2 7/8" high nitrogen explosive gun, using the surface well test package to

connect the Xmas tree to production system. There was a minor issue with e-line unit while perforating due to its electronic device. In the dummy run, the guns found difficult to pass the liner with gun hanger releasing tool that was subsequently decided to replace with a bullnose and keep the gun hanger at the setting depth after perforation. The operation was conducted safely, and the well was then handed over to production with LMH 20-30 perforated as per plan.

- The B-7P well was completed without any issue, and then perforated in the UMA10 while the rig was drilling B-8P. The perforation gun was 3 3/8" high melting explosive (HMX), deployed with a braided line and gun hanger system ensuring sufficient rat-hole for dropping the guns.

- The B-8P well was completed as shown in Figure 3. Since the clean-up tool experienced the overpull at the 10" Tieback, the cement bond log was then omitted in the 5 1/2" section. While deploying completion string, the DHG lost signal after 1,357 m string in-hole. A back-up DHG was then installed on completion, causing the DHG being positioned higher than planned.

- The B-4P well was completed without any problem and then perforated in the LMH 20-30-40 reservoirs while the rig was drilling the B-9P well. The perforation gun is 2 7/8" HNS with coiled tubing perforation system. The B-9P well was completed. The operation was executed as per plan until the completion string found obstruction at 2,771 m. The attempts to run the completion string through obstruction had caused the production packer prematurely set. To address this, the upper tubing section was cut using an e-line remote control torch cutter and retrieved on surface. The production packer was then

Table 1. Completion time and NPT distribution

No.	Well	Completion duration (hours)	NPT (%)	NPT code
1	A-1P	281	4	Completion services
			9	Fluids services
2	A-3P	427.5	2	Wellhead services
3	A-6P	863.5	6	Fluids services
4	A-2X	476.0	4	Wireline logging services
5	B-3P	223.5	16	Wellhead services
6	B-1P	268.5	17	Wellhead services
7	B-8P	199.5	5	Clean up
8	B-4P	371.0	48	Wait on weather
9	B-9P	596.5	72	Well problems
10	B-9PST	223.0	1	Wireline logging services
11	A-5P	197.5	4	Wireline logging services
12	A-4P	185.5	18	Wireline logging services

Table 2. The process of evaluating NPT caused by wireline logging services

Category	Assessment
Pre-job planning/equipment Preparation	<ul style="list-style-type: none"> ✓ All equipment was delivered for load-out on time; ✓ Contingent equipment was ready for load out on time; ✓ Procedures and simulations were provided in advance of jobs; × Lack of coordination and preparation for mobilizing zone 2 logging unit.
Job execution (equipment)	<ul style="list-style-type: none"> ✓ Successful open-hole logging performance in HPHT environment (PCL and WL); ✓ Successful cased-hole logging performance (cement bond integrity measurements); ✓ Successfully completed 15 interventions with WHP > 5,000 psi; × Some major issues and equipment failures were identified for certain jobs.
Job execution (personnel)	<ul style="list-style-type: none"> ✓ Effective communication between the field crew and operator’s supervisors; × Intermittent levels of crew competency observed throughout the campaign.
Onshore support	<ul style="list-style-type: none"> ✓ Effective communication between support staff and operator engineering team via various meetings held before operation and weekly updates during job preparation progress; × Technical support and assistance between coordinator and project team need to be further enhanced.
Lessons learned/Follow up	<ul style="list-style-type: none"> ✓ Being proactive in failure investigation and root cause analysis; ✓ Corrective actions were effectively applied, yielding good results for cased-hole logging; × The timeliness of failure investigation reporting requires improvement, including frequent status updates.

Table 3. NPT have been analyzed, evaluated, and lessons learned

Category	Assessment
Pre-job planning/equipment Preparation	<ul style="list-style-type: none"> ✓ Equipment was correctly prepared, serviced and maintained according to company’s procedures and delivered on time. × Services contractor’s equipment “just in time” delivery strategy reduced flexibility. × Poor QA/QC on some manufactured equipment.
Job execution (equipment)	<ul style="list-style-type: none"> ✓ Equipment worked as designed. × High NPT at the start of project as this was the first time this system was run in the world. ✓ NPT was reduced once new procedures and right service hands was assigned.
Job execution (personnel)	<ul style="list-style-type: none"> ✓ Dedicated service hands did a good job. × Services contractor’s personnel crew competency was questionable at the start of the project. Service hands were changed out until the expected level of support was achieved.
Onshore support	<ul style="list-style-type: none"> ✓ Good equipment preparation & support from Vung Tau workshop. ✓ The additional of Operator wellhead specialist to the team significantly reduced downtime attributed to Services contractor. × Poor levels of customer technical support from Services contractor’s office.
Lessons learned/Follow up	<ul style="list-style-type: none"> × Having the right people using the right equipment and knowing how the equipment works is required for efficient operations. × This was specifically designed equipment and needed specifically trained personnel - “on the job training” was not appropriate for this work. × Low improvement, response to failure investigation, root cause analysis.

milled and recovered although the lower slip segments were missing. Consequent attempts to clean the slip segments resulted in the wellbore clean-up string stuck in the hole. This serious stuck pipe led to a series of fishing run and ended up with the fish of a 27/8” drill pipe left inside the 5½” liner. The whipstock was then set above the 5½” liner hanger, and the well was side-tracked. And the completion of B-9PST was executed without any further problem.

4. Major completion lesson learned

During the well completion process in the A and B fields, the issues occurring at the wells, as mentioned

above, resulted in non-productive time (NPT). Table 1 shows the total well completion time and the corresponding non-productive time for each well. For example, the total well completion time of the well A-4P was 185.5 hours, with 18% of the time attributed to NPT due to wireline logging services. The lesson learned was applied to subsequent wells for reducing NPT related to this specific issue.

Each type of NPT code will be evaluated step by step to draw lessons learned. Table 2 provides a specific example of the evaluation of NPT code related to wireline logging services. The three wells A-4P, 5P, and B-9PST were drilled

during phase 2 of the project. Based on the statistics in Table 1, it is clear that well A-4P was drilled first and had an NPT related to Wireline logging services of 18%. A deeper analysis reveals that the primary causes of NPT in this well are issues encountered during equipment preparation and equipment failures during operation. The root causes are lack of coordination and preparation for mobilizing zone 2 logging unit, therefore, the installation time took longer than expected. The results of the analysis, evaluation, and lessons learned, summarized in Table 2, form the basis for a significant reduction in NPT for subsequent wells (4% for well A-5P and, notably, only 1% for well B-9PST).

Table 3 provides another example of the evaluation of NPT code related to wellhead services. As summarized in Table 1, the three wells with NPT related to wellhead services are B-1P, B-3P, and A-3P. The causes leading to NPT at these wells have also been analyzed, evaluated, and lessons learned are presented in Table 3.

Other NPT codes were also analyzed and evaluated using the same method to draw lessons learned for each type of well completion service as below.

4.1. Wellbore clean-up

- Do not place shear-activated tools on one string: In wells A-1P and A-2X, the CTC tool (circulating sub) was prematurely activated during the inflow test, causing operational delays. The lesson learned is to closely monitor pressure during the test and replace the CTC with a PBL sub activated by a ball-drop.

- Incorporate clean-up tools into one string: Instead of performing wellbore clean-up in two separate runs, it is recommended to combine the tools into a single string to reduce rig time and ensure efficient well cleaning.

4.2. Fluid cleanliness

Use appropriate cleanliness criteria: In well B-1P, using total settling solids (TSS) instead of nephelometric turbidity unit (NTU) as a cleanliness criterion was proved to be more accurate and practical for assessing the return brine, which minimizes excessive circulation time.

4.3. Pilot test before mixing old and new brine

Conduct pilot testing: In wells A-6P and B-9P, mixing old and new brine without prior testing caused unwanted precipitation. The lesson learned is to always perform pilot testing before mixing to avoid unexpected chemical reactions.

4.4. Completion equipment and tools

- Special ball requirements for PBL sub in heavy mud: In wells A-6P and B-5P, standard balls failed to work in heavy mud, resulting in delays. The lesson is to use heavier dart-type balls that can perform in high-viscosity fluids.

- Mark completion equipment: In well A-1P, a production packer came loose due to insufficient marking. The lesson learned is to ensure that all completion equipment is clearly marked for monitoring during installation.

- Avoid excessive work on completion string: In well B-9P, excessive work on the completion string caused the production packer to set prematurely, leading to severe operational issues. The lesson learned is to pull out of hole (POOH) when encountering obstructions instead of forcing the string.

4.5. Perforation and intervention operations

- Use gun hanger for depth correlation: In well B-1P, using a gun hanger as a depth correlation tool for perforation with coiled tubing avoided off-depth perforation issues.

- Surface pressure test with water: Methanol was found to damage O-rings due to gas reactions. The lesson learned is to use water for pressure tests to maintain the integrity of seals.

- Design for snubbing wireline tools in high wellhead pressure: In well A-2X, tools couldn't be snubbed into a high-pressure well due to insufficient weight. The lesson learned is to calculate the proper tool weight with a safety margin for HPHT conditions.

4.6. Other operational issues and lessons

- Wireline tool issues: Several instances of tool malfunction were noted, such as tools failing to pass through heavy mud, being unable to snub due to high wellhead pressure, or centralizers breaking. The key lesson learned is to carefully design tool strings, considering the specific working conditions (HPHT) and ensuring adequate weight and flexibility.

- Increase safety margin for cable tension in PLT logging: During PLT logging in HPHT wells, excessive cable tension was encountered. The lesson learned is to design jobs with a higher safety margin for flowing

conditions and ensure that proper friction factor is applied to calculate cable specifications.

In summary, the application of the lessons learned as mentioned above in well completion for future drilling projects will contribute to reducing NPT. Reducing construction time will, in turn, lower drilling costs and enhance the economic efficiency of the project.

5. Conclusion

The conclusion of the paper emphasizes the importance of applying real-world experiences to optimize operations and minimize NPT in drilling and well completion activities. The lessons gathered stem from challenges encountered across various phases of operations, including wellbore clean-up, fluid cleanliness checks, well completion, perforation and well intervention, and wireline tool use. Key lessons learned include:

- Integration of tools and processes: Combining tools into a single string and optimizing processes such as wellbore clean-up and fluid cleanliness checks significantly reduces time and resources. Instead of performing separate runs, tools should be integrated to minimize downtime and enhance operational efficiency.

- Accurate criteria application: Shifting from the nephelometric turbidity unit to total settling solids as the fluid cleanliness criterion greatly improves the ability to assess solid content in the filtered brine, preventing unnecessary circulation. This demonstrates the importance of applying the correct standards suitable to specific well conditions.

- Pre-testing critical steps: Conducting pilot tests before mixing old and new brine or performing other critical operations helps prevent unexpected chemical reactions and precipitations. These proactive measures protect equipment and ensure smoother operations in the wellbore.

- Attention to equipment design and supervision: Well completion equipment requires careful design and supervision, such as clear markings or precise weight calculations when deployed in specialized conditions like HPHT wells. Ineffective planning can lead to significant issues, including additional runs or equipment failure.

- Tool modifications and adaptations to actual conditions: The challenges with wireline tools, perforation guns, and other downhole equipment highlight the need for constant improvements and adjustments to suit real-world working conditions, especially in HPHT environments. Tools must be calibrated for weight, pressure, and other operational factors to ensure safety and efficiency.

References

- [1] Gunnar DeBruijn, Craig Skeates, Robert Greenaway, David Harrison, Mike Parris, Simon James, Fred Mueller, Shantonu Ray, Mark Riding, Lee Temple, and Kevin Wutherich, "High-pressure, high-temperature technologies", *Oilfield Review*, Volume 20, Issue 3, pp. 46 - 60, 2008. [Online]. Available: <https://www.slb.com/-/media/files/oilfield-review/high-pressure-high-temperature>.
- [2] Vietnam Petroleum Institute, "*Research and compile the Petrovietnam HPHT well completion manual*", 2024.
- [3] Schlumberger, "The defining series: HPHT wells", 2016. [Online]. Available: <https://www.slb.com/resource-library/oilfield-review/defining-series/defining-hpht>.
- [4] Bien Dong POC, "*End of project report - Bien Dong 1 drilling campaign*", 2017.
- [5] Idemitsu, "*Sao Vang and Dai Nguyet wells completion operation and lessons learnt summary*", 2020.

STUDY ON APPLIED TECHNOLOGIES TO PROPOSE SOLUTIONS FOR ENHANCING HYDRAULIC FRACTURING EFFICIENCY IN TIGHT SANDSTONE RESERVOIRS OF THE CUU LONG BASIN

Hoang Long¹, Phung Dinh Thuc², Nguyen Minh Quy¹, Trinh Viet Thang³, Pham Trung Giang¹, Bui Viet Dung¹, Le Thi Thu Huong¹

¹Vietnam Petroleum Institute (VPI)

²Vietnam Petroleum Association (VPA)

³Vietnam Oil and Gas Group (PVN)

Email: longh@vpi.pvn.vn

<https://doi.org/10.47800/PVSI.2024.06-03>

Summary

The main objective of this study is to evaluate hydraulic fracturing technologies applied in the oil fields of the Cuu Long basin to obtain lessons learned and propose solutions to improve the efficiency of hydraulic fracturing methods for the tight clastic formations therein. For that purpose, an assessment of representative hydraulic fracturing cases in oil production wells is conducted, focusing on well candidate selection, lithological composition, and reservoir rock properties for calculating geomechanical parameters and stress fields. Geomechanical models that simulate fracture development are compared to actual applications, namely in terms of effective treatment radius, required fracturing injection pressure, proppant size, injection pressure control processes, as well as flow return and well monitoring methods. The study also reviews modern and effective hydraulic fracturing technologies currently applied worldwide, particularly advanced geomechanical simulations, to accurately predict fracture networks, permeability, conductivity, the length, width, and height of fractures within productive fracturing zones. Based on the research outcome, solutions are proposed to improve the efficiency of hydraulic fracturing for the Miocene and Oligocene formations in the Cuu Long basin.

Key words: Hydraulic fracturing, fracking, geomechanical model, fracture prediction model, proppant, fracturing fluid, oil incremental, tight Oligocene formation, tight sandstone reservoir.

1. Introduction

Currently, oil and gas industry remains an irreplaceable and essential resource for global economic development, including in Vietnam. In recent years, oil and gas production in Vietnam has shown a strong declining trend as major oil fields in the Cuu Long basin - such as Bach Ho, Rong, Su Tu Den, Te Giac Trang, Rang Dong, and Hai Su Den oil field have entered the late stages of their production lifecycle. Newly discovered fields are mostly small reserves or located at edges of structures, with limited in-place reserves, or they belong to tight Oligocene formations with challenging production conditions, making development difficult and insufficient to offset declining production. Detailed production forecasts for Vietnam's oil fields through 2035

predict a rapid decline, with output expected to fall to only 10 million tons per year after 2024 and below 2 million tons per year by 2035 [1].

To counter this decline in production, oil field operators have implemented various well interventions to enhance oil recovery of the producing wells. Such interventions are especially crucial for maintaining and increasing production to meet annual targets, given the limited number of new wells being drilled, declining field output, and the need for economically viable technical solutions amidst low oil and gas prices [2]. As a result, well intervention techniques like add-perforation, acidizing, water/gas shut-off, hydraulic fracturing, and electric submersible pump installations have been applied in Cuu Long sandstone basin, particularly in tight Oligocene formations. These measures have significantly contributed to increasing production and recovery in these fields [3, 4].



Date of receipt: 8/11/2024.

Date of review and editing: 8 - 21/11/2024.

Date of approval: 21/11/2024.

In Vietnam, hydraulic fracturing applications in the Cuu Long basin have primarily focused on the Miocene and Oligocene formations. The basement formation has been applied to a limited extent due to its natural fractures, which cause severe fluid loss during fracturing and prevent achieving the necessary pressure differential for effective fracturing [2]. Therefore, implementing production enhancement methods in existing wells or newly production wells in tight sedimentary formations, such as the Oligocene, is now a pressing issue.

The initial part of this study focuses on analyzing and assessing the current methods used for hydraulic fracturing, identifying technical uncertainties in well selection and design. Due to limited assessments of the geomechanical properties in the selected well area and various risks in evaluation, the well selection process is analyzed based on geological characteristics, reservoir permeability, appropriate permeability ranges, lithology, geomechanical parameters, stress fields, and geomechanical modeling for hydraulic fracturing to predict fracture aperture, fracture volume, fracturing fluid, proppant diameter, proppant volume, fracturing pressure, and closure pressure. Technical controls are applied during pre-fracturing testing, fluid injection, deep placement of proppants within fractures, and closure pressure control to stabilize proppants in fractures, creating and maintaining new fracture channels that connect the well with the reservoir in targeted zones.

The study assesses post-fracturing effectiveness by monitoring fluid flow rates, production dynamics, and the process of returning the hydraulically fractured well to production. It analyzes typical wells for specific geological formations and technological stages, focusing on simulating fracture network patterns and hydraulic

fracturing parameters for wells that have achieved significant oil production increases in the Cuu Long basin. Additionally, the study evaluates advanced and effective fracturing technologies used globally, particularly advanced geomechanical simulations for hydraulic fracturing, to accurately predict fracture networks, fracture permeability and conductivity, as well as fracture length, width, and height in targeted fracturing intervals. Based on these research findings, solutions are proposed to modernize and improve hydraulic fracturing efficiency for the Miocene and Oligocene formations in the Cuu Long basin.

2. Overview of hydraulic fracturing in the Cuu Long's sandstone

Curently, there are 26 oil fields in the entire Cuu Long basin, of which 20 fields are in production and the remaining 6 planned for development in the near future. Production is mainly concentrated in the Cuu Long basin from several large oil fields, such as Bach Ho, Rong, Rang Dong, Su Tu Den, which have been producing for around 20 years. The remaining producing fields are smaller in reserves. Hydraulic fracturing has been experimentally applied to various geological formations, including the basement, Lower Oligocene, Upper Oligocene, and Lower Miocene - particularly in areas with very poor reservoir permeability, wells with high contamination levels, and wells where production cannot be improved by conventional production methods or acid treatments. Hydraulic fracturing for sedimentary reservoirs in the Cuu Long basin has been extensively implemented in fields managed by VSP, such as Bach Ho, Rong, Ca Tam, and Kinh Ngu Trang [5], with the majority of projects concentrated in the first two listed (Table 1).

Table 1. Hydraulic fracturing projects applied in Cuu Long sandstone reservoirs

No.	Oil fields	Project number	Reservoir
1	Bach Ho	118 projects	Miocene, Upper Oligocene, Lower Oligocene
2	Ca Tam	6 projects (102, 104, 2X, 108)	Upper Oligocene, Lower Oligocene
3	Gau Trang	GTC1-1P	Miocene
4	Rong	21 projects (RP2, RP3, RC7, RC6, RC5, RC9)	Miocene, Upper Oligocene, Lower Oligocene
5	Tho Trang	ThTC1-2X	Miocene
6	Hai Su Den	HSD-4X	Oligocene
7	Te Giac Trang	TGT-15X	Oligocene
8	Lac Da Vang	LDV-2X, LDV-4X	Oligocene
9	Su Tu Nau	SNS-1P	Oligocene
10	Kinh Ngu Trang	KNT-1X	Oligocene
11	Block 01 & 02	RBA 14XP, Jade 4X, Emerald 2X	Miocene, Oligocene

Hydraulic fracturing in the Upper and Lower Oligocene accounts for nearly 77% of treatments, whereas in the Miocene, it comprises only about 21%. Fracturing is rarely performed in the basement formation, only 2%, due to geological and production characteristics that make this method unsuitable. The basement formation is rarely targeted because of its low effectiveness, mainly due to large natural fractures that lead to severe fluid loss during fracturing and an inability to create sufficient pressure differentials for effective fracturing.

The success of these methods depends on the technology used, implementation approach, reservoir properties, well characteristics, geological targets, and the specific characteristics of each oil and gas field. Hydraulic fracturing for oil fields of Cuu Long basin faces numerous challenges due to offshore production conditions and extreme operating environments. These include the significant depths of tight Oligocene formations (3,000 - 4,300 m), high temperatures (120 - 150°C), high pressures (250 - 400 bar), high clay content in lithology, poor permeability and connectivity, and high heterogeneity. For tight Oligocene targets, characteristics such as high abnormal reservoir pressure and low permeability (1 - 10 mD) are typical. Criteria for assessing hydraulic fracturing applications for this target are presented in Table 2.

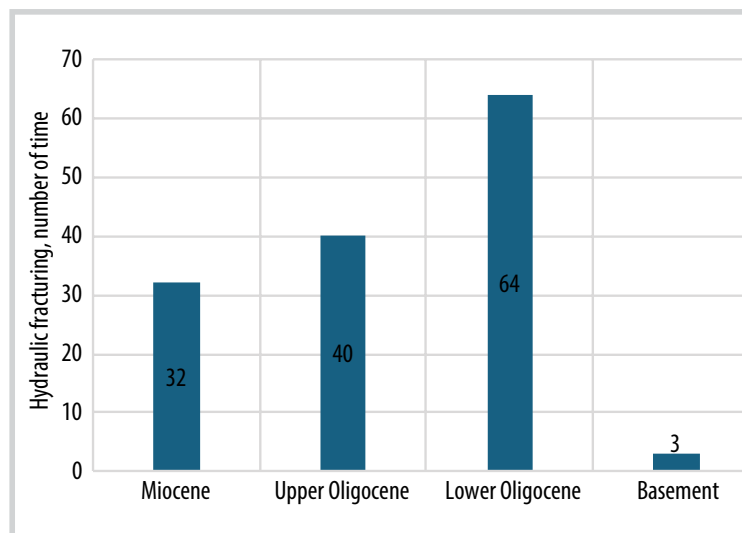


Figure 1. Statistics of hydraulic fracturing projects for reservoirs of Cuu Long basin.

According to statistics on hydraulic fracturing projects in Vietnam, the effectiveness of hydraulic fracturing projects evaluated for each target shows that the Miocene formation has a success rate of approximately 69%, the remaining 31% being less effective. For the Oligocene formation, the application effectiveness is better, with a success rate of around 76%.

3. Simulation studies for hydraulic fracturing forecasting and application effectiveness in the Cuu Long basin

The selection and application of hydraulic fracturing methods on production wells targeting tight Oligocene formations in the Cuu Long basin are significantly affected by substantial technical and economic risks due to various factors. To analyze the reasons behind the successes and failures of hydraulic fracturing projects, it is essential to fully evaluate the three main stages of the fracturing process under the production conditions of wells in the Cuu Long basin, as follows:

- Well candidate selection: This involves analyzing geological characteristics, reservoir engineering parameters, production rates, near-wellbore permeability, geomechanical stress fields, and historical production data. Additionally, well structures and technical issues, such as casing, cement quality, and downhole equipment, are considered to assess wells for treatment.
- Design of the hydraulic fracturing process and well preparation: This stage includes assessing the geomechanical model, reservoir and rock properties to conduct in-depth

Table 2. Criteria for Oligocene reservoirs

No.	Criterion	Commentary
1	Geographical location	Regional proximity to offshore Vietnam
2	Formation pressure, anomaly coefficient	Over 300 atm, anomaly coefficient 1.1 - 1.7
3	Reservoir	Oligocene, Miocene (second priority)
4	Composition of rocks	Sandstones, clays, siltstones
5	Depth of reservoirs	Over 3,000 m
6	Permeability	0.5 - 10 mD
7	Formation thickness	From 50 m
8	Porosity	Up to 20%

analyses for selecting proppant volume and size, additives, and pressure parameters based on stress fields. It also involves designing fracturing options/ technologies, pump rates, pressure control, and injection fluid volume, as well as preparing wellbore equipment for hydraulic fracturing operations.

- Implementation of hydraulic fracturing in stages: This phase includes performing a minifrac test, injecting fracturing fluid, and pumping proppant to stabilize fractures and create new channels that connect the well with the reservoir. After fracturing, well effectiveness is assessed by an evaluation program that monitors fluid flow rates, production dynamic parameters, and observes the process of putting the fractured well back into production.

Several wells have been successfully hydraulically fractured thanks to the correct selection of wells and the accurate assessment of geomechanical parameters, lithology, reservoir permeability, and well productivity. This process enabled the construction of a fracture simulation model to determine the fracture width, volumetric distribution in various directions within the reservoir, permeability, and fracture conductivity. As a result, the correct proppant size and amount were selected, along with the appropriate volume and properties of the fracturing fluid. The pumping pressure and closure pressure were accurately calculated to optimize fracture creation and maintain long-term stability of the proppants as well as the conductivity of the oil channel from the reservoir to the well. The paper presents two typical hydraulic fracturing projects successfully applied to the tight Oligocene formation of the Cuu Long basin.

3.1. Case study 1: Well BO-01

The BO-01 well, located in the Oligocene formation, has a production interval from 3,790 - 3,940 m, with an effective reservoir thickness of approximately 36 m. The average porosity is around 14%, and the average permeability is approximately 1.3 mD. The lithology composition, represented by a QFR diagram (quartz-feldspar-rock fragment), shows that quartz comprises about 55 - 65%, typically the dominant component that helps achieve a low Young's modulus while maintaining high material strength. Feldspar makes up around 25 - 30%, contributing to the overall hardness but keeping the

Young's modulus at a low to medium level. Rock fragments account for approximately 10 - 15%, contributing minimally to strength but helping maintain a low Poisson's ratio, which aids in controlling deformation and elasticity.

The well has been in operation since 2014 with an initial production of around 40 sm³/day, but it quickly dropped to 10 sm³/day within about 3 years of operation. The well was assessed to have potential for increased production due to the significant remaining oil reserves in the area and the very low water cut in the well or the surrounding area.

Based on the criteria for selecting wells for hydraulic fracturing, well BO-01 was chosen for in-depth studies on geomechanics, lithology, and the development of a hydraulic fracturing simulation model to predict fracture aperture, proppant size, proppant volume, as well as fracturing pressure and closure pressure. The design included pre-fracturing test, pumping process for hydraulic fracturing, injection of proppants deep into the fractures, and controlling the closure pressure to stabilize the proppants in the fractures, creating and maintaining new fracture networks connecting the well to the reservoir and the affected area of the well. An evaluation program was developed to assess the effectiveness of the fracturing treatment, monitor fluid production rates, production dynamics, and oversee the process of bringing the hydraulically fractured well back into production.

Geomechanical parameters such as stress field, Young's modulus, Poisson's ratio, and borehole logs were incorporated into the hydraulic fracturing simulation model for analysis. The results of the comparison between the simulated and

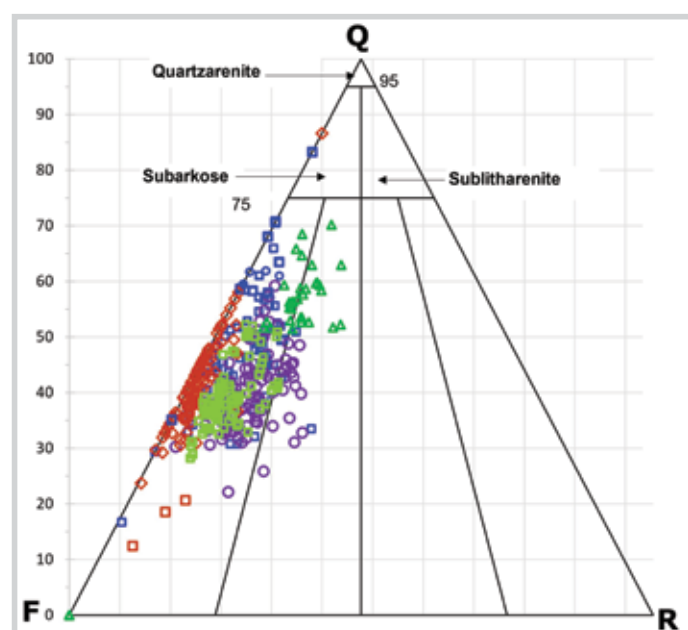


Figure 2. Lithological composition characteristics of the Oligocene formation.

actual hydraulic fracturing outcomes are presented in the figure below. The results show that the differences between the design and actual results are not significant, particularly with respect to fracture volume, where the actual fracture length, height, and width are all larger than those in the initial simulated design (Table 3).

The results show that the effectiveness of the pumping process is better than expected. 131 tons of proppant were pumped into the created fractures, the pump pressure was raised to 540 atm, and the pumping time lasted for 3 hours.

The production after hydraulic fracturing in well BO-01 shows that it increased from 10 sm³/day to over 80 sm³/day, then decreased and stabilized at a production rate above 20 sm³/day for the next 2 years of operation. The cumulative oil production, as shown in Figure 5, demonstrates the effectiveness of the hydraulic fracturing method for well BO-01.

3.2. Case study 2: Well BO-02

Hydraulic fracturing was performed in the Oligocene layer at a depth range of 3,880 - 4,040 m, with an effective reservoir thickness of about 32 m and permeability ranging from 0.5 to 1.2 mD. The production behavior of surrounding wells in the area showed high production rates initially (>100 sm³/day), but it declined rapidly after about 1 - 2 years of operation. During the later stages of decline, the wells sustained low but stable production rates of around 10 - 15 sm³/day over 5 - 7 years. Well BO-02 was also designed and subjected to pumping according to the prescribed design procedure. The fractures were evaluated based on actual data and re-simulated, as shown in Figure 6.

Table 3. Comparison of the design and actual results of hydraulic fracturing application

Parameters	Simulation design	Actual implementation
Propped fracture length (m)	56.8	62.8
Propped fracture height (m)	88.5	110.7
Average propped fracture width (cm)	0.55	0.86
Fracture conductivity (mD.m)	525.9	454.4
Fcd	3.1	9
Proppant volume (tons)	136.5	131.1

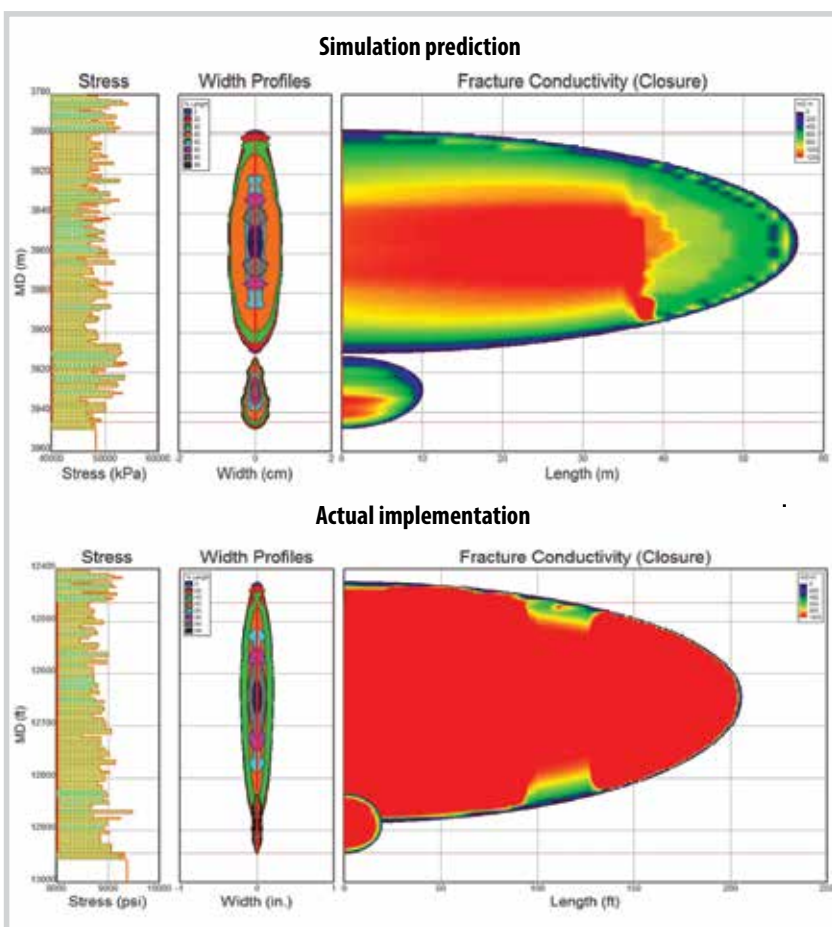


Figure 3. Evaluation of the accuracy of the hydraulic fracturing model and practical application.

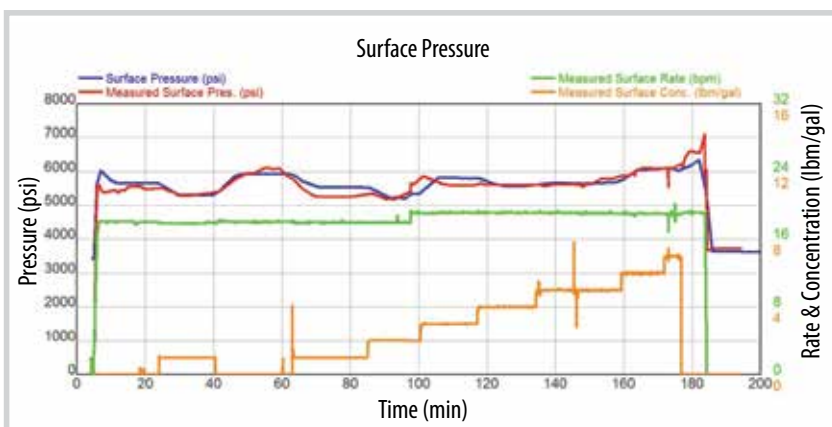


Figure 4. Graph of pressure monitoring during the hydraulic fracturing pumping process.



Figure 5. Production of well BO-01 before and after hydraulic fracturing.

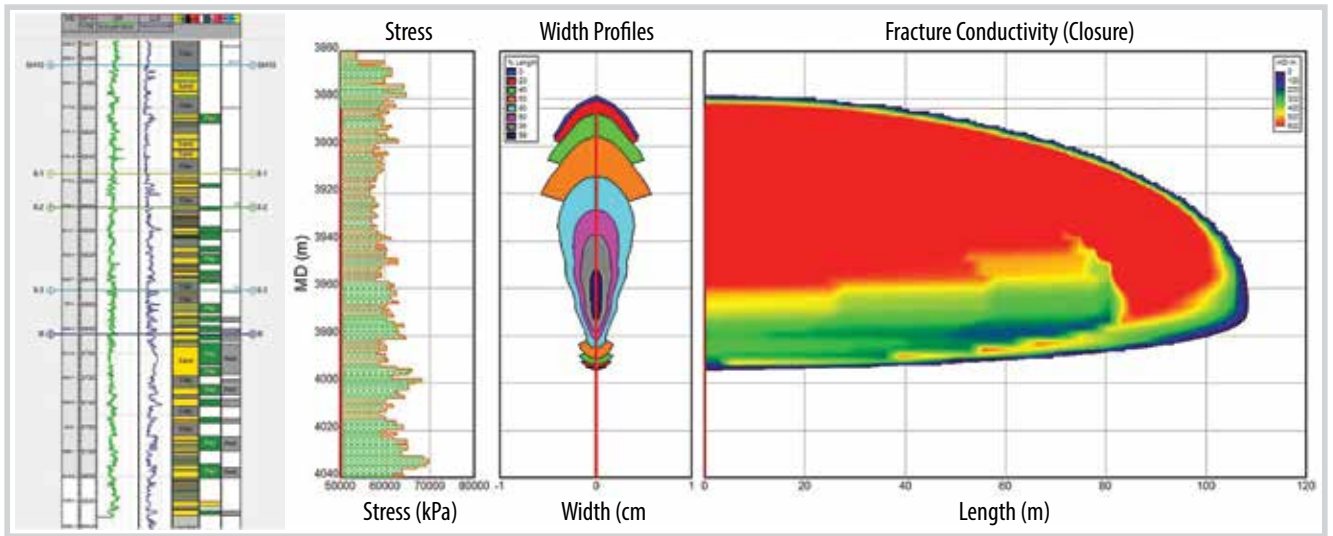


Figure 6. Simulation of the actual fractures during the hydraulic fracturing implementation.

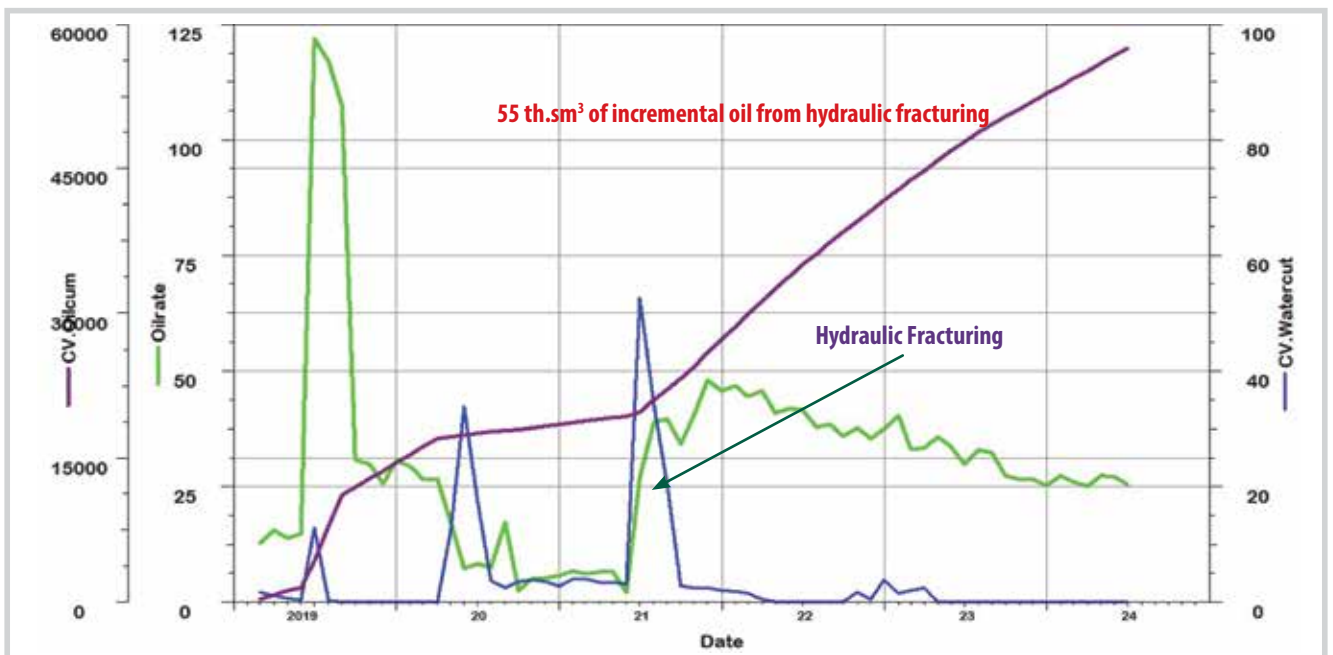


Figure 7. Flow rate and increased oil production after hydraulic fracturing in the tight Oligocene formation.

The production rate increased from 5 sm³/day to over 45 sm³/day, then gradually declined and maintained an average of over 25 sm³/day for nearly 3 years of operation. The total oil increase from hydraulic fracturing to the present time has reached 55 thousand sm³. The hydraulic fracturing project has been highly successful both technically and economically, contributing to increased production across the entire field.

4. Evaluation of technologies and geomechanical models that can be appropriately applied to the Cuu Long basin

The typical hydraulic fracturing cases above have demonstrated the effectiveness of applying this process to oil wells in the clastic reservoirs of the Cuu Long basin. Application procedures must be followed in selecting wells with suitable lithology for fracturing, ensuring that the remaining oil volume in the reservoir is sufficient to sustain production through the created fractures. The injection process must control fracture pressure according to design and maintain the appropriate injection rate. The proppant concentration must be injected with precise volume and timing to ensure fracture stability as closure pressure is reduced, as shown in cases BO-01 and BO-02. Based on the applied research steps and hydraulic fracturing technology in Vietnam, as well as the evaluation results from over 150 hydraulic fracturing projects implemented for the Miocene and Oligocene targets in the Cuu Long basin, several causes for success or failure can be summarized as follows:

- Failure causes: One possible cause of failure could be the inaccurate geological assessments, particularly the geomechanical evaluations of the selected wells. The reservoir structure, stress field of the formation according to the well depth, may not have been studied in detail or may not match the actual conditions of the selected well, leading to incorrect calculations of the required pumping pressure and the fracturing fluid systems used to create effective fractures. Therefore, the geomechanical model plays a crucial role in providing parameters to predict the length, width, height, and permeability of the created fractures. This allows for detailed calculations on the effective area of hydraulic fracturing, proppant size, fracture fluid volume, and proppant-carrying fluid volume to be pumped, as well as the decision on the appropriate hydraulic fracturing technology for the well [9].

- Another cause of failure may arise from non-optimal evaluations and application procedures, leading

to several issues affecting the well being treated, such as the inability to bring the packer to the surface due to deformation of the production tubing caused by improper fracturing pressure and the influence of the stress field in the formation.

- The effectiveness of hydraulic fracturing technology could also be influenced by situations where treatments were applied in wells with multiple product layers but without adequate evaluations of the well structure, equipment, or appropriate technology. In such cases, when fracturing was performed in the lower perforated interval, communication with the upper perforated interval occurred, causing fluids to migrate upward through the casing outside the production tubing due to poor quality cementing, leading to treatment failure.

- One of the causes of failure in well treatment is the selection of unsuitable proppant fluids or the non-optimized fracturing pumping process. The pumping process did not manage to inject the full calculated volume of proppant-carrying fluid into the fractures, resulting in a large volume of proppant remaining in the production tubing. This required implementing multiple solutions after the treatment to release the packer in the well, such as using coiled tubing, pulling the tubing out of place, or perforating the production tubing to flush it, leading to a failed treatment. Additionally, in some wells, the treatment was carried out without pumping fracturing fluid to create fractures, and instead, proppant-carrying fluid was directly pumped into the well. In this fracturing method, the proppant-carrying fluid serves both to open and develop the fractures and to stabilize them, preventing the fractures from closing. However, this method carries significant risks, such as proppant getting stuck in the pumping column due to failure to pump the full amount of proppant-carrying fluid as designed, forcing the pump to stop when the pressure suddenly rises above the limit (screen out), especially in wells with a high loss coefficient, and it may not be effective. Therefore, nowadays, most hydraulic fracturing operations are carried out in a fully sequential manner: first, high-pressure fracturing fluid is pumped to create fractures, then a continued injection of fluid containing proppant and proppant-carrying fluid follows, followed by the injection of chemicals and additives to push the proppant deep into the formation through the fractures and maintain fracture stability after the treatment.

Based on the research output and the adoption of advanced technologies worldwide, and by comparing with the current hydraulic fracturing technology applied in Vietnam, the following technologies and geomechanical modeling approaches can be appropriate to the tight sandstone formations of the Cuu Long basin:

- Hydraulic fracturing models: With the reservoir conditions of high pressure and temperature, low permeability (0.01 - 100 mD), and multiple sandstone layers in the reservoir, geomechanical models combined with fluid flow simulations are suitable.

- + P3D model (Pseudo-3D) [6]: It is suitable for simulating the shape and size of fractures in reservoirs with low permeability. The model accounts for factors that limit the vertical and horizontal extent of fractures, helping predict the fracture propagation in formations with permeability ranging from low to medium.

- + Planar 3D model: It can simulate the development of fractures in a 3D space, both horizontally and vertically. This model is useful when dealing with reservoirs with multiple sandstone layers, where fracture propagation needs to be precisely controlled to ensure efficient hydrocarbon extraction from different layers.

- + Coupled geomechanical-fluid flow models with DFN (discrete fracture network) simulation [7]: This model helps calculate the interaction between rock and fracturing fluids, which is crucial for dealing with reservoirs that have high temperature and low permeability. It allows the optimization of fracture propagation while maintaining pressure stability and fluid flow in the reservoir. The DFN model simulates systems of both natural and induced fractures, aiding in the optimization of oil and gas flow through fracture networks in multi-layered reservoirs.

- Fracturing fluids and proppants suitable for high temperatures in the Cuu Long basin:

- + High-temperature stable fracturing fluids [8]: Fracturing fluids such as polymer-based gel systems or cross-linked gel can be used. Cross-linked gel helps stabilize the structure of the fluid and maintain the necessary viscosity at high temperatures, thereby keeping the proppant in the fractures for longer periods.

- + High-temperature, high-pressure proppants: In high-temperature environments like the Cuu Long basin, it is necessary to use specialized proppants with high thermal resistance, such as ceramic proppants or bauxite proppants with advanced plastic coating technology.

These proppants offer excellent strength and thermal resistance, ensuring they do not break under high-temperature and high-pressure conditions.

- Effective multi-stage fracturing technology for multi-layered sandstone reservoirs: The method divides the well into multiple segments and performs hydraulic fracturing in each segment, aiming to maximize the contact area with the reservoir and extract oil and gas from different layers.

- Technology for high flow rate and high-pressure control: Given the high-temperature and high-pressure conditions, a high-flow high-pressure control system is necessary, such as sliding sleeve or plug-and-perf technologies. These systems help regulate and optimize the hydraulic fracturing process for each segment of the well while maintaining the required flow rate and pressure for each wellbore section.

5. Conclusions

The hydraulic fracturing process in sandstone oil fields requires strict adherence to standards, from well selection and design to construction and long-term maintenance. Lessons learned from real-world failures show that each stage can significantly impact the overall effectiveness of a hydraulic fracturing project. By applying the solutions derived from these experiences, it is possible to optimize the fracturing process and increase extraction efficiency.

A thorough assessment of geological characteristics, lithological composition, geomechanical parameters, rock stress fields, reservoir permeability, and remaining in-place oil reserves within the well's influence radius is crucial to select the appropriate well, build an accurate fracture simulation model, and implement the fracturing design using the optimal pumping process.

For geological targets with poor and tight properties currently being exploited in the Cuu Long basin, such as the Oligocene formations of the Bach Ho, Rong, and Ca Tam fields, or potential targets like Te Giac Trang, Kinh Ngu Trang, and Lac Da Vang, it is essential to consider the application of new technologies. These include geomechanical modeling combined with flow simulation for fracture modeling, using fracturing fluids and proppants with optimal size and properties suited for the high temperatures of the Cuu Long basin. Effective technologies such as multi-stage fracturing for multi-layered sandstone reservoirs should be applied to achieve

significant production increases without technical risks during the fracturing process.

Acknowledgments

The authors would like to express their sincere gratitude to the Vietnam Petroleum Institute (VPI), the Vietnam Oil and Gas Group, the University of Mining and Geology, and the Vietsovpetro Joint Venture for their professional support, resources, and funding in carrying out this research. This paper is part of the results from the Contract No. 8074/HD-DKVN.

References

[1] Hoàng Long, "Nghiên cứu lựa chọn các giải pháp công nghệ và thực nghiệm đánh giá các tác nhân nâng cao hệ số thu hồi dầu cho đối tượng trầm tích lục nguyên của các mỏ dầu thuộc bể Cửu Long", (Mã số ĐTĐLCN.26/19), Viện Dầu khí Việt Nam, 2021.

[2] Phùng Đình Thực, Dương Danh Lam, Lê Bá Tuấn, và Nguyễn Văn Cảnh, *Công nghệ và kỹ thuật khai thác dầu khí*. Nhà xuất bản Giáo dục, 1999.

[3] Từ Thành Nghĩa, Nguyễn Thúc Kháng, Lê Việt Hải, Dương Danh Lam, Nguyễn Quốc Dũng, Nguyễn Văn

Trung, và Phan Đức Tuấn, *Công nghệ xử lý vùng cận đáy giếng các mỏ dầu khí ở thềm lục địa Nam Việt Nam*. Nhà xuất bản Đại học Quốc gia TP. Hồ Chí Minh, 2016.

[4] Vietsovpetro, "Xử lý vùng cận đáy giếng bằng công nghệ bơm các thành phần không có tính axit để tạo thành hỗn hợp axit tại đáy giếng", 2012.

[5] Vietsovpetro, "Sơ đồ công nghệ điều chỉnh mới khai thác và xây dựng mỏ Bạch Hổ", 2003, 2008, 2012, 2018.

[6] T.K. Perkins and L.R. Kern, "Widths of hydraulic fractures", *Journal of Petroleum Technology*, Volume 13, Issue 9, pp. 937 - 949, 1961. DOI: 10.2118/89-PA.

[7] Bin Chen, Beatriz Ramos Barboza, Yanan Sun, Jie Bai, Hywel R Thomas, Martin Dutko, Mark Cottrell, and Chenfeng Li, "A review of hydraulic fracturing simulation", *Archives of Computational Methods in Engineering*, Volume 29, Issue 5, pp. 1 - 58, 2022. DOI: 10.1007/s11831-021-09653-z.

[8] D. Mader, "Hydraulic proppant fracturing and gravel packing", *Developments in Petroleum Science*, Volume 26, 1989.

EVALUATION OF THE APPLICABILITY OF SUBSEA WELLHEADS RUNNING BY JACK UP RIG FOR OIL AND GAS EXPLORATION PROJECTS IN SHALLOW WATER, OFFSHORE VIETNAM

Nguyen Trong Tai¹, Trieu Hung Truong², Nguyen The Vinh², Le Quang Duyen², Nguyen Van Thinh²

¹Zarubezhneft EP Vietnam

²Hanoi University of Mining and Geology

Email: tai.nguyen@vn.nestro.org

<https://doi.org/10.47800/PVSI.2024.06-04>

Summary

An overview of the oil and gas production in Vietnam reveals that certain major oil and gas projects, which account for large-scale operations and dominate the oil and gas production in the continental shelf of Vietnam, are entering a declining production phase. This affects not only the efficiency of individual projects but also the national energy security. Consequently, the research and application of new technical solutions to supplement and maintain oil and gas production become the most critical tasks in the current phase. However, based on the assessment of oil and gas potential in the basins on the continental shelf of Vietnam, few major offshore oil and gas prospects can be developed using conventional methods to achieve high economic efficiency. Therefore, two development concepts with the highest feasibility, both economically and technically, are: the development of marginal fields in shallow water conditions and the execution of exploration/production activities in new prospects at existing production projects by drilling additional infill wells and connecting them to the central processing platform (CPP).

The article evaluates the potential and proposes a solution using subsea wellheads & X-mas Tree, operated by jack-up rigs, to develop marginal oil and gas fields in shallow water conditions and existing oil and gas fields with potential prospects located far from the CPP. This approach aims to reduce operational costs and enhance the overall efficiency of the project.

Key words: Subsea wellheads, shallow water, X-mas tree, OPEX, CAPEX.

1. Introduction

The concept of "shallow water" in oil and gas exploration and production is defined based on the nature of work in each specific sector. For the scope of this article, shallow water is defined by the depth at which drilling and completion activities can be conducted using a jack-up rig with a maximum water depth of approximately 115 m in oil and gas fields. This depth is lower than the actual working specifications of jack-up rigs due to operational limitations related to the leg penetration during the rig positioning. In particular, the leg penetration at basins on Vietnam's continental shelf can vary between 3 m and 23 m, depending on the seabed's geological characteristics in each area.

Based on this concept, current producing oil and gas fields and future potential development fields in shallow water are primarily distributed across the Cuu Long basin, Nam Con Son basin, Malay - Tho Chu basin and Song Hong basin. The distribution of these oil and gas fields is shown in Figure 1.

In these basins, oil and gas fields have been developed and continuously produced over long periods using conventional technical methods. The equipment structure consists of a central processing platform (CPP) and fixed production platforms without processing systems, which are connected to the CPP through an underwater pipeline network. The production wells are drilled directionally/horizontally from the fixed platforms to reach prospects located at a maximum horizontal displacement of approximately 4.5 km.

Currently, the potential for large oil and gas fields that



Date of receipt: 13/11/2024.

Date of review and editing: 13 - 21/11/2024.

Date of approval: 21/11/2024.

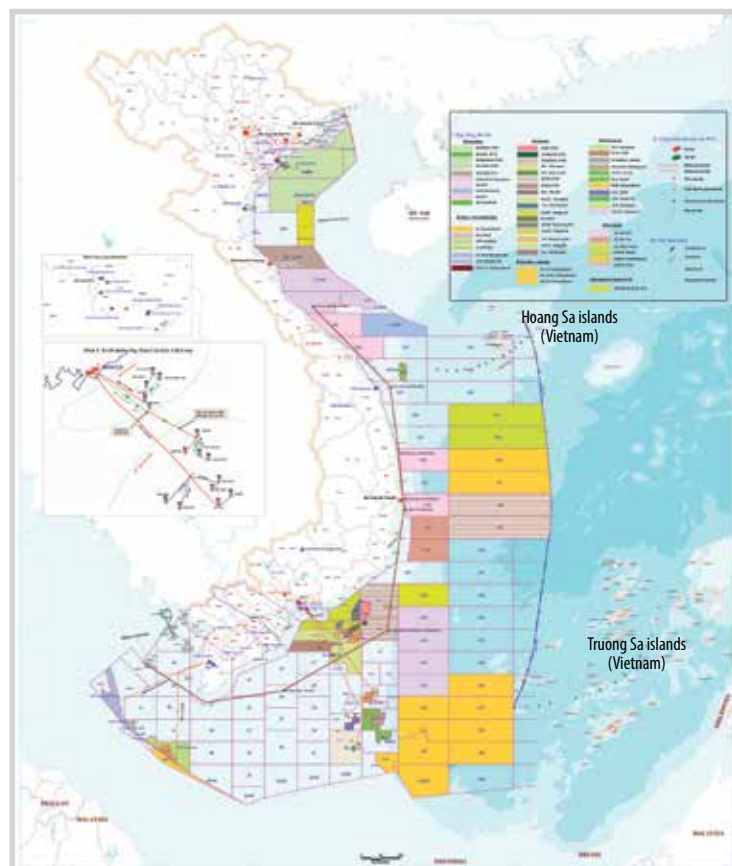


Figure 1. The distribution of oil and gas activities in Vietnam.

could apply the conventional methodology for development phase on the Vietnam continental shelf has diminished. The in-place and recoverable reserves are not large, and high development costs, including drilling and production facilities, often result in project net present values (NPV) falling below expectations. Therefore, to increase oil and gas production, alternative approaches are necessary, focusing on the following aspects:

- Enhance exploration/production activities in ongoing projects by increasing the number of infill wells and constructing pipeline systems to connect to the CPP.
- Develop marginal fields using new technologies suited to the natural and geological conditions of the area to reduce capital expenditure (CAPEX).

In evaluating technological approaches, the authors identified that one promising solution for reducing drilling and CAPEX costs is the use of subsea wellheads and X-mas Tree systems installed with jack-up rigs. This method has demonstrated high efficiency in numerous global projects, yet it remains unimplemented in Vietnam.

2. Assess the development methodologies currently applied for oil and gas fields in Vietnam

Generally, development plans for oil and gas projects are established based on several key factors, including reservoir

evaluation and feasibility, technology and equipment, the field’s natural environment, offshore facility capacity, and innovative drilling and production techniques.

In Vietnam, most major oil and gas discoveries have been developed using conventional methods, including the construction of central processing platforms, fixed platforms, floating production storage and offloading (FPSO) units, and subsea pipeline systems for transporting oil and gas to shore. However, few oil and gas fields can efficiently apply this methodology. Meanwhile, the demand for oil and gas production continues to grow, highlighting the importance of developing marginal fields and exploring new prospects within ongoing production projects.

2.1. Exploration and development of new prospects in ongoing production projects

For production projects experiencing declining production rates, technical approaches are being considered to maintain and sustain production, including:

- a. Drilling additional infill/deviated wells from the fixed platform or CPP to reach the prospects within a drillable horizontal range (currently achievable with conventional technology at approximately 4,500 m).
- b. With prospects located far apart, exploration/appraisal drilling of potential prospects beyond the reach of feasible deviated drilling is necessary. This involves installing lightweight wellhead platforms (with only the wellhead and X-mas Tree systems and connecting to the CPP via subsea pipelines).

It can be observed that this technical methodology is applied in most oil and gas projects in Vietnam. However, they also have limitations in terms of both technical factors and project efficiency, including the following:

- Some of CPPs or platforms have already reached the maximum number of wells per template slot; therefore, to drill a new development infill well, one of the existing wells must be abandoned and a sidetrack drilled to the new prospect. This will reduce the production rate along with additional drilling costs.

- The infill wells to be drilled from the platform will be designed with high inclination/complex well profile leading to prolonged operations time and higher risk of stuck pipe which may necessitate abandoning the well or drilling a new bore, thereby increasing project costs.

- The reservoir pressure is depleted after a production duration, resulting in reduced fracture gradient pressure while the pore pressure in the cap rock remains at its original values. This phenomenon leads to the risks of blowouts and fluid loss, significantly affecting the design and drilling operations

- The fixed costs for constructing new wellhead platforms (CAPEX) for new development wells are substantial, leading to a decreased NPV for the project (which will be specifically determined in the subsequent section).

- The preparation time for the installation of fixed platforms is lengthy, resulting in delayed first gas/oil production.

2.2. Development of marginal fields in shallow water areas

- For marginal fields, factors affecting project feasibility include: recoverable reserves, geological conditions, natural conditions at the field site and drilling and facility costs. Fields with varying conditions require different development approaches, resulting in varied development costs. Thus, once recoverable reserves are established, CAPEX and OPEX costs become decisive factors. If a conventional development methodology is applied to marginal fields, the following limitations are observed: Independent development for marginal fields: In cases where prospects in the field are located far apart and beyond the feasible radius for deviated drilling, the concept of development involving the construction of CPP platforms and/or lightweight platforms is considered. However, that development concept incurs high costs, making in the project inefficient.

- Development of marginal fields based on adjacent field facilities: In this scenario, the lightweight platforms are selected for installation on the main reservoirs location. Oil and gas shall be transported to the adjacent field's CPP via a subsea pipeline system. However, for fields with low recoverable reserves, the cost of constructing lightweight platforms may reduce overall project efficiency.

3. Application of subsea wellhead system for shallow water areas

3.1. Geological conditions

At this stage, the newest technology for sealing devices used to connect the subsea suspension system to surface equipment has not yet met the requirements for high - temperature and high - pressure (HTHP) conditions. Therefore, the subsea wellhead system for shallow water fields is only applicable to formations with the following conditions:

- Wellbore pressure $P < 10,000$ psi,
- Wellbore temperature $T \leq 150^{\circ}\text{C}$.

3.2. Field environment conditions

As mentioned above, oil and gas fields in shallow water are developed using a jack-up rig solution under the following conditions:

- Water depth of approximately 115 m, which may vary based on the technical specifications of the rig and the penetration depth of the rig legs at the well location.
- Well location within a 10 km radius, which depends on the estimated cost of the subsea pipeline system from the well location to the central processing platform, or CPP.

3.3. Structure of exploration/development wells

Depending on geological, pressure, and temperature conditions, the well structure is designed accordingly. However, the most common casing structure for exploration/development wells in shallow water basins in Vietnam is 30" x 20" x 13 $\frac{3}{8}$ " x 9 $\frac{5}{8}$ " x 7".

Additionally, the well structure may omit or add casing sizes. Following the design principles of the subsea wellhead system for shallow waters, the well structure only affects the configuration and scale of the system, without impacting functionality. Therefore, this document outlines the simplest structure with the applied casing schematics of 30" x 16" x 9 $\frac{5}{8}$ " x 7".

3.4. Use of subsea wellhead and X-mas Tree systems

During the exploration phase, to reduce drilling and development costs, it is recommended to consider converting the exploration well into a development well by using the MLS (mudline suspension system) after completing the exploration stage.

In general, the design of subsea wellhead and X-mas Tree should be based on the specific well schematic and well design. Therefore, in this paper, for economic evaluation purpose, the concept design and installation

of the MLS are based on the casing scheme of 30" x 16" x 9 5/8" x 7", as outlined in the running procedures and illustrated in Figure 2.

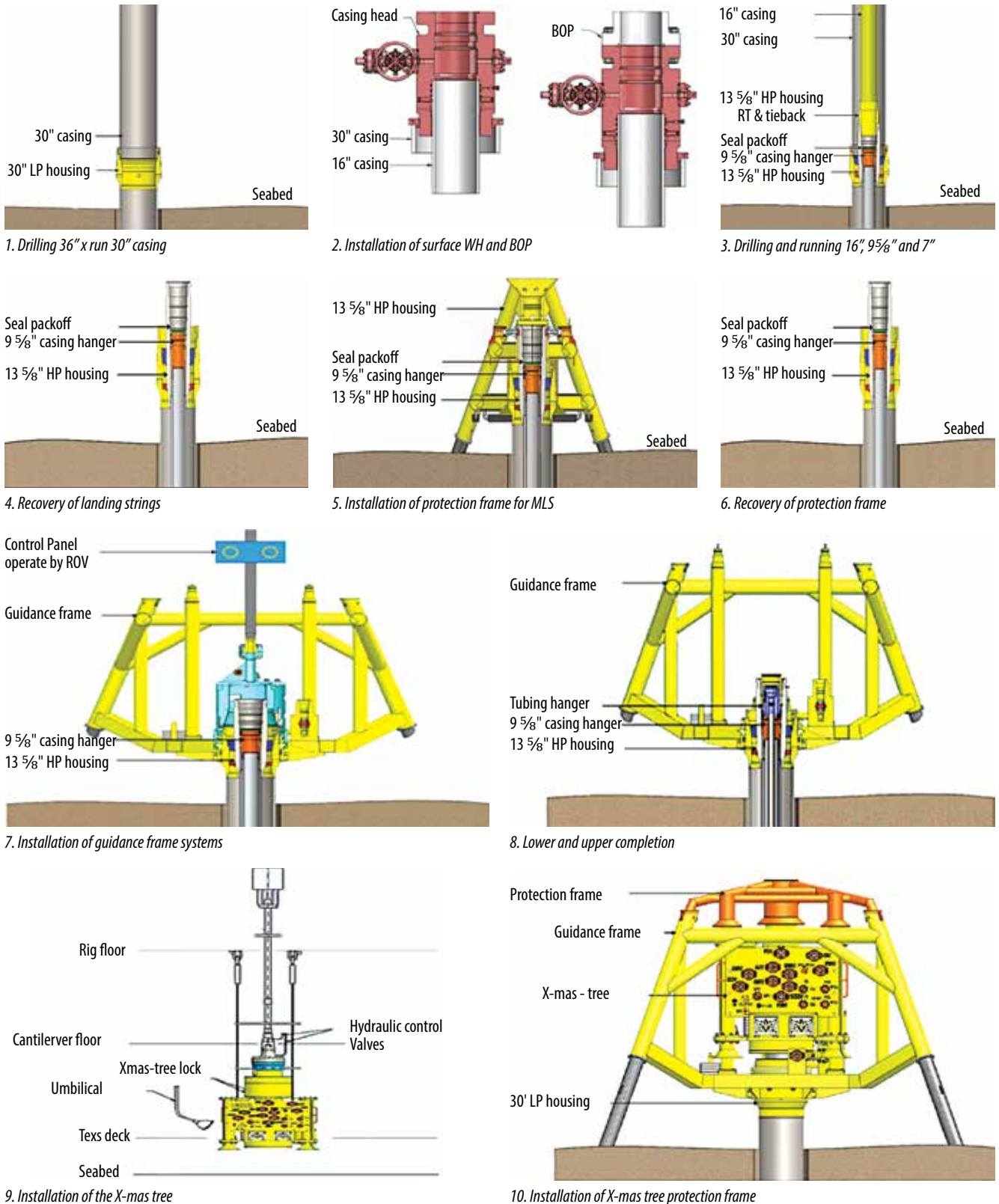


Figure 2. Running procedures of subsea wellhead and MLS systems.

3.5. Structure of subsea facilities utilizing subsea wellhead and X-mas Tree systems

Essentially, the structure of subsea facilities utilizing subsea wellhead and X-mas Tree systems in shallow water conditions is similar to that in deep water. The production wells are positioned based on the evaluation results of prospects. Three main types of structures are designed and constructed, including (Figures 3 - 5).

Applicable for prospects with small reserves, a single well wellhead and X-mas Tree shall be connected to the central processing platform or a lightweight platform via a subsea pipeline system (Figures 3).

In cases where prospect have big reverser or prospects are located relatively close to each other, drilling can be carried out using a subsea template or an independent drilling location through the cantilever system of a jack-up rig (Figures 4).

Applicable to large prospects or those located close to each other, the wells are drilled from various locations and connected to a flow manifold, which is then linked to the central processing platform (Figures 5).

4. Assessment of technical and economic efficiency

The subsea wellhead system used in shallow water has been designed and deployed with jack-up rigs in several major field areas worldwide, such as the Gulf of Mexico, the North Sea, and the Black Sea. These projects have demonstrated that the system meets both technical and economic efficiency requirements. However, it has not yet been applied in Vietnam, underscoring the need to evaluate the feasibility of using a subsea wellhead system for exploration and development. This

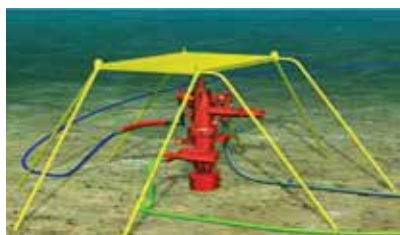


Figure 3. Single production well [1].

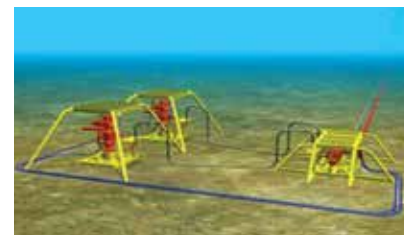


Figure 4. Structure of the well cluster [1].

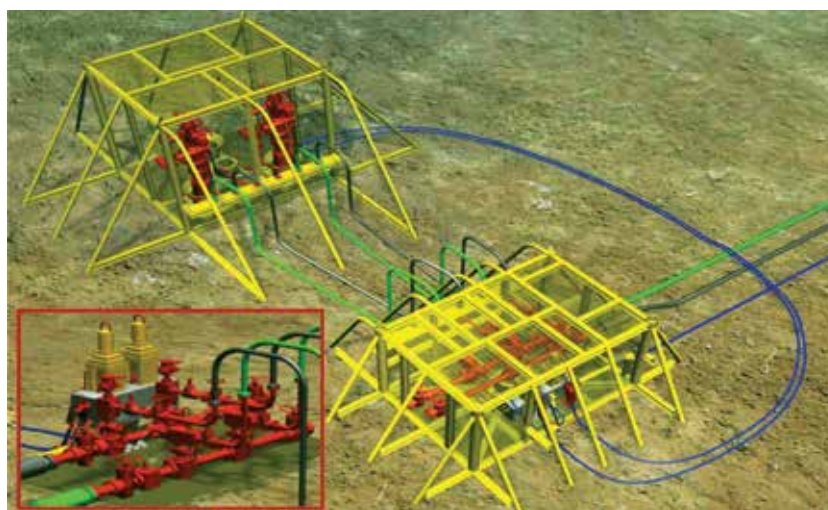


Figure 5. Structure of the well series [1].

approach aims to supplement production in declining fields or to develop marginal fields in shallow water conditions.

Considering the current circumstances of Vietnam's oil and gas industry, the author presents an option for a development plan for oil and gas fields in shallow water areas, focusing on technical and economic efficiency as follows:

4.1. Technical efficiency

- Shortened time to first oil/gas [2]

In principle, once a field development plan (FDP) is approved by the authorities, the project will proceed through the stages of preparing bidding documents, signing contracts, manufacturing, handover, and equipment installation.

With projects using the conventional development methodology, the preparation and installation of the production platform require approximately 24 - 30 months, with drilling and completion taking about 3 months. Therefore, the total time from project approval to first oil and gas flow is around 27 - 33 months. An alternative approach involves pre-drilling with a subsea template before installing a wellhead platform to shorten project time. However, this method can be delayed due to the waiting period for the wellhead platform installation, after which the jack-up rig must return for well connection and completion. Additionally, this method carries higher risks related to positioning the production platform onto the well template.

In contrast, applying a subsea wellhead system in shallow water can achieve first oil/first gas approximately 14 - 16 months after project approval. Essentially, this approach shortens the time to first oil/gas flow by about 12 - 17 months, depending on the scale of the project.

- Simplified facility structure [2]

For fields with multiple prospects located 8 - 10 km apart and with moderate reserves, the simplest operational approach is to use a structure with single wells or well clusters, operated with direct hydraulic control. In cases where clustered well structure is applied, a jack-up rig with cantilever movement can be used for drilling and completion without requiring frequent rig repositioning.

In addition to these advantages, applying a shallow-water subsea wellhead approach with a simple profile for production well can penetrate prospects located in areas that can not be reached by drilling from the production platform. This increases both production rate and overall project efficiency.

- Reduced drilling risks

The design of wells in shallow-water subsea wellhead systems typically features simple schematic and trajectories, avoiding wellbore penetrating through abnormal geological conditions. Consequently, using a jack-up rig for drilling in these wells minimizes operational risks, such as stuck pipe, hydraulic issues while also shortening drilling time.

4.2. Economic efficiency

- Minimized drilling expenditures

For conventional development plans, the lightweight fixed platforms with wellhead systems installed on the surface require the deck to be elevated above sea level to withstand storm conditions. Consequently, the length of the legs of the jack-up rig must be longer, leading to higher specifications and, therefore, higher daily rental rates (USD/day). In contrast, using a subsea wellhead system enables the use of a rig with lower specifications, thereby reducing daily rental costs.

According to current market surveys of jack-up rigs, the rental price of a rig with a leg length of 477 ft is approximately 10 - 20% lower to compare to a rig leg length of 517 ft (or longer). Additionally, the well strategy design is simplified when applying a subsea wellhead, thus shortening construction time by approximately 5%, thereby reducing drilling costs.

- Reduced CAPEX

The value of CAPEX for each project is determined based on the scale of offshore facilities and drilling methodology, which depends on the scope of each project. With the exploration/development projects by drilling infill wells in ongoing production fields or developing marginal fields, the following costs will decrease to compare to conventional methodology:

- + Subsea wellhead/tree systems and pipeline connections to the CPP: Costs include operational equipment and vessel chartering for pipe laying, which are lower than the design, construction, and installation costs of lightweight fixed production platforms.

- + No cost for surface wellhead/tree systems.

- + Costs for supporting services, including service vessels, logistics bases, transportation, and import/export activities.

- Reduced OPEX

The value of OPEX for a project primarily includes items such as chartering security vessels, maintenance, upkeep of equipment and platforms, and periodic surveys. Therefore, using a subsea wellhead system can affect costs for the following items:

- + No annual maintenance costs for surface equipment, as with fixed platforms.

- + Lower logistics costs, including service vessels and personnel for maintenance and repairs of equipment throughout the field's life, compared to fixed platforms.

- + Higher well intervention costs, as a jack-up rig must be mobilized for each individual well repair task.

Nevertheless, in overall comparisons, using a subsea wellhead system results in lower OPEX than lightweight fixed production platforms.

- Overall project economic efficiency

For oil and gas projects globally and in Vietnam, economic efficiency is primarily evaluated using the Net Present Value (NPV) of the entire project. Furthermore, based on the assessment results of oil and gas potential on Vietnam's continental shelf, the use of a subsea wellhead systems are often utilized for developing moderately scale. This makes the NPV a key factor in determining whether to proceed with project implementation.

In this article, the authors aim to evaluate the

Table 1. Comparison of overall costs for development of gas project in Vietnam

Descriptions	Estimated cost of project applied the lightweight platform (Million USD)	Estimated cost of project applied subsea wellhead methodology (Million USD)
Estimated cost of drilling and completion	124.5	118
Estimated cost of wellhead and X-mas Tree	1.5	2.8
Estimated cost of building a fixed lightweight platform (unmanned)	51.5	0
Estimated costs of subsea pipelines, control and umbilical systems and vessel subsea pipe layer	90.5	95
Estimated value of CAPEX	268	215.8
Estimated value of OPEX and well intervention	415	181
Abandonment expenditure	50	34
Net profit of partners	145	145
Net profit of contractor	432	432
Total income of government	650	650
Taxes	85	85
Other fees	20	20
Total CAPEX, OPEX	2,333	1,978.6
Revenue from the sale of products	2,427	2,427
NPV	39.5	222.3

economic efficiency of a gas field case study in Vietnam. The scope of work is defined as follows:

- The gas field is currently in production, with facilities including a central processing platform and a development plan that involves drilling infill wells to maintain the gas production rate.
- Total 4 production wells designed with TD @ 4,000 m TVD SS with casing structure 30" x 20" x 13³/₈" x 9⁵/₈" x 7" and 5¹/₂" completion for a field life of 15 years.
- Jack up rig 10,000 psi BOP shall be utilized for drilling activities, the daily rate 130,000 USD/day [3].
- The light fixed unmaned platform including jacket and topside with estimation of weight 1,700 MT and 1,400 MT respectively.
- The gas is transported to the central processing platform over a distance of 30 km.
- Production is expected to decline gradually over 15 years, with a total output of 5,500 million m³.
- The estimated gas price under the contract is 12.5 USD/MMBTU.

The economic efficiency of the proposed development project is assessed through a comparison of various development methodologies, based on the estimated costs associated with a gas project in Vietnam. The key cost components and their details are outlined in Table 1.

Note:

The estimated costs listed in Table 1 for a specific gas project are assumed based on the following criteria:

- Estimated costs for each item are based on the average values of gas projects in Nam Con Son basin, offshore Vietnam.
- Costs are estimated for a project with the following scale:
 - + Service costs are estimated based on market prices for the year 2023.
 - + The discount rate - 10%.

Estimated costs are calculated in detail for each specific project, using the estimated service prices at the time the project is executed.

Based on the estimated NPV table for the two options, it is evident that with the same production volume, the option using the subsea wellhead/tree system incurs lower total costs, resulting in a higher NPV compared to the option using lightweight fixed platforms.

5. Conclusion

Based on the assessments of oil and gas reserves on Vietnam's continental shelf to date, the fluctuations in the market for services related to the exploration and development of oil and gas fields, the preliminarily evaluation of technical and economic efficiencies, and the

results demonstrating effectiveness in several projects worldwide, the application of the subsea wellhead/tree system for development in shallow water is a feasible option for fields with the following characteristics:

- Currently producing fields that plan to increase production rates by drilling infill wells to access distant prospects located far from the central processing platform.
- Marginal oil and gas fields with natural environmental conditions suitable for operations using jack-up rigs.

However, during the development planning process, oil and gas operators need to consider several issues related to the operation of production wells, including:

- Assessing potential reserves and prospect locations to select the optimal development structure, maximizing operational efficiency and minimizing CAPEX costs.
- Selecting appropriate service providers with the necessary capabilities and experience in executing similar projects.

- Evaluating the technical options and equipment used for well intervention to minimize risks and project costs.

- Utilizing data collected during production to update the production plateau for each specific formation, enabling a reasonable well-opening strategy.

Reference

[1] FMC Technologies, "Shallow water subsea production systems", *The 4th Tunisian Oil & Gas*, 2014.

[2] Jerry Streeter, "Shallow water subsea systems improve NPV", *Offshore Engineer Magazine*, 2013. [Online]. Available: <https://www.oedigital.com/news/457434-shallow-water-subsea-systems-improve-npv>.

[3] Westwood Global Energy Group, "Global offshore rig dayrate forecast". [Online]. Available: <https://www.westwoodenergy.com/reports/global-offshore-drilling-rig-dayrate-forecast>.

PRODUCTION AND OPTIMISATION OF A WELL BY HYBRID ARTIFICIAL ACTIVATION

Rolande Tsapla Fotsa¹, Isidore Komofor Ngongiah^{2,3}, Sifeu Takougang Kingni^{3,6}, Fritz Maxwell Yebchue Tchachue⁴
Nazaire Pierre Kenmogne³, Gaetan Fautso Kuate^{5,7}

¹Department of Mechanical Engineering, College of Technology, University of Buea

²Department of Physics, Faculty of Science, University of Bamenda

³Department of Mechanical, Petroleum and Gas Engineering, National Advanced School of Mines and Petroleum Industries, University of Maroua

⁴University Institute of Entrepreneurship, University of Douala

⁵Department of Physics, Higher Teacher Training College, University of Bamenda

⁶Laboratory of Products Development and Entrepreneurship, Institute of Innovation and Technology

⁷Department of Mechanical and Industrial Engineering, National Higher Polytechnic Institute, University of Bamenda

Email: ngongiahisidore@gmail.com

<https://doi.org/10.47800/PVSI.2024.06-05>

Summary

This paper focuses on proposing a hybrid activation mechanism for the production and optimisation of a well called X101 (for confidentiality reasons), which has become non-eruptive. Completion, pressure, volume, temperature (PVT), reservoir, and the X101 well profile data are processed by Pipesim and Excel software and integrating a certain number of calculations using nodal and decline curve analysis methods. The activation of the X101 well by an electric submersible pump (ESP) having 450 stages provided an oil production flow rate of 9189.329 stock tank barrels per day with a bottom-hole pressure of 2746.151 psi. Over time, the X101 well activated by the ESP having 450 stages faces a succession of maintenance operations occurring in very short time intervals following the reduction in the efficiency of the ESP. To overcome the problem of frequent maintenance which disrupts production times, the gas lift is added to the X101 well activated by a new ESP having 199 stages. The installation of the gas lift reveals that the adequate gas injection flow rate is 2 million standard ft³ per day and 2 valves must be installed at 4,959 ft and 3,966 ft to suitably meet the production requirements. The X101 well activated by the combination of ESP and gas lift delivered a production flow rate of 7954.601 stock tank barrels per day with a bottom-hole pressure of 2873.623 psi and its optimisation made it possible to obtain a net oil flow rate of 9,035 stock tank barrels per day at the bottom-hole pressure of 2,762 psi. The profitability of the X101 well activated by the combination of ESP and gas lift is USD 73,163,517 for a return on investment after 9 months and 22 days for 13 years of production.

Key words: Non-eruptive well, hybrid activation, gas lift, electric submersible pump, nodal analysis, sensitive analysis, payback period.

1. Introduction

The natural exploitation of the so-called primary oil deposits involves the energy stored in the reservoir as pressure in the rock and the compressed fluid [1 - 3]. As the wells are exploited, over time, their reservoirs begin to be depleted, and the productive capacity of wells decreases [4 - 6]. This decline is caused by a decrease in the reservoir's ability to deliver fluid to the well (a drop in blowout energy) and in some cases is caused by increased pressure losses in the production string [1, 7 - 9]. When

this energy does not meet production constraints despite the reserves in place being significant, well-activation techniques (artificial lift) and secondary recovery are introduced in order to improve the well potential and enhance production [7, 10]. This is the case of the reservoir of the X101 well, which is a horizontal well producing simultaneously in three distinct zones of the same reservoir in the field called X (for confidentiality reasons). After a few years of production, the X101 well was unable to continue to adequately deliver hydrocarbons to the surface due to total depletion occurring in its reservoir. Following an in-depth analysis of this constraint, the operating company of the field took the initiative to activate the X101 well with the ESP while considering its advantages over other



Date of receipt: 19/1/2024.

Date of review and editing: 19/1 - 6/8/2024.

Date of approval: 6/8/2024.

well activation mechanisms, namely: The gas lift, the progressive cavity pump, the hydraulic pump and the rod pump [11 - 15]. Under the effect of the depth, the number of layers to be produced, and the requirements on the minimum production flow, the motor of this pump was subjected to a very high number of stages (450) which mainly led to the shortening of its lifespan. Concerned by maintenance operations, which were very recurring due to the short lifespan of the installed ESP, the authors of this paper propose to the company a hybrid artificial lift. This technology, which is still little known in the oil industry, consists of combining two activation mechanisms in the same oil well [16 - 19]. This hybrid artificial lift aims to reduce the number of stages of the ESP in order to extend its lifespan and obtain a greater margin of time between maintenance operations.

The problem is to know which configuration of the hybrid artificial lift is the best to properly produce the hydrocarbons at the desired flow rate (minimum 7,500 stock tank barrels per day). Thus, this study aims to propose a combination of two activation mechanisms making it possible to maximise production in the X01 well in an efficient manner. To accomplish this research investigation, the following steps (specific objectives) were considered (which gives the necessary steps in implementing this oil well activation technique):

To carry out the initial design of the X101 well to highlight its profile;

To evaluate the nodal analysis to have an idea of the state of the X101 well with and without the contribution of the ESP having 450 stages;

To choose and justify the use of the second artificial lift;

To design the design of the combination of the 2 artificial lifts selected;

To evaluate the performance of the well while taking into account the combination of these 2 mechanisms;

To optimise production to better understand how the parameters relating to the activation mechanisms influence the production rate and produce an economic assessment of the operations.

To achieve these objectives, the nodal analysis method and the method relating to the design of the different activation mechanisms are used to better assess the performance and optimisation of the well with this combination of artificial lift. Analysis and manipulation of data are done using Pipesim and Excel software. The other parts of the paper are formatted in sections. The preceding section is the data and results while the conclusion is presented in the last section of the paper.

2. Data and results

The data in Tables 1 to 3 consist of completion data, reservoir or PVT data, and petro-physical data.

The data in Tables 1 - 3 make it possible to carry out and design the completion, the design of the activation mechanisms and also the simulations involving nodal and sensitivity analysis in the X101 well using the Pipesim software. The Excel software is employed for calculations concerning predictions and the economic balance sheet.

Figure 1 shows the profile and nodal analysis of the X101 well in the initial state.

The initial design of the X101 well allows the observation of the well profile and the depth of the equipment as shown in Figure 1a. The X101 well is a deviated well going from the surface to 15,000 ft, which should be producing normally at three distinct zones of the same reservoir simultaneously. The X101 well is non-eruptive because the IPR and VFP curves do not meet as shown in Figure 1b.

Table 1. Completion data

Parameters	Depth (ft)	ID (inch)	OD (inch)	Grade
Conductor casing	1,000	27.75	30	B
Surface casing	4,500	19	20	M65
Intermediate casing	9,000	12.375	13.625	L80
Production casing	10,000	8.435	9.625	L80
Tubing	11,000	3	4.5	L80
Liner	10,000 - 15,000	6.004	7	L80
Packer	10,900			
Choke		3		
SCSSV	1,500			
Flow line	2,500	2.5		

Table 2. Reservoir data

Parameters	Values
Pressure and temperature of the first zone	3,500 psi and 120°F
Pressure and temperature of the second zone	3,600 psi and 205°F
Pressure and temperature of the third zone	3,700 psi and 210°F
PI for the three zones	2.5 stock tank barrels/Psi.d
Average permeability	80 md
Medium porosity	20%
Water salinity	10,000 ppm
Skin	0
API	38°
GOR	100 SCF/STB
Water cut	70%
Oil formation volume factor	1.2
Oil viscosity	1.3 CP
Number of stages	450 to 250 maximum
Wellhead pressure	300 psi

Table 3. Deviation data

MD (ft)	TVD (ft)	MD (ft)	TVD (ft)
0	0	8,000	7831.951
1,000	1,000	9,000	8539.058
2,000	2,000	10,000	8556.51
3,000	3,000	11,000	8565.237
4,000	4,000	12,000	8565.237
5,000	5,000	13,000	8565.237
6,000	6,000	14,000	8565.237
7,000	6965.926	15,000	8565.237

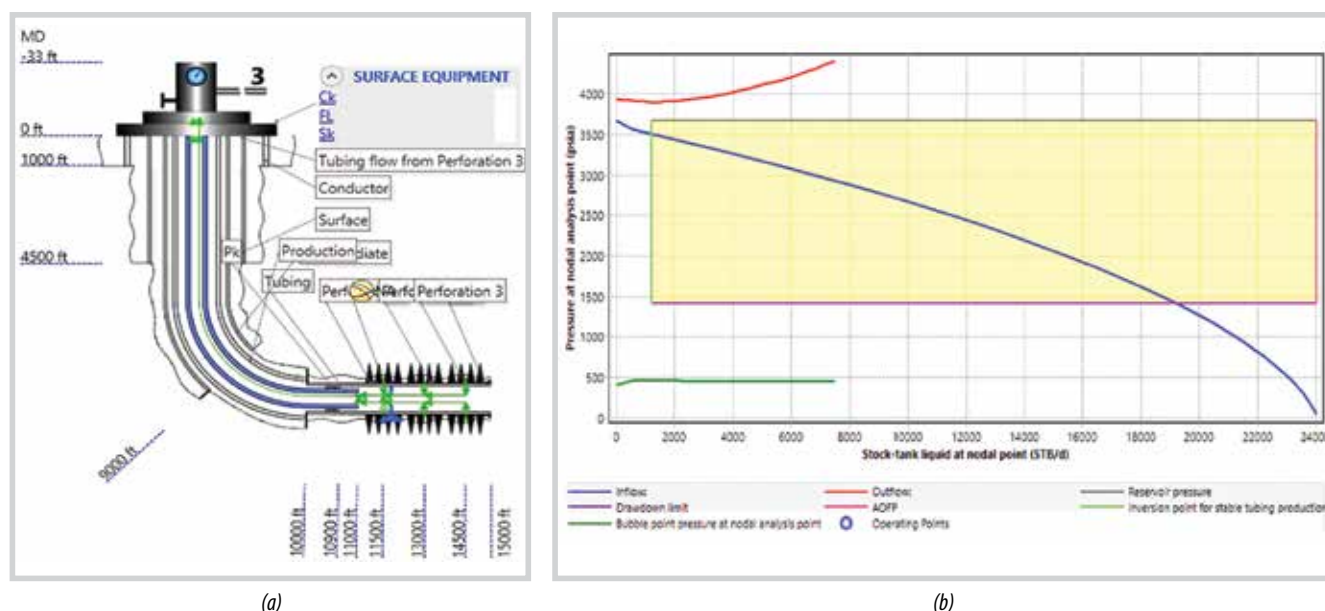
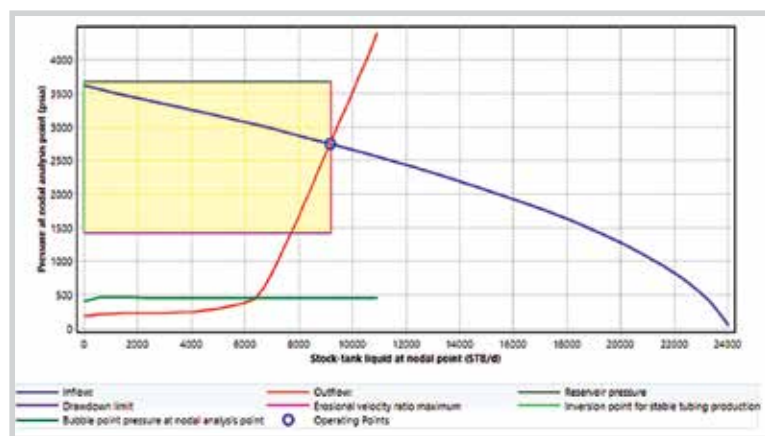


Figure 1. Profile (a) and nodal analysis (b) of the X101 well in the initial state.

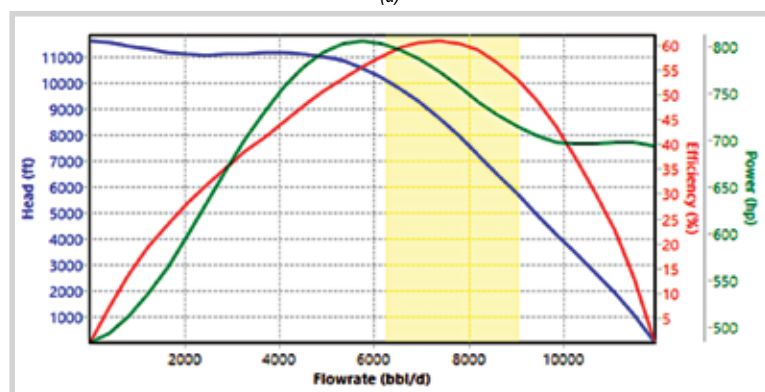
2.1. Production of the X101 well activated by the combination of ESP and gas lift

To make the X101 well eruptive again, an ESP must be installed as an activation mechanism that meets the

requirements of the well and the production conditions. Figure 2 highlights the production results following the activation of the X101 well by the ESP and the performance curves of the ESP respectively.



(a)



(b)

Figure 2. (a) Nodal analysis of the X101 well activated by the ESP and (b) ESP performance curves for the X101 well.

Table 4. Parameters of the new ESP

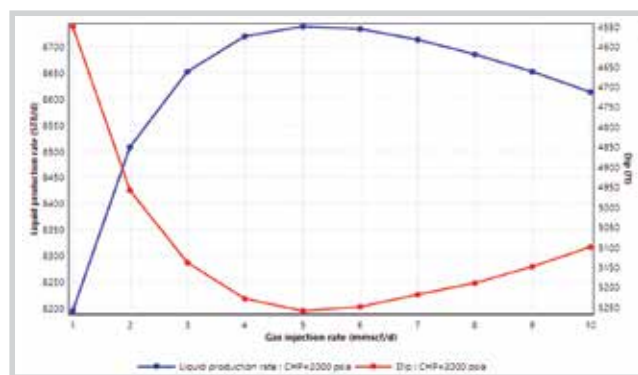
Parameters	Values
Pump	ALNAS ANA545 55Hz
Stages	199
Speed	3499.992 rpm
Efficiency	60.25224%
Power	314.4059 HP
Head	3506.842 ft
Differential pressure	1427.495 psi
Discharge pressure	4345.753 psia
Fluid temperature rise	3.471007°F

The ESP activation of the X101 well yields an oil production rate of 9189.329 stock tank barrels per day and a bottom-hole pressure equal to 2746.151 psi as shown in Figure 2a. Figure 2b indicates that the ESP operates at its maximum capacity at 450 stages, a speed of 3,500 RPM, and a frequency of 55 Hz. It is important to remember here that the X101 well is centrally located in a horizontal field that has become non-eruptive and a candidate for the ESP. This well had been put into production with an optimal flow rate greater than 7,500 stock tank barrels per day and its activation by the ESP makes it possible to continue to adequately produce at this flow rate despite the depletion occurring in the reservoir. Over time, the operating company faced a succession of maintenance operations occurring in very short time

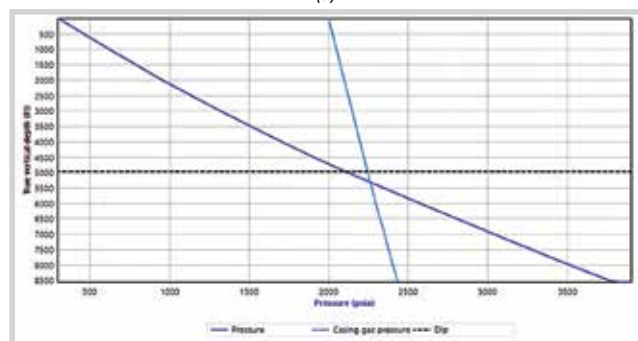
intervals because of the reduction in the efficiency of the ESP. This reduction in ESP's efficiency is largely due to a high number of stages (450), which created a certain load on the engine and pushed the ESP continuously to work with its maximum capacity. This load associated with corrosion occurring on pumps can considerably reduce the lifespan of this ESP and increase maintenance operations. Hence, the authors of this paper propose to install a second activation mechanism associated with the ESP to benefit from increased production time and extended maintenance intervals. After implementing components such as the desirable oil recovery flow rate, the inside diameter of the casing, the pressure at the head of the well, the data relating to the X101 well and the reservoir, and the placement of the separator at the bottom, Pipesim allows one to obtain the characteristics of the new ESP used to activate the X101 well as presented in Table 4.

After obtaining the parameters linked to the new design of the ESP, the new ESP is installed in the X101 well and serves as a support (reference) for the realisation of the gas lift design. Designing the gas lift system consists of finding the injection points, the flow rate with which the gas is to be injected as well as the number of valves necessary to facilitate the rise of the oil as shown in Figure 3.

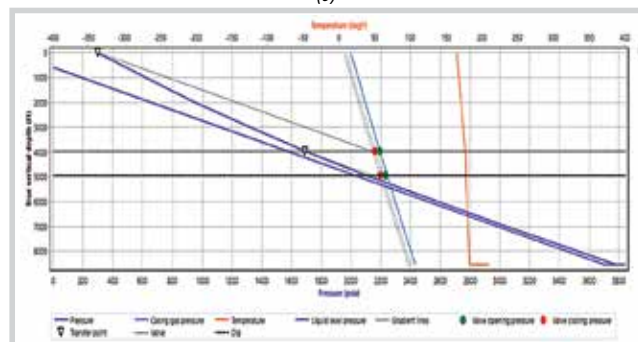
Figure 3a reveals that the value of 2 million standard ft³ per day is retained as the injection rate and used for the simulations presented in Figures 3b and 3c. Figure 3b reveals that the first valve will be placed at a depth of 4,959 ft for a good design of the system combining the two activation mechanisms. Figure 3c reveals that two SLB (Camco), Series R20, IPO type valves are to be installed, where the deepest of which will have a minimum port size of 0.5 inches and the tallest, a port size of 0.25 inches. It also provides the depth of the second valve which is equivalent to 3,966 ft. Figure 4 presents the profile and nodal analysis of the X101 well activated by the ESP and gas lift combination.



(a)



(b)



(c)

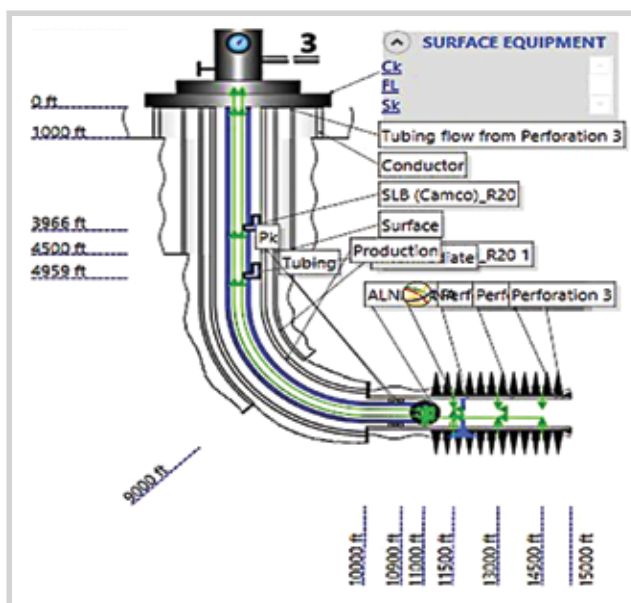
Figure 3. (a) Gas lift response, (b) deepest injection point, and (c) gas lift design.

The initial design of the X101 well activated by the ESP and gas lift combination allows the observation of the profile of the X101 well and the depth of the equipment as shown in Figure 4a. Figure 4b reveals that the X101 well activated by the ESP and gas lift combination has an oil production flow rate of 7954.601 stock tank barrels per day and a bottom-hole pressure of 2873.623 psi.

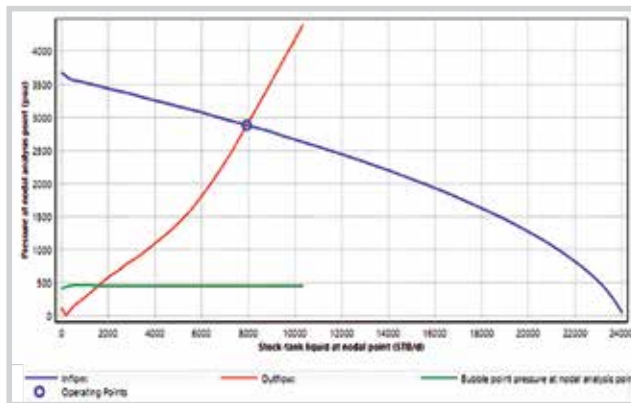
2.2. Optimisation of the production of the X101 well activated by the combination of ESP and gas lift

It is imperative to recall here that the factors on which this optimisation was focused are: The gas injection rate, the diameter of the flowline, the pressure at the wellhead, the number of stages, and the frequency of the ESP.

- Sensitivity analysis on the X101 wellhead pressure



(a)



(b)

Figure 4. (a) Profile and (b) nodal analysis of the X101 well activated by the combination of the ESP and gas lift.

Wellhead pressure has a major influence on production flow. For the X101 well activated by the ESP and gas lift combination, the reduction in pressure at the wellhead led to a remarkable increase in production flow rate. This can be explained by the fact that it allows an increase in the volume of oil sucked up by the ALNAS ANA545 55Hz pump and tends to reduce pressure losses in the production tubing. Choosing to reduce the pressure at the wellhead is an efficient idea because it increases the efficiency of the pump without affecting it. The optimal wellhead pressure value retained for the X101 well is 100 psi. This pressure will allow the well to produce safely while avoiding a significant production of successive sand from eroding the production tubing and the pump.

- Sensitivity analysis on the number of stages

The number of stages directly increases the production flow rate. An increase in the number of stages

could increase the production flow but at the risk of creating a load on the pump’s motor which could lead to a reduction in its lifespan. The X101 well was activated by the combination of the ESP and gas lift with a reduced number of stages set at 200 to limit the load on the engine and the long lifespan of the pump which will allow a greater margin of time for maintenance operations.

- Sensitivity analysis on the pump’s frequency

The production flow rate is proportional to the frequency of the ESP. For this purpose, to avoid a very large production which could

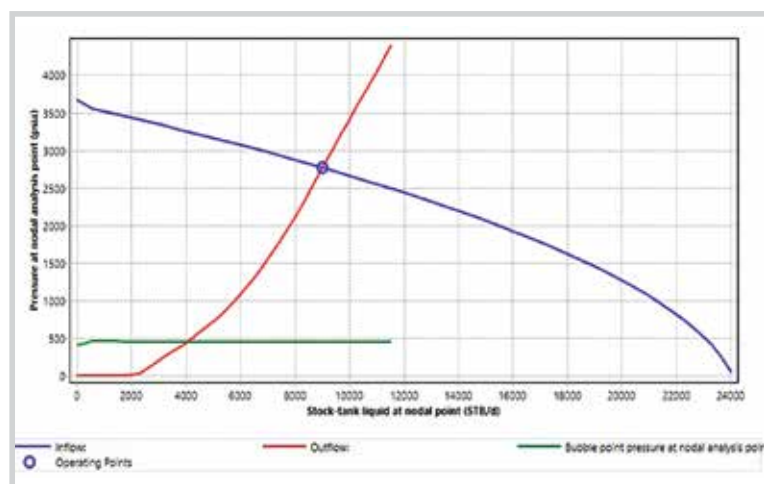


Figure 5. Nodal analysis of the X101 well activated by the combination of ESP and gas lift with the integration of optimal values.

Table 5. Capex and Opex

Capex	
Services	Cost
Gas lift equipment	USD 150,000
Downhole and surface equipment for ESP	USD 100,000
Opex	
Services	Cost
Water treatment	USD 160,000
Annual maintenance	USD 45,000
Cost of oil	USD 10 per barrel
Energy cost	USD 20 per day

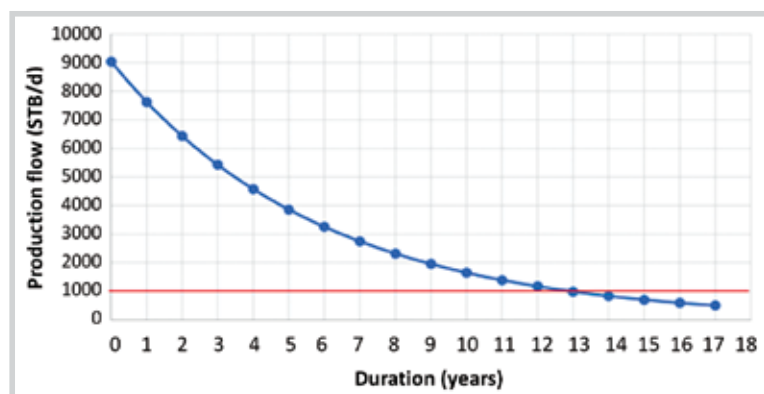


Figure 6. Production decline curve for the X101 well activated by the ESP and gas lift combination.

lead to the production of sand, the appropriate frequency for the ESP ALNAS ANA545 is 55 Hz and it can be adjusted after the installation of the VSD for the adjustment of the pump’s parameters.

- Sensitivity analysis on the gas injection flow

In the X101 well activated by the ESP and gas lift combination, it is easy to see that from a certain gas injection flow rate, the production flow rate is inversely proportional to the injected gas flow rate. Indeed, from the injection interval of 1 to 2 million standard ft³ per day, the injection rate is fairly stable and from 2 to 5 million standard ft³ per day the injection rate was inversely proportional to the production rate. When we continue to increase the injection flow rate, the injected gas creates turbulence which will reduce the production flow rate and give rise to high gas production. Therefore, 2 million standard ft³ per day is maintained and used as the optimal value for the gas injection flow.

- Sensitivity analysis on the diameter of the flowline

The production rate increases with the diameter of the flowline. In the X101 well activated by the combination of ESP and gas lift, the optimal value of the internal diameter of the flowline retained is 3.5 inches simply because it allows production with a flow rate approximated to that of the first ESP. Using the optimal values obtained, Figure 5 presents the nodal analysis of the X101 well activated by the combination of ESP and gas lift.

Figure 5 reveals that the X101 well activated by the combination of ESP and gas lift produces at a constant flow rate of 9,035 stock tank barrels per day and a bottom-hole pressure of 2,762 psi while having an acceptable time margin between maintenance operations.

2.3. Economic assessment

Table 5 presents the Capex and Opex.

Before calculating the entire expenses

Table 6. NPV of the project

Expenses	Income	Cash flow	NPV
USD 57,430,786	USD 535,238,417	USD 358,355,723	USD 73,163,517

associated with putting the X101 well into production with the proposed artificial lift combination, it is first necessary to have an idea of the future production of the well based on the analysis of the curve of decline. This analysis revealed the behavior of production up to the production limit set by the company (100 stock tank barrels per day). Future production rates are plotted graphically in Figure 6.

With the production limit of 1,000 stock tank barrels per day, the interpretation of Figure 7 leads to a prediction about the next 13 years of production. So, to have the total expenses, it is necessary to add up all the investments as follows while taking into account the oil flow:

$$\text{Expenses} = 150,00 + 160,00 + \text{Total energy cost} \\ (20 \times 365 \times 13) + \text{Total cost of oil} + (45,000 \times 13)$$

This results in a total expenditure of USD 57,430,786. The NPV is obtained by applying the discount rate to the net cash flow after taxes. The result of this operation is given in Table 6.

Table 6 shows that the NPV of the project is positive. Therefore, the use of an ESP and the gas lift to activate the X101 well is indeed a profitable project. The payback period $(PBP = \frac{57,430,786}{9,035 \times 0.3 \times 365 \times 95 \times (1-0.25)} = 0.81)$ is obtained from the 9th month and 22nd day of production.

3. Conclusion

This paper aimed to propose a hybrid activation mechanism that made it possible to activate and maximise production at the X101 well while having an acceptable time margin between maintenance operations. For this purpose, data containing information on the completion, the reservoir, the profile of the X101 well, and the installed electric submersible pump were used. Firstly, it was necessary to highlight the initial design of the X101 well and its nodal analysis which showed that the X101 well had become non-eruptive.

The X101 well was initially activated using an electric submersible pump with 450 stages, which provided an oil production flow rate of 9189.329 stock tank barrels per day at a bottom-hole pressure of 2746.151 psi. But over time, it faced frequent maintenance issues due to the reduced

efficiency of the electric submersible pump. To overcome this problem, a gas lift system was added to the well, using a new electric submersible pump (ALNAS ANA545 55Hz) with 199 stages, requiring an injection flow rate of 2 million standard ft³ per day and the installation of two valves at 4,959 ft and 3,966 ft, which provided a production flow rate of 7954.601 stock tank barrels per day at a bottom-hole pressure of 2873.623 psi. Further optimisation of this system allowed the well to achieve a net oil flow rate of 9,035 stock tank barrels per day at a bottom-hole pressure of 2,762 psi. The economic assessment showed the profitability of the solution proposed in this study by presenting an NPV of USD 73,163,517 and a payback period of approximately 9 months and 22 days of production over 13 years of production.

References

- [1] Boyun Guo, William C. Lyons, and Ali Ghalambor, *Petroleum production engineering, A computer-assisted approach, 1st edition*. Gulf Professional Publishing, 2011.
- [2] Jr. Harry Dembicki, *Practical petroleum geochemistry for exploration and production*. Elsevier, 2017. DOI: 10.1016/C2014-0-03244-3.
- [3] Ricardo Michael Kamga Ngankam, Eric Donald Dongmo, Madeleine Nitcheu, Josephine Fleur Matateyou, Gabriel Kuitse, and Sifeu Takougang Kingni, "Production step-up of an oil well through nodal analysis", *Journal of Engineering*, Volume 2022, Issue 1, 2022. DOI: 10.1155/2022/6148337.
- [4] Frank Jahn, Mark Cook, and Mark Graham, *Hydrocarbon exploration and production, 2nd edition*. Elsevier, 2008.
- [5] S. John, *Forecasting oil and gas producing for unconventional wells, 2nd edition*, 2018.
- [6] Michael J. Economides, A. Daniel Hill, and Christine Ehlig-Economides, *Petroleum production systems*. Prentice Hall, 1994.
- [7] John R. Fanchi and Richard L. Christiansen, *Introduction to petroleum engineering*. Wiley, 2016.
- [8] Jonathan Bellarby, *Well completion design, 1st edition*. Elsevier, 2009.

[9] Chang Samuel Hsu and Paul R. Robinson, *Petroleum science and technology*, 1st edition. Springer, 2019. DOI: 10.1007/978-3-030-16275-7.

[10] D. Katz and W. Barlow, *"Relation of bottom-hole pressure to production control"*. American Petroleum Institute, 1995.

[11] Michael J. Economides, A. Daniel Hill, Christine Ehlig-Economides, and Ding Zhu, *Petroleum production systems*, 2nd edition. Prentice Hall, 2013.

[12] Stéphanie Laure Biloa, Sifeu Takougang Kingni, Eric-Donald Dongmo, Sop TAMO Berthelot, Komofor Isidore Ngongiah and G. Kuate Fautso, "Heightened the petroleum productivity of an eruptive well by an electric submersible pump with a free gas separator", *International Journal of Energy and Water Resources*, Volume 8, pp. 327 - 339, 2023. DOI: 10.1007/s42108-023-00250-3.

[13] Victorine Belomo, Madeleine Nitcheu, Eric Donald Dongmo, Kasi Njeudjang, Gabriel Kuate and Sifeu Takougang Kingni, "Activation of a non-eruptive well by using an electric pump to optimise production", *Petrovietnam Journal*, Volume 6, pp. 36 - 42, 2022. DOI: 10.47800/PVJ.2022.06-04.

[14] Kermit E. Brown, *The technology of artificial lift methods*. Pennwell Books, 1977.

[15] Ruichao Zhang, Zenglin Wang, Xinhui Wang, Jincheng Wang, Guangzheng Zhang, and Dechun

Chen, "Integrated diagnostics method and application of ground and downhole working condition in rod pumping well", *Journal of Applied Science and Engineering*, Volume 21, Issue 4, pp. 615 - 624, 2018. DOI: 10.6180/jase.201812_21(4).0015.

[16] Candra Kurniawan, Hendra Kusuma, Prayudha Rifqi Shafiraldi, Hilman Lazuardi, and Bonni Ariwibowo, "Re-shifting of a single string packer-less electric submersible pump gas lift hybrid to fit the up-to-date environment", *Journal IATMI*, 2022.

[17] A.F. Rohman, Y.I. Arseto and K. Hamzah, "Redesign of a single string packerless ESP-gas lift hybrid", *SPE/IATMI Asian Pacific Oil and Gas Conference and Exhibition, Nusa Dua, Bali, Indonesia, 20 October 2015*. DOI: 10.2118/176291-MS.

[18] Vu Le and Son Tran, "Hybrid electrical-submersible-pump/gas-lift application to improve heavy oil production: From system design to field optimization", *Journal of Energy Resources Technology*, Volume 144, Issue 8, 2022. DOI: 10.1115/1.4052979.

[19] Noke Fajar Prakoso, "Single string packerless ESP gas lift hybrid; Optimizing production and minimizing loss", *SPE Oil and Gas India Conference and Exhibition, Mumbai, India, January 2010*. DOI: 10.2118/128974-MS.

PARAFFIN TREATMENT OF CRUDE OIL PRODUCED FROM THE CENTRAL OF RONG AND NAM RONG - DOI MOI FIELDS DURING TRANSPORTATION THROUGH UNINSULATED SUBSEA PIPELINES

**Chu Van Luong¹, Tran Duy Hai², Pham Thanh Vinh², A.G. Alberta², Nguyen Huu Nhan², Doan Tien Lu²
Chau Nhat Bang², Le Thi Doan Trang², Tran Thi Thanh Huyen², Vu Hong Khuong²**

¹Vietsovetro Joint Venture

²Science Research and Engineering Institute, Vietsovetro Joint Venture

Email: vinhpt.rd@vietsov.com.vn

<https://doi.org/10.47800/PVSI.2024.06-06>

Summary

Due to being developed in the early stages, several major oil subsea pipelines in Vietsovetro Joint Venture are not equipped with insulation systems, causing significant difficulties in transporting high-paraffin crude oil. Specifically, the lack of insulation leads to intensive heat loss through pipeline walls, resulting in paraffin deposition on the pipe surface. Additionally, the temperature drop significantly increases oil viscosity, leading to high pressure losses during transportation.

This article analyses the difficulties in crude oil transportation through the uninsulated RP-1 → FSO-3 pipeline, the major route from Central of Rong, Nam Rong - Doi Moi fields to FSO-3 and presents the technical solutions that Vietsovetro has researched and implemented to successfully resolve these problems.

Key words: High-paraffin crude oil, uninsulated subsea pipeline, pour point depressant (PPD), Central of Rong field, Nam Rong - Doi Moi field.

1. Introduction

Crude oil produced in the Central of Rong and Nam Rong - Doi Moi fields has high-paraffin content, ranging from 13.8% to 23% by mass. The asphaltene-resin content ranges from 3.69% to 18.8% by mass. The oil density varies between 832 kg/m³ and 890 kg/m³. The pour points temperatures of the produced oils range from 30°C to 36°C. The main properties of crude oil from Rong field are presented in Table 1.

The high-paraffin and asphaltene-resin contents result in complex rheological properties of the produced crude oil. When the crude oil temperature approaches its pour point (< 37°C), wax deposits form intensively in both the tubing and the gathering-transportation system, leading to reduced pipeline internal diameter and increased pressure losses.

2. Pipeline system connected to RP-1 platform

Initially, Vietsovetro’s crude oil gathering, processing and transportation system was constructed following field development model in Caspian sea. According to this model, pipelines were laid on the seabed without burial or insulation. After 1998, Vietsovetro began insulating its subsea pipelines with composite or foam materials.

Nam Rong - Doi Moi fields have the main platform RP-1 and satellite platforms of RC-DM, RC-4, and RC-5. Crude oil from RC-DM, RC-4, RC-5 is transported to RP-1 as gas-saturated oil, while the one from RC-6 is transported to RP-1 as a gas-oil mixture. The combined oil stream from

Table 1. Main properties of crude oil from Nam Rong - Doi Moi fields

Parameters	Values
Gravity at 20°C (kg/m ³)	832 - 890
Paraffin content (% mass)	19 - 23
Asphaltene (% mass)	3.69 - 18.8
Viscosity at 50°C (mm ² /s)	5.6 - 27
Pour point (°C)	30 - 36
WAT (°C)	55 - 60



Date of receipt: 22/10/2024.

Date of review and editing: 22/10 - 23/11/2024.

Date of approval: 23/11/2024.

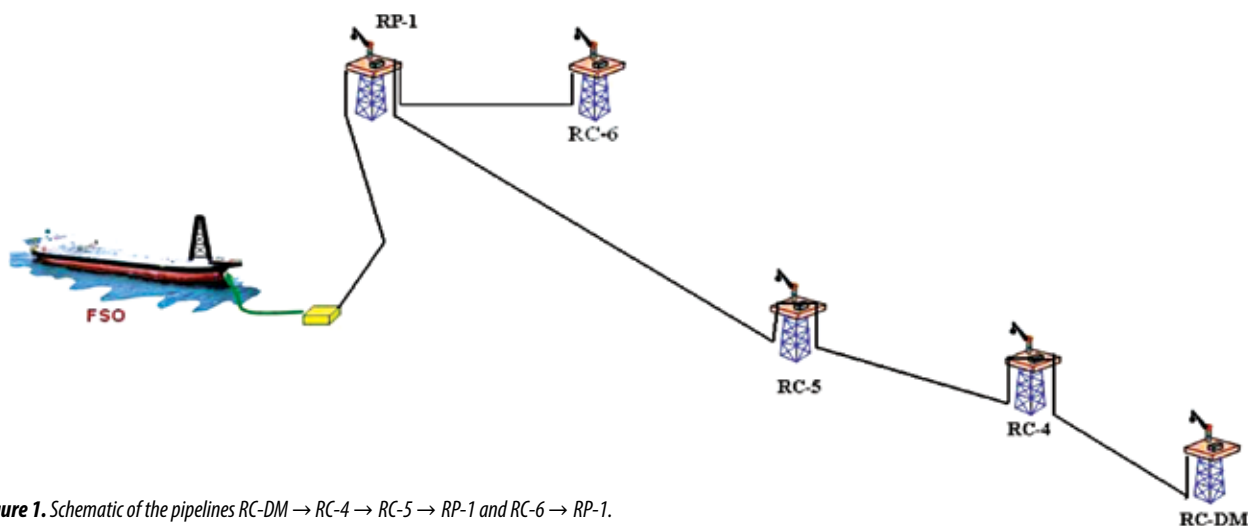


Figure 1. Schematic of the pipelines RC-DM → RC-4 → RC-5 → RP-1 and RC-6 → RP-1.

these satellite platforms is then transported to FSO-3 for processing to meet commercial specifications (Figure 1).

As mentioned above, the pipeline from platform RP-1 to FSO-3 is uninsulated, while other subsea pipelines from RC-DM, RC-4, RC-5, and RC-6 platforms are insulated with composite or foam materials.

Therefore, the most critical problem for the Nam Rong - Doi Moi field’s transportation pipeline system is to maintain flow assurance in the uninsulated section RP-1 → FSO-3. This is the sole pipeline transporting oil from this field to FSO-3.

3. Challenges in high-paraffin crude oil transportation through uninsulated pipeline RP-1 → FSO-3

The seabed water temperature ranges from 22°C to 28°C. Crude oil produced from RC-DM, RC-4, RC-5, RC-6 and RP-1 platforms has high content of paraffin, asphaltene and resin. The pour points of the produced oils range from 30°C to 36°C. The transportation of crude oil through RP-1 → FSO-3 pipeline faces the following risks:

- Paraffin crystallization: Wax crystal deposit on the internal pipeline walls, reducing the internal diameter and increasing pressure loss;
- High transport pressure: Required due increased oil viscosity when the temperature approaches the pour point.

Simulation results indicate that in the uninsulated pipeline RP-1 → FSO-3, paraffin deposits can

Table 2. Dependence of incoming liquid FSO-3 on seabed temperature

Seabed temperature (°C)	Temperature of incoming liquid FSO-3 (°C)
23	32,2
24	32,4
25	33,0
26	33,4
27	34,0
28	34,2
29	34,5

form a layer approximately 40 mm thick. While this solid wax layer acts as a natural insulation, reducing heat loss to the surrounding environment, it also causes significant pressure increase.

As the seabed water temperature decreases, the oil temperature in the pipe drops rapidly, causing the transported oil’s viscosity to increase significantly and leading to high pressure drops. Depending on the seabed water temperature, the oil temperature at FSO-3 fluctuates from 32 - 35°C if pumped from RP-1 at 37 - 40°C. The treated crude oil has a pour point of approximately 32°C. When seabed water temperature falls below 23°C, the temperature of crude oil arriving at FSO-3 approaches its pour point. In these conditions, the averaged pump pressure increases to 25 - 35 bar, creating high risks for the transportation system.

4. Optimization of high-paraffin crude oil transportation via uninsulated RP-1 → FSO-3 pipeline

The study focused on improving crude oil treatment using pour point depressants in combination with demulsifier to achieve maximum efficiency in lowering the pour point and viscosity of the oil mixture.

In general, chemical treatment efficiency depends on multiple factors: chemical dosage, product temperature, water content, produced water form in the product, among which product temperature plays the most crucial role. To maximize the effec-

tiveness of pour point depressant (PPD), Vietsovpetro implemented a method of injecting PPDs through capillary tubes at 2,000 - 2,500 m depth, where the crude oil temperature exceeds its wax appearance temperature.

At the Central of Rong and Nam Rong - Doi Moi satellite platforms, chemical dosage has been uniform across all oil wells, without considering well-specific parameters such as crude oil properties, product temperature at

pump locations, water content, and individual well production rates. This highlighted the critical need for a study to determine optimal dosage for each oil well.

The rheological properties of crude oil from each well were analyzed using different dosage of the PPD currently applied in Vietsovpetro’s fields. The tested dosage was based on current operational levels. The results are presented in Figures 2 - 5.

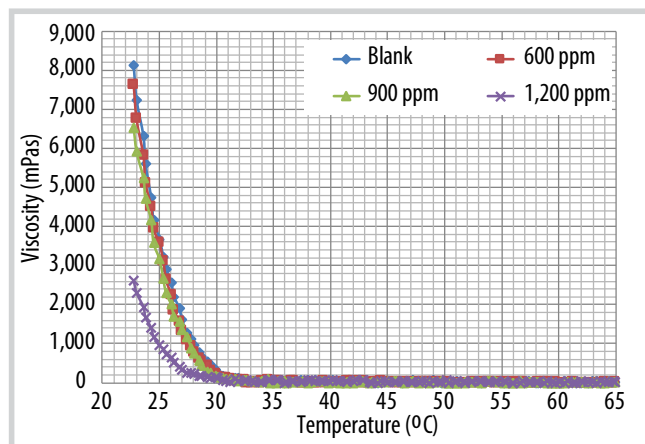


Figure 2. Rheological properties of crude oil of the wells 425, 424 RC-4.

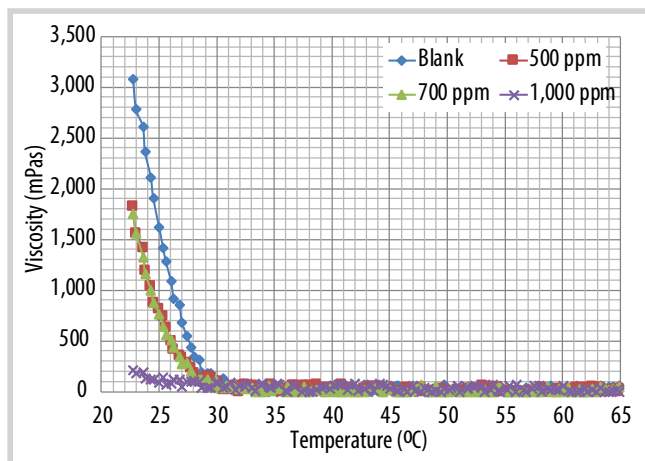
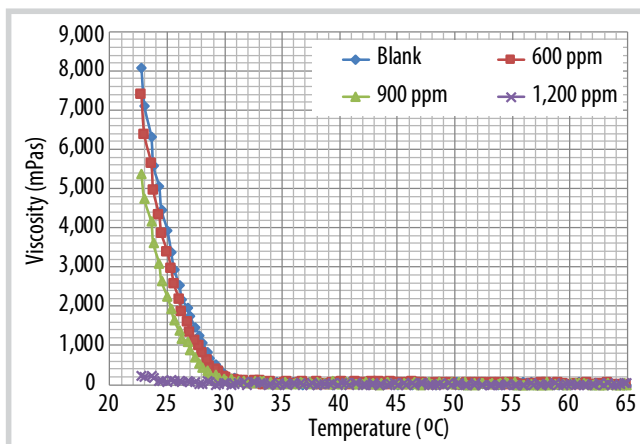


Figure 3. Rheological properties of crude oil of the wells 15, 17 RC-5.

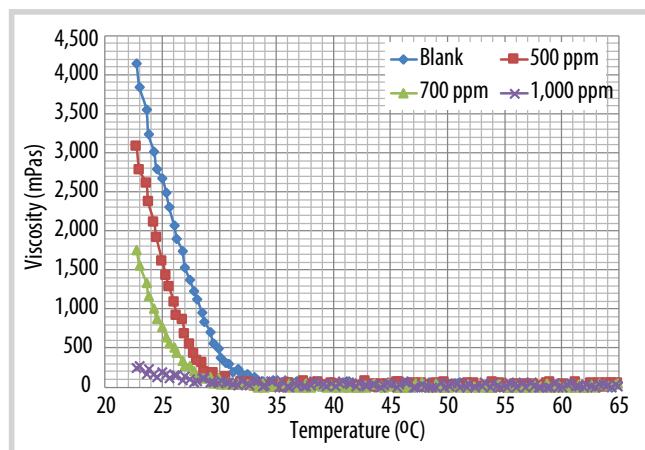
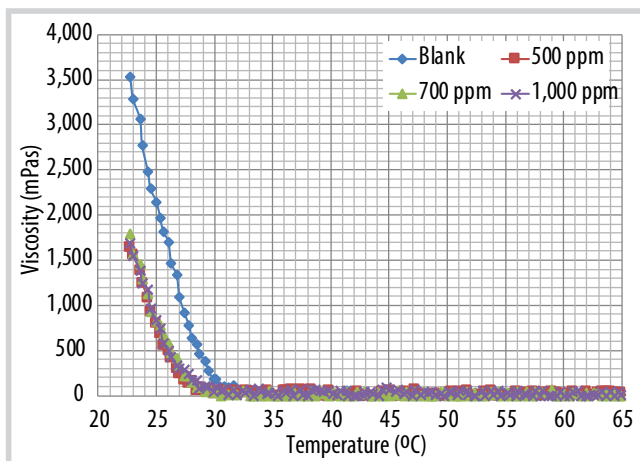
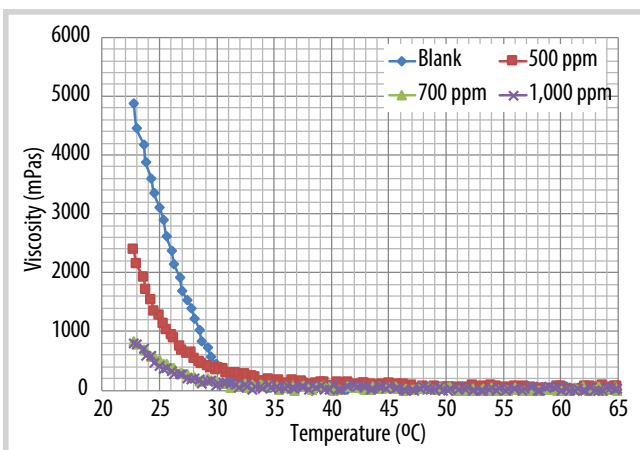


Figure 4. Rheological properties of crude oil of the wells 503, 506 RC-5.



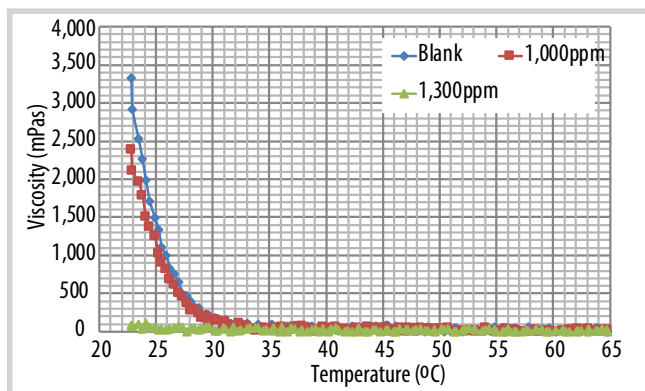
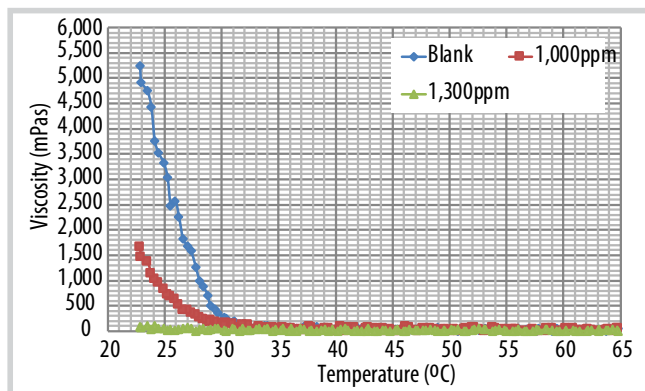


Figure 5. Rheological properties of crude oil of the wells 410, 407 RC-DM.

Table 3. Deposition of paraffin of crude oil RC-DM treated by cold finger method

Wells	Deposition of paraffin (kg/m ²) Temperature of bulk oil at 37°C Temperature of cold finger at 32°C			
	0 ppm	700 ppm	1,000 ppm	1,300 ppm
20	6.75	5.39	3.27	1.75
25	4.59	3.13	2.14	0.65
421B	7.01	3.80	3.26	1.27
422	7.20	4.81	2.48	2.09
423	6.88	2.53	1.42	1.21
424	8.09	6.76	5.04	2.82
425	8.11	6.55	5.11	5.01
426	8.52	6.86	5.23	2.11

Table 4. Deposition of paraffin of crude oil RC-4 treated by cold finger method

Wells	Deposition of paraffin (kg/m ²) Temperature of bulk oil at 37°C Temperature of cold finger at 32°C			
	0 ppm	600 ppm	900 ppm	1,200 ppm
20	4.23	3.39	3.12	2.02
25	8.23	6.25	5.07	3.01
421B	10.15	8.85	7.13	3.57
422	5.25	4.98	2.21	2.10
423	8.02	3.46	3.22	3.15
424	8.05	7.79	3.54	3.08
425	6.69	2.53	2.41	2.32
426	7.32	6.51	5.23	2.84

Table 5. Deposition of paraffin of crude oil RC-5 treated by cold finger method

Wells	Deposition of paraffin (kg/m ²) Temperature of bulk oil at 37°C Temperature of cold finger at 32°C			
	0 ppm	500 ppm	700 ppm	1,000 ppm
15	2.19	1.41	1.38	0.77
17	1.79	1.32	1.23	1.17
503	1.89	1.46	1.12	0.31
506	7.02	2.51	2.44	2.18
507	6.89	5.44	4.90	4.76
508	6.57	3.42	3.30	3.22
509	8.47	5.38	4.86	4.74
510	2.78	2.76	2.71	2.70

Table 6. Optimized PPD dosage

Well	Used dosage before Optimization (ppm)	Optimized dosage (ppm)
20/RC-4	900	1,200
25/RC-4	900	1,200
412B/RC-4	900	1,200
422/RC-4	900	900
423/RC-4	900	900
424/RC-4	900	1,200
425/RC-4	900	600
426/RC-4	900	1200
15/RC-5	700	1,000
17/RC-5	700	500
503/RC-5	700	1,000
506/RC-5	700	700
507/RC-5	700	500
508/RC-5	700	500
509/RC-5	700	500
510/RC-5	700	0
2X/RC-DM	1,300	1,300
405/RC-DM	1,300	0
406/RC-DM	1,300	1,300
407/RC-DM	1,300	1,300
410/RC-DM	1,300	1,300

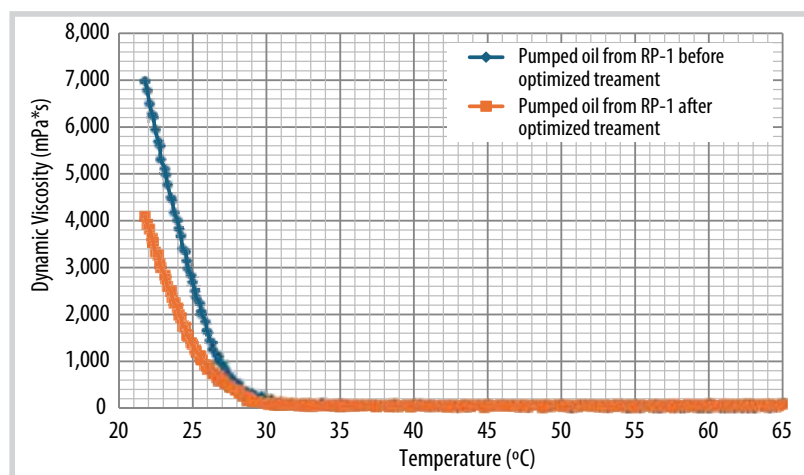


Figure 6. Rheological properties of crude oil pumped from RP-1.



Figure 7. Wax tendency of crude oil pumped from RP-1, before (a) and after (b) optimized treatment.

Based on the study results of the rheological properties of treated crude oil from oil wells in the Central of Rong and Nam Rong - Doi Moi fields, optimal chemical dosages were determined and implemented in field trials (Table 6).

The optimization of chemical treatment using PPDs was implemented on platforms RC-DM, RC-4, and RC-5 with the optimal dosages mentioned above. After field trials, the pour point of crude oil pumped from RP-1 to FSO-03 decreased from 31 - 32°C to 29 - 30.5°C.

In addition to optimizing PPD treatment, demulsifiers are also used on the RC platforms to treat the produced liquid mixture, improving water separation and reducing mixture viscosity.

Lowering the pour point helps reduce the pressure drop in pipelines. The transportation operations from RP-1 to FSO-3 remain stable, with all system operating parameters consistently maintained within allowable technical limits.

Table 7. Deposition of paraffin of treated crude oil pumped from RP-1

Chemical	Deposition of paraffin (kg/m ²)	Deposition reduction (%)
	Crude oil pumped from RP-1	
Before optimized treatment	7.20	70.8
After optimized treatment	2.45	

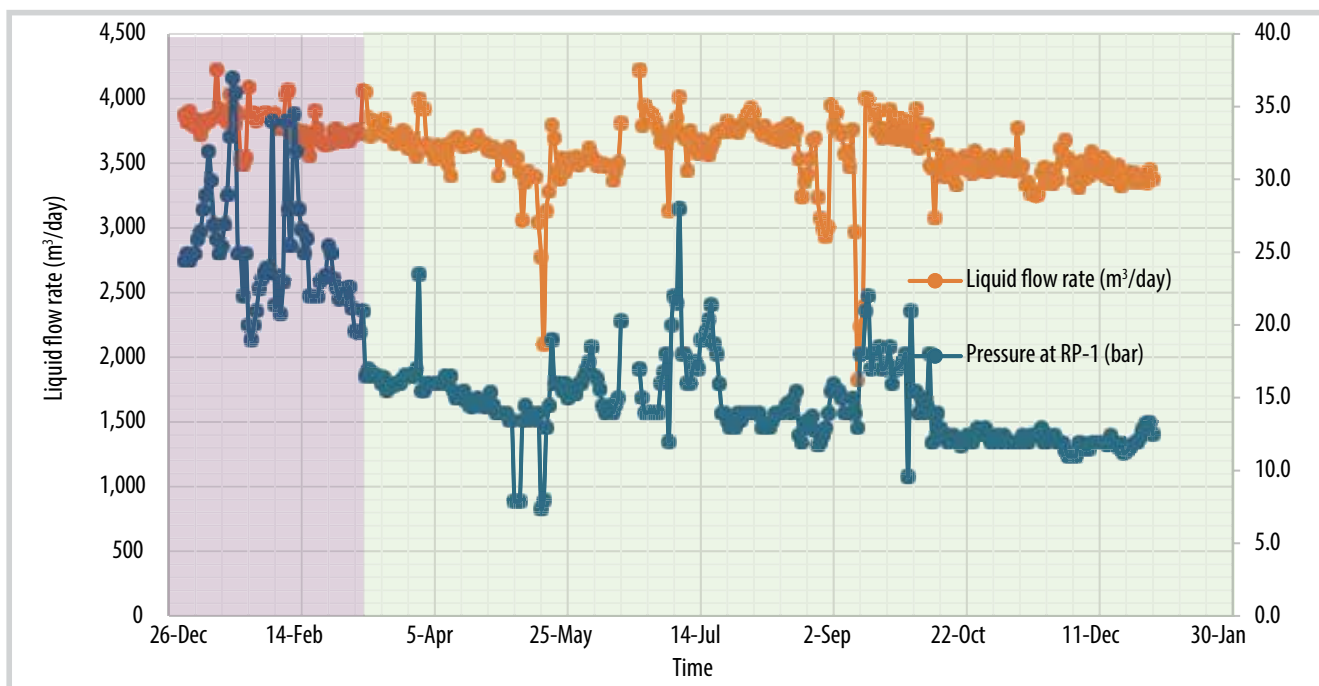


Figure 8. Operating parameters of RP-1 → FSO-3 pipeline before (green zone) and after (yellow zone) optimization.

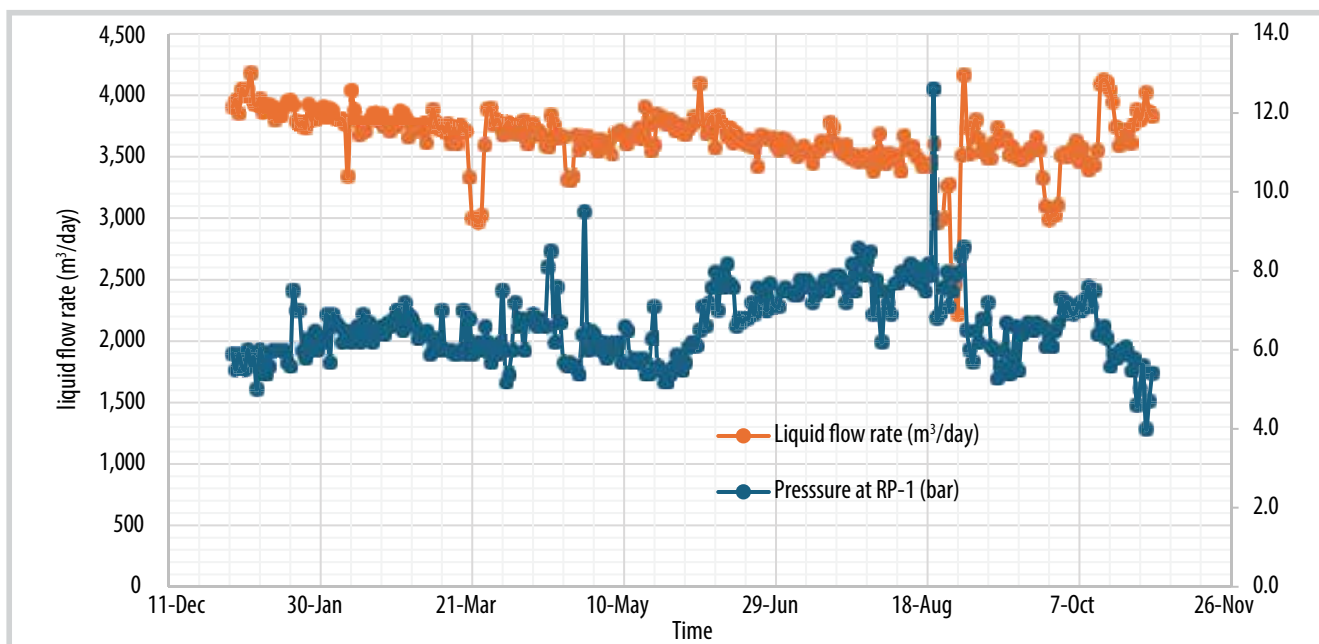


Figure 9. Operating parameters of RP-1 → FSO-3 pipeline in the latest period.

5. Conclusion

The transportation of high-paraffin crude oil through uninsulated pipelines is inherently risky and complex. The main problem is intensive heat loss, which promotes

paraffin deposition on the inner surface of pipelines and increases fluid viscosity, resulting in substantial pressure loss during transportation.

The study results indicate that crude oil properties

vary significantly among wells within the same satellite platform. Notably, the effectiveness of pour point depressant treatment fluctuates considerably from well to well.

For optimal PPD usage, applying uniform dosage to all oil wells can result in either ineffective treatment or chemical waste. Through rheological and deposition studies of crude oil from individual wells, optimal treatment regimes can be determined. The optimal PPD dosage should be established based on well-specific treatment requirements.

In particular, the uninsulated RP-1 → FSO-3 pipeline operates with oil temperature approaching the pour point, leading to increased average pump pressure and creating high risks for the transportation system.

Therefore, PPD treatments enhance pour point reduction effectiveness, lower viscosity, and minimize wax deposition. However, the conventional approach of applying uniform dosage across all wells has not adequately reduced back pressure. The well-specific optimization approach has proven to be more effective in maximizing PPD treatment efficiency.

The study results of the Central of Rong and Nam Rong - Doi Moi fields demonstrate that implementing these concepts has significantly improved crude oil treatment efficiency. As a result, the field's crude can now be safely transported through the uninsulated RP-1 → FSO-3 pipeline.

The results of study have been applied for another oil fields produced by Vietsovpetro, especially for the small and marginal oil fields.

References

[1] А.Г. Ахмадеев, Фам Тхань Винь, Буй Чонг Хан, Ле Хыу Тоан, Нгуен Хоай Ву, и А.И.Михайлов, "Оптимизация безнасосного транспорта продукции скважин в условиях морской нефтедобычи", *Нефтяное Хозяйство*, № 11, с. 140 - 142, 2017.

[2] А.Г. Ахмадеев, Тонг Кань Шон, и С.А.

Иванов, "Комплексный подход к обеспечению транспортировки высокопарафинистых нефтей шельфовых месторождений", *Нефтяное Хозяйство*, № 6, с. 100 - 103, 2015.

[3] Từ Thành Nghĩa, Phạm Bá Hiển, Phạm Xuân Sơn, Tống Cảnh Sơn, Nguyễn Hoài Vũ, Ngô Thường San, Nguyễn Văn Minh, và Nguyễn Thúc Kháng, "Những khó khăn, thách thức của Vietsovpetro trong vận chuyển dầu nhiều paraffin bằng đường ống ngầm ngoài khơi", *Tạp chí Dầu khí*, Số 5, trang 20 - 25, 2015.

[4] Phung Dinh Thuc, Ha Van Bich, Tong Canh Son, V.P.Vygovskoy, and Le Dinh Hoe, "A new approach to study on thixotropic properties of waxy crude oil from Dragon and White Tiger fields offshore Vietnam", *SPE Asia Pacific Oil and Gas Conference and Exhibition, Jakarta, Indonesia, 20 - 22 April, 1999*.

[5] Phung Dinh Thuc, Ha Van Bich, Tong Canh Son, Le Dinh Hoe, and V.P.Vygovskoy, "The problem in transportation of high waxy crude oils through submarine pipelines at JV Vietsovpetro oil fields, offshore Vietnam", *Journal of Canadian Petroleum Technology*, Volume 42, Issue 6, pp. 15 - 18, 2003.

[6] Nguyen Thuc Khang, Ha Van Bich, Tong Canh Son, and Le Dinh Hoe, "Transporting oil and gas mixture in gathering system at White Tiger oil field", *SPE Asia Pacific Oil and Gas Conference and Exhibition, Jakarta, Indonesia, 9 - 11 September, 2003*.

[7] Nguyen Thuc Khang, Ha Van Bich, Tong Canh Son, Le Dinh Hoe, and Phung Dinh Thuc, "A new approach for regime optimization of oil and gas mixture pipeline transportation", *SPE Asia Pacific Oil and Gas Conference and Exhibition, Perth, Australia, 18 - 20 October, 2004*.

[8] Tong Canh Son, Le Dinh Hoe, and Nguyen Quang Vinh, "Schematic of oil and gas transportation from Nam Rong - Doi Moi to RP-1 of Rong oil field subsea pipelines from a marginal offshore oil field", *Petrovietnam Journal*, Volume 10, pp. 38 - 43, 2015.

RESEARCH AND APPLICATION OF HIGH-PERFORMANCE DRILLING FLUID SYSTEMS IN VIETSOVPETRO JOINT VENTURE

Hoang Hong Linh, Bui Van Thom, Mai Duy Khanh, Pham Dinh Lo

Vietsovpetro Joint Venture

Email: linh.h.rd@gmail.com

<https://doi.org/10.47800/PVSI.2024.06-07>

Summary

Since 2015, starting with the KGAC system, the authors of Vietsovpetro have diligently researched and rationally combined conventional and modern drilling fluid (DF) systems. As the result, the KGAC was upgraded to the KGAC Plus. Then, during the testing and application of the KGAC and KGAC Plus systems to more than 100 wells, some adjustments to the system composition were made and KGAC Plus was improved to KGAC Plus M1. Particularly, Polyhib was used instead of NaOH and AKK to regulate the pH degree and prevent the clay from swelling. Not satisfied with the achievement, the Vietsovpetro team continued to study and test to advance KGAC Plus M1 to KGAC Plus M1*, which has greatly improved the drilling quality and efficiency at Vietsovpetro.

Key words: Water-based drilling fluid, clay inhibitive chemicals, anti-bit balling (anti-accretion) chemicals, borehole stability, thermal stability.

1. Drilling fluid system KGAC

1.1. General information

The KGAC drilling fluid system uses two inhibitors (FCL, AKK) of the traditional FCL-AKK system and two inhibitors (KCl, Glycol) of the advanced KCl/glycol system. In KGAC, FCL inhibits by dispersion mechanism, AKK by flocculation, KCl by binding K⁺ ions, glycol by forming a film around the clay components. All 4 inhibitory agents are compatible with each other and with other components such as xanthangum, PAC-LV, lubricants, etc. in the KGAC system. After the laboratory test, the KGAC drilling fluid system was applied at 2 wells of Vietsovpetro with very good results, significantly reducing complexity and non-production time. Its calculated economic efficiency yielded a million dollars. Since then, the KGAC system has been widely used in more than 50 wells of Vietsovpetro.

1.2. Laboratory testing results of drilling fluid system KGAC

The KGAC drilling fluid system is analyzed, tested and compared to 3 systems of FCL/AKK, Glydril, Ultradril.

All the drilling fluid systems are prepared on freshwater base. Their parameters are measured at 25°C before heating. Then, the samples were hot rolled in a roller oven at 130°C for 40 hours. After heating, the parameters are re-checked, especially the swelling degree of clay (clay inhibition test).

Testing results of main parameters are shown in Table 1 and Figures 1 - 3

Table 1. Parameters of drilling fluids systems before and after heating

No.	System	Fluid loss		YP		Gel _{1/10}	
		Before heating	After heating	Before heating	After heating	Before heating	After heating
1	GLYDRIL	5	5	33	30	7/9	7/8
2	ULTRADRIL	5	5	43	39	8/12	7/11
3	FCL/AKK	4.5	8	7	9	3/5	1/2
4	KGAC	5.2	5.7	28	26	9/11	8/12

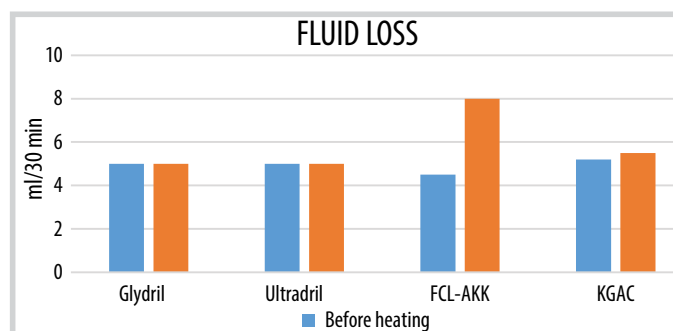


Figure 1. Fluid loss.



Date of receipt: 3/1/2024.

Date of review and editing: 3/1 - 6/2/2024.

Date of approval: 6/2/2024.

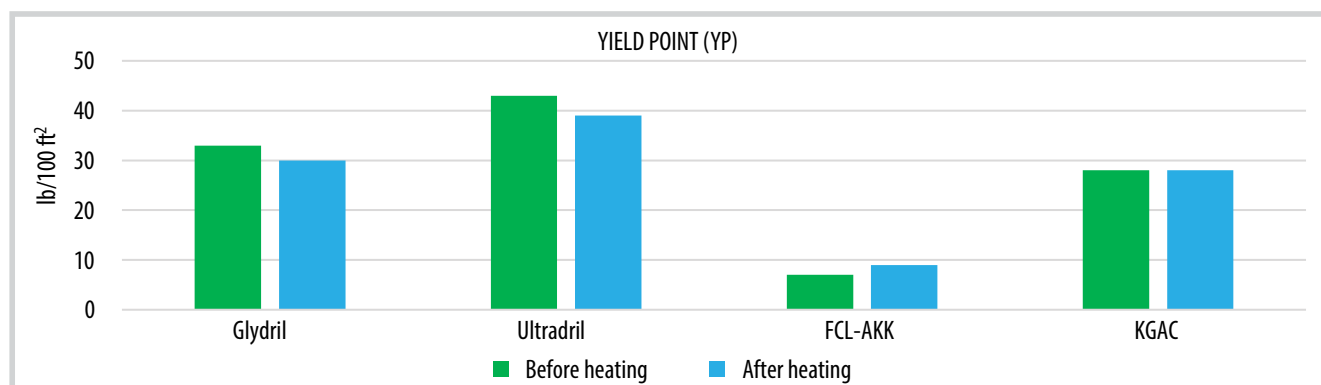


Figure 2. Yield point (YP) of drill water-based drilling fluid system.

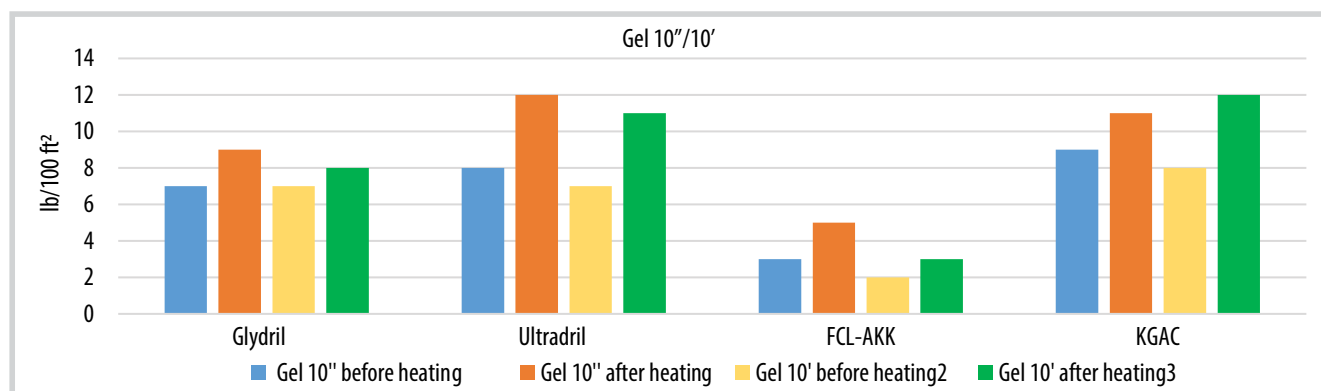


Figure 3. Gel 10''/10'' of drill water-based drilling fluid systems.

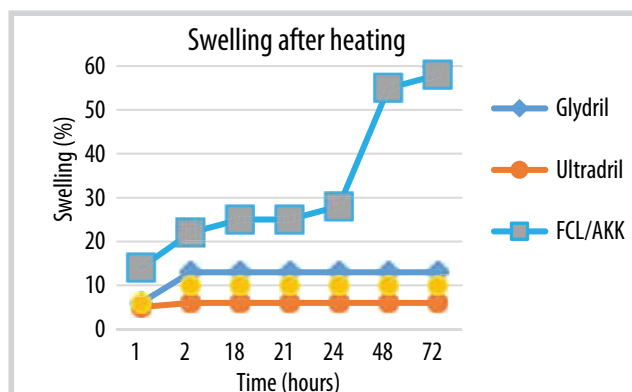
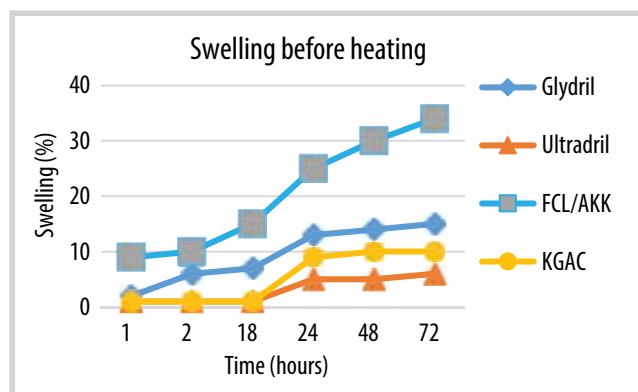


Figure 4. Comparison of clay swelling between drilling fluids systems (before and after heating).

The obtained results (Figures 1 - 3) show that the new inhibitor drilling fluid system KGAC is superior to the traditional FCL/AKK and equivalent to Glydril system, which was widely used by contractors at Vietsovetro's wells, as below.

- Fluid loss: The fluid loss value is equivalent to other systems before heating, while better than the FCL/AKK and comparable to the Glydril after heating.
- Yield point (YP): Both values before and after heating are much better than that of FCL/AKK system, and equivalent to Glydril system.
- Gel: The value shows that the DF is thermally stable

after heating, better than the FCL/AKK and equivalent to the Glydril.

The experiment comparing the degree of clay swelling inhibition between some advanced systems is conducted on a swellmeter: The clay sample used is activated clay and compressed at 6,000 psi (408 atm). With geological conditions of Vietsovetro's wells, the experimental conditions are equivalent to the Oligocene layer containing many active clays. Exposure time of clay core samples in drilling fluid is up to 72 hours.

The new DF system KGAC (Figure 4) has shown high swelling inhibition level, equivalent to and somewhat

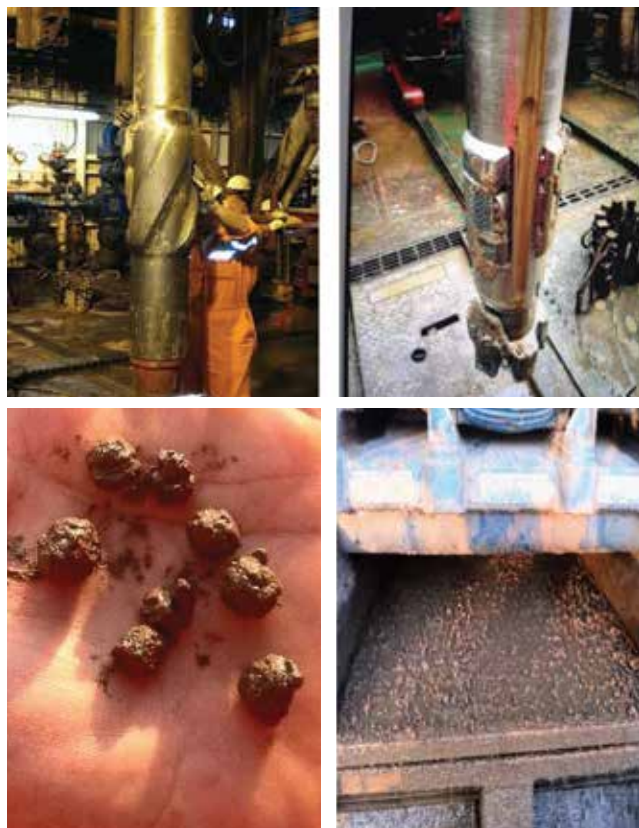


Figure 5. Field tests on Tam Dao 2 rig: There was very little clay adhesion on BHA pulled out, drilled cuttings were well inhibited, dry and nonsticky.

superior to the Glydril system of MI-SWACO company. The authors conducted a series of experiments with different concentrations and mixing sequences in order to select one recipe that suits the technical requirements of Vietsovpetro.

1.3. Field-test results

From the positive results in the laboratory, KGAC DF system were then applied in 2 wells on Tam Dao 2 rig. The tests at these 2 wells were both successful, achieving technical requirements, lower cost and less negative impact on the environment. Some actual results are presented in Figures 5 and 6.

The actual values of the DF parameters in Figure 6 show that the KGAC meets technical requirements when drilling Vietsovpetro's wells. They fall within design range and are quite stable throughout the drilling period. After successful field tests, in 2015, KGAC system was widely applied in many wells of Vietsovpetro with positive results.

1.4. Initial economic efficiency

To initially evaluate the economic efficiency of the KGAC, the authors make a comparison between the cost

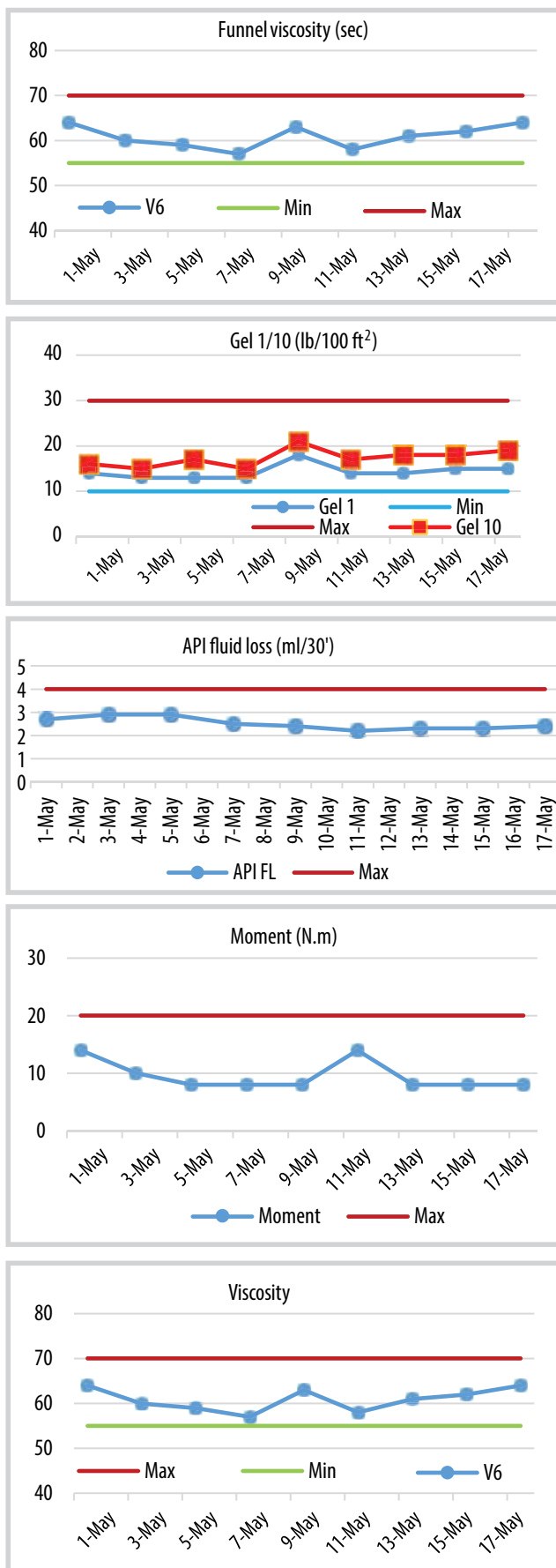


Figure 6. Actual parameters of KGAC DF when applied to well drilling.

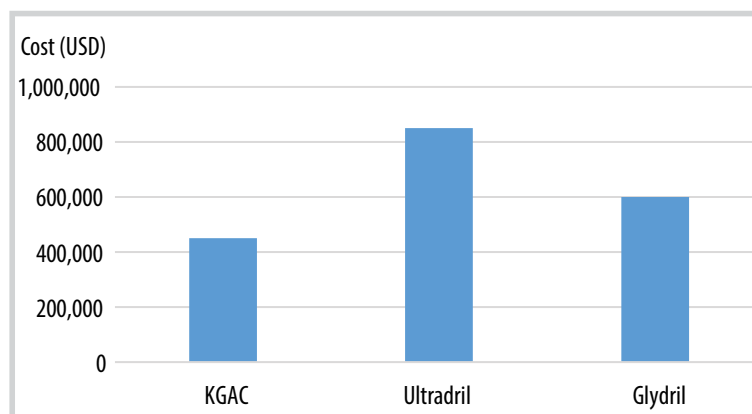


Figure 7. Cost comparison of DF systems.

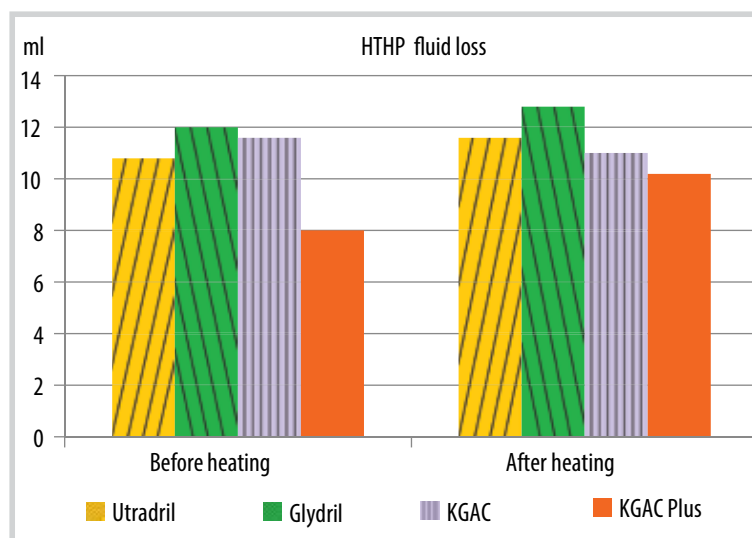
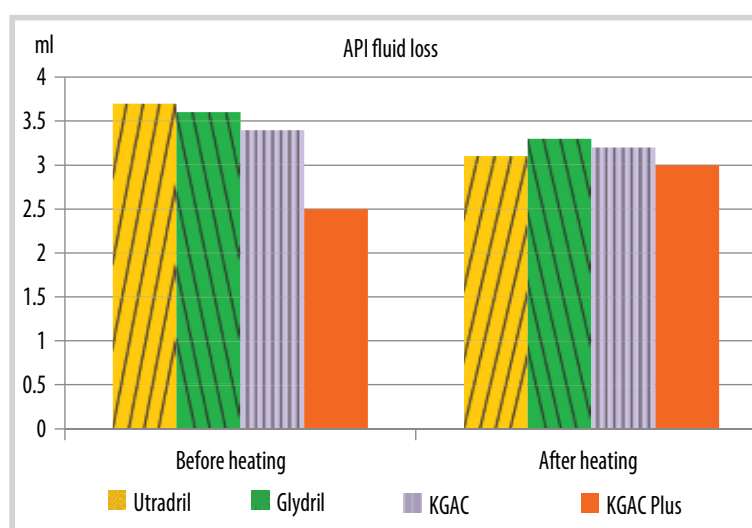


Figure 8. API and HTHP fluid loss of DF systems (before and after heating).

of DF service at well A1 (using Glydril system) and that of self-service construction at well A2 (using KGAC system). These two wells are drilled by the same rig in similar geological conditions (Figure 7).

In fact, during well completion, the highest cost is typically the 12¼" and 8½" sections (when drilling through active clay

formations). Through the wells, on average, about 1,000 m³ of DF must be used to drill this stage. Using the KGAC solution system can save about USD 160,000 compared to the Glydril.

2. KGAC Plus drilling fluid system

2.1. General information

The Vietsovpetro drilling fluid team continued their research and added the encapsulation inhibitor chemical HyPR-CAP, which is analogous to ID-CAP D in the Glydril system or ULTRACAP in the Ultradril system. This chemical is compatible with other components of the KGAC and the KGAC Plus system was created, which has the quality equivalent to the best water-based drilling fluid system currently used on the Vietnamese continental shelf. In the first year of use, the KGAC Plus drilling fluid system successfully maintained its cost-effectiveness, reaching more than USD 2 million. In 2018, two drilling fluid systems KGAC and KGAC Plus were certified for ecological and environmental safety and awarded a gold medal by the World Intellectual Property Organization (WIPO).

2.2. Laboratory testing results of KGAC Plus system

Encouraged by the success of the KGAC system, the authors have investigated adding a new encapsulation inhibitor component HyPR-CAP with different concentrations and mixing processes. Compatibility, stability of DF parameters, inhibition ability, thermal stability, lubricity, etc. were studied in comparison with ULTRADRIL and some other advanced DF systems. Testing results are shown in Figures 8 - 10.

From Figures 8 - 10, we can see that:

- API and HTHP fluid loss are better when compared to other systems.
- Rheological properties and lubricity of KGAC Plus system are improved compared to KGAC and equivalent to Ultradril.
- The inhibition ability of KGAC Plus system is improved compared to KGAC and comparable to Ultradril.

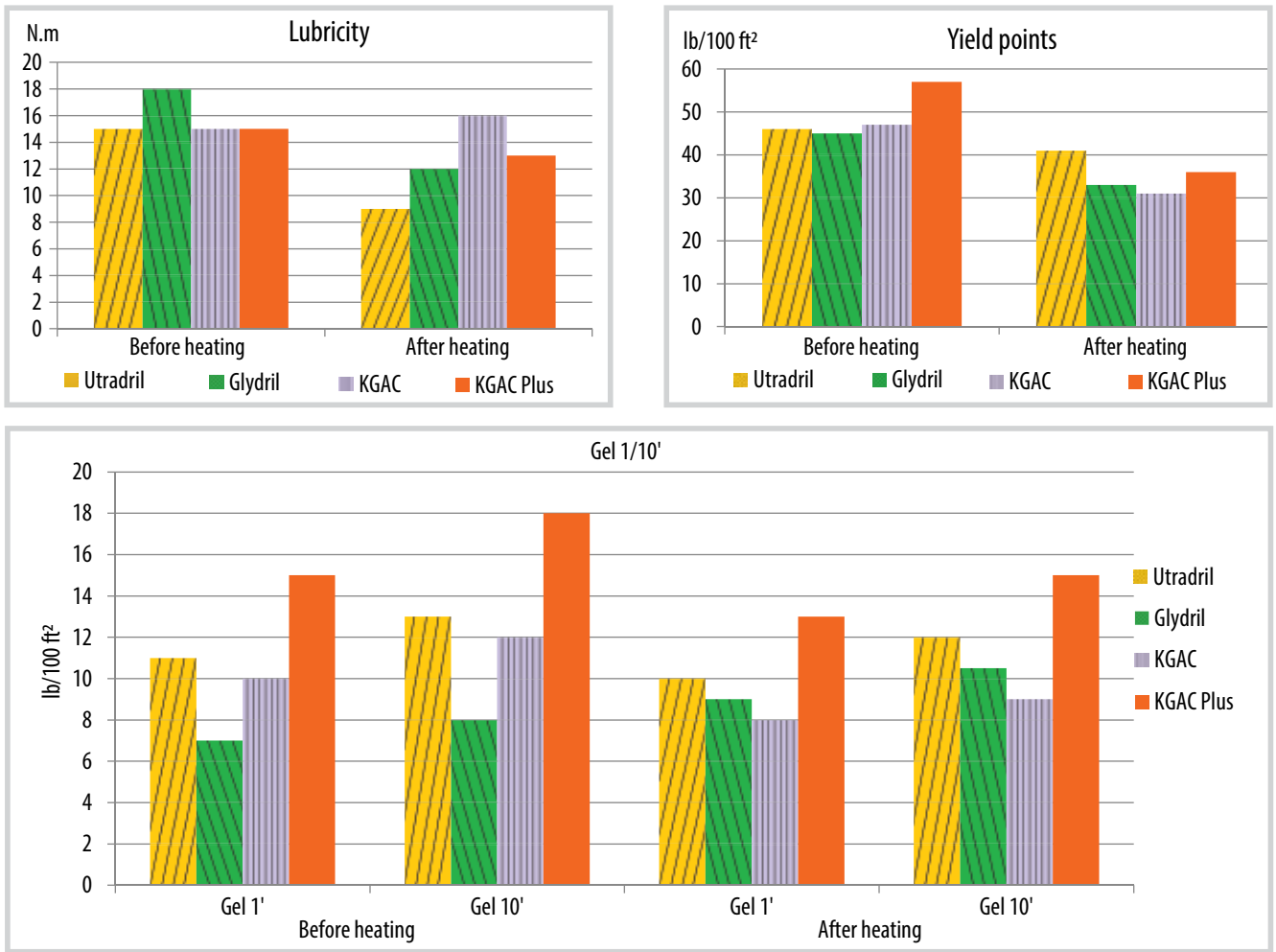


Figure 9. Rheological properties (YP, Gel) and lubricity of DF systems.

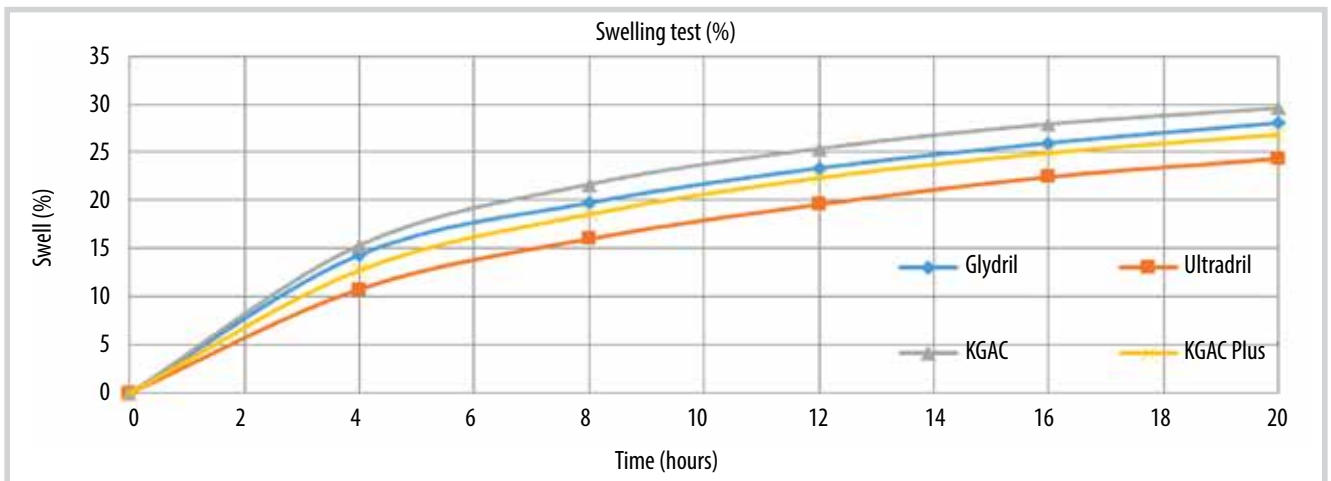


Figure 10. Inhibition ability of DF systems.

2.3. Field test results

The KGAC Plus DF system was successfully field-tested for drilling 2 wells using Tam Dao-03 and Cuu Long rigs. No complications or problems occurred during the drilling and casing of these wells.

Figure 11 shows that the parameters of DF KGAC Plus during field tests are stable within the design values.

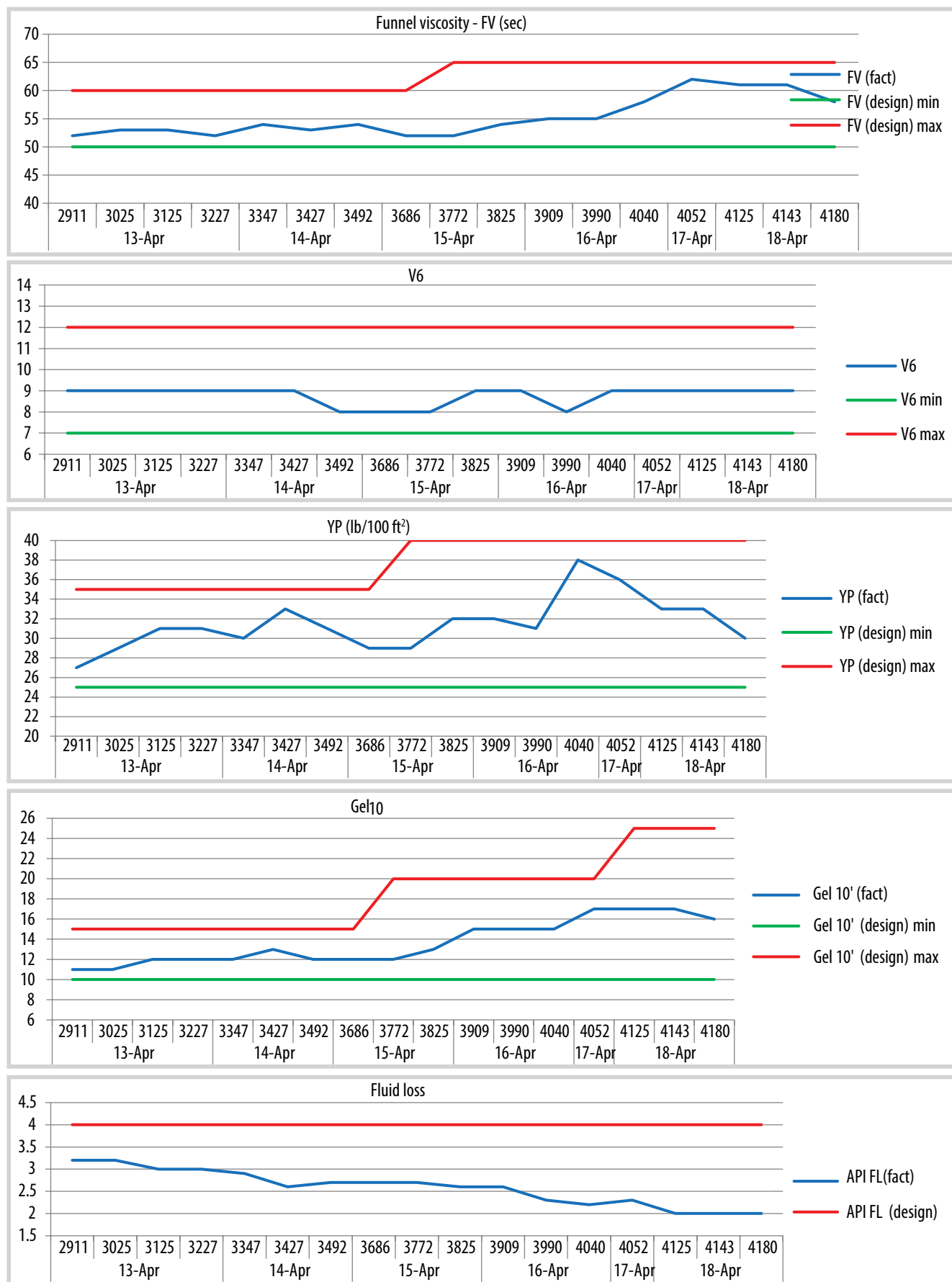


Figure 11. Parameters of KGAC Plus DF during field tests.

2.4. Initial economic efficiency

Experimental results show that the quality of the KGAC Plus system is equivalent to Ultradril (the best water-based inhibitive system currently offered by MI SWACO-USA and applied worldwide). Figure 12 shows that the cost of preparing the KGAC Plus system is only about 60% of that of Ultradril. If this system is applied, about USD 300,000 per well can be saved, not counting other factors. With an annual average construction rate of 20 - 25 wells, Vietsovpetro is expected to save about USD 6 - 7 million per year.

2.5. Eco-environment safety certificate of DF systems KGAC and KGAC Plus

After successful application at the fields, samples of DF systems KGAC and KGAC Plus were sent to the Research and Development Center for Petroleum Safety and Environment - Vietnam Petroleum Institute (CPSE VPI) for analysis and assessment of ecological safety level.

The toxicity of these 2 DF samples against marine algae *Skeletonema* and larvae of Black tiger shrimp *Penaeus monodon* was assessed in accordance with the quality management standard procedures ISO 9001: 2008 and TCVN ISO/IEC 17025: 2007. Conclusions of CPSE-VPI stated: "Based on the acute toxicity test results against marine algae *Skeletonema* and larvae of the Black tiger shrimp *Penaeus monodon*, the KGAC and KGAC Plus DF systems are classified in group E - the best group according to the toxicological classification system OCNS (Offshore Chemicals Notification Scheme, UK)".

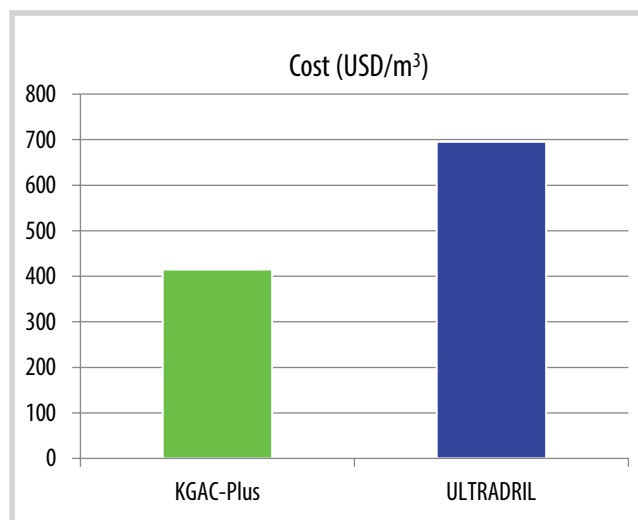


Figure 12. Cost comparison of KGAC Plus and Ultradril systems.

3. KGAC Plus M1 drilling fluid system

3.1. General information

KGAC Plus M1 DF system has changed in composition compared to KGAC Plus system. Specifically, Polyhib is used as an alternative to NaOH and AKK to maintain pH value and inhibit clay swelling. Its inhibition mechanism is the formation of ionic bonds by NH_2^+ . KGAC Plus M1 system is being successfully applied to drill more than 100 wells of Vietsovpetro. In 2020, this fluid drilling system won the first prize at the National Technical Innovation Contest (VIFOTEC).

3.2. Laboratory test results of KGAC Plus M1 system

The results of laboratory test on the degree of clay swelling inhibition of KGAC Plus M1 system compared with other systems are presented in Figure 13.

Research and experimental results show that the new inhibitor system KGAC Plus M1 is superior to Vietsovpetro's other KGAC systems and is equivalent to Ultradril of MI SWACO company.

3.3. Field-test results of KGAC Plus M1 system

KGAC Plus M1 system was field-tested at 2 wells with results presented in Figures 14 and 15.

During the drilling of the test well, DF parameters were stable within the allowable design value and met the technical requirements.

3.4. Economic efficiency

Experimental and field-test results show that the quality of KGAC Plus M1 system is equivalent to that of Ultradril (the best water-based DF system available

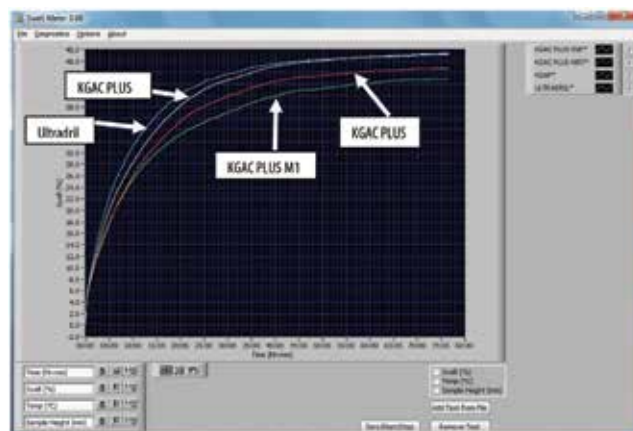


Figure 13. Laboratory testing results on the degree of clay swelling inhibition of KGAC Plus M1 system compared with other systems.



Figure 14. Clean BHA without adhering clay.



Figure 15. Drilled cuttings were well inhibited, dry and not sticky.

currently). KGAC Plus M1 system with cost of 357 USD/m³ is much cheaper than Ultradril with 698 USD/m³. Typically, about 1,000 - 1,500 m³ of inhibitive DF is needed to drill sections with highly active shale. Therefore, if KGAC Plus M1 system is applied, it can save about USD 340,000 - 520,000, not to mention other factors (dilution level, thermal stability, clay tolerance, rig rental time, labor, etc.).

Based on actual consumption, the chemicals cost of KGAC Plus M1 system for 4 field-test wells is USD 933,496, compared to USD 2,467,092 for drilling 4 wells with similar conditions using the Ultradril system or equivalent. Thus, about USD 1,500,000 is saved. On average, annually Vietsovetro constructs about 20 wells, therefore, it is expected to save around USD 8 million per year.

4. KGAC Plus M1* drilling fluid system

To enhance the quality and effectiveness of the KGAC Plus M1 DF system, Vietsovetro's DF team has conducted research and experiments to upgrade the system to KGAC Plus M1* DF.

4.1. To improve inhibitive level

Experiments were conducted to find a suitable polyamine inhibitor to replace Polyhib in KGAC Plus M1 system:

Table 2. Cuttings dispersion test results

	KCl 7%	Poly-Hib	EC301	VH-258	Ultrahib
Initial mass of cuttings (g)	30	30	30	30	30
Dried cuttings remaining on 150 µm sieve (g)	9.8	23.7	25.2	27.55	24.35
% reserved	32.67	79	84	91.83	81.17



Figure 16. Anti-accretion test in KGAC Plus M1 DF system.

Table 3. Anti-accretion test in KGAC Plus M1 DF system

	Base mud	3% Ultrafree	3% Vietfree
Accreted shale (g)	18	0.5	5
Anti-accretion percentage (%)	-	97.2	72

Once extracted from the formation, water will be absorbed into drilled cuttings, causing them to disperse into smaller particles. One function of the inhibitors is to reduce the dispersion of drilled cuttings such that they are large enough to be removed from the shale shaker.

In this experiment, artificial drilled cuttings were made from API bentonite with the size of 2 - 5 mm. A 30 g sample of artificial drilled cuttings was immersed in 450 ml of the test solution and rotated at 120°C for 4 hours in roller oven. Then, the solution and cuttings were filtered through a 150 µm sieve for 2 minutes using a dedicated vibrator. The cuttings remaining on the sieve were dried to a constant weight. The test solution was prepared on a 7% KCl solution, with polyamine chemical used at a 3% concentration. Experimental results are shown in Table 2.

Experimental results indicate that the polyamine inhibitors have a good effect in reserving drilled cuttings, in which the sample containing Viethib-258 is somewhat better than the sample containing Ultrahib. Additionally, it also shows that polyamine chemicals can be used effectively in combination with KCl.

4.2. To improve anti-accretion ability

Figure 16 and Table 3 show that the experimental

Table 4. DF samples after adding CaCO₃ F/M và Celba F/M

	Tam Dao 01 rig	Tam Dao 03 rig	Cuu Long rig
Before adding			
Mud cake durability (seconds)	26	31	28
Moment (lb.in)	130	145	125
After adding CaCO ₃ F/M and Celba F/M			
Mud cake durability (seconds)	56	62	61
Moment (lb.in)	95 - 100	90 - 100	80 - 85

Table 5. Test results of KGAC Plus M1* system

STT	Parameters	Unit	Results		Requirements
			Before heating	After heating 150°C/16 hours	
1	Density	g/cm ³	1.63	1.63	1.60 - 1.70
2	Funnel viscosity	Sec	76	68	60 - 70
3	API fluid loss	ml/30 minutes	2.8	3.2	≤ 3.5
4	Mud cake	mm	1	1	≤ 1.5
5	V600/V300	-	164/106	121/80	
6	PV	cP	58	41	ALAP
7	YP	lb/100 ft ²	48	39	40 - 50
8	V6		12	11	10 - 14
9	Gel 1/10'	lb/100 ft ²	11/24	10/15	10 - 16/12 - 25
10	pH	-	10	9.5	9.5 ± 0.5
11	Moment	N.m	15	14	≤ 20
12	Content of K ⁺	g/l	96	93	80 - 100
13	Content of Cl ⁻	g/l	70	70	≤ 80
14	MBT	Nm	20	22	≤ 35
15	HTHP FL 150°C@500psi	ml/30 minutes x 2	12.2	13.4	≤ 14

Table 6. DF parameters when drilling 2,846 - 4,627 m

Section		Parameters								
		γ (g/cm ³)	FV (seconds)	FL (cm ³ /30 minutes)	K (mm)	Gels _{1/10'} (lb/100 ft ²)	PV (cPs)	YP (lb/100 ft ²)	V6 (grad.)	pH
2846 - 3033 KGAC + M1*	Designed	1.12 - 1.14 ± 0.02	50 - 65	< 3.5	1	8 - 14/9 - 15	ALAP	25 - 40	8 - 12	9 ± 0.5
	Actual	1.14	58 - 61	3 - 3.5	1	8/9	28 - 31	35 - 38	8 - 9	9.5
3033 - 4011 KGAC + M1*	Designed	1.16 ± 0.02	50 - 65	< 3.5	1	9 - 14/9 - 16	ALAP	25 - 40	9 - 13	9 ± 0.5
	Actual	1.15 - 1.18	57 - 60	2.6 - 3.0	1	9/12	33 - 35	38 - 42	9 - 11	9.3
4011 - 4445 KGAC + M1*	Designed	1.18 ± 0.02	50 - 65	< 3.5	1	9 - 15/10 - 18	ALAP	25 - 40	9 - 13	9 ± 0.5
	Actual	1.19 - 1.23	56 - 59	2.6 - 2.8	1	10/13	33 - 36	40 - 44	10 - 11	9.1
4445 - 4627 KGAC + M1*	Designed	1.20 - 1.26 ± 0.02	55 - 70	< 3.5	1	9 - 15/10 - 22	ALAP	25 - 40	9 - 14	9 ± 0.5
	Actual	1.24 - 1.28	57 - 64	2.6 - 2.7	1	10/15	37 - 41	40 - 46	10 - 12	9.0
	BHA with 2 stabilizers	1.27	60 - 64	2.8 - 3.0	1	9/12	33 - 35	38 - 39	9 - 10	9.0

chemical samples (Ultrafree, Vietfree) used in the KGAC Plus M1 system reduce the ability of shale to adhere to metal surfaces.

4.3. To improve borehole stability

Improving the shale inhibition ability of KGAC Plus M1 system will contribute to the stability of the borehole. Through research, experiments and testing at wells, the inhibition ability of the KGAC Plus M1* system has been enhanced with polyamine-based chemicals. Moreover,

adding materials such as CaCO₃ F, CaCO₃ M and Celba F, Celba M help to increase durability of mud cake and reduce adhesion moment, ensuring borehole stability suitable for each specific geographical condition.

Experimental results in Table 4 show that, when DF sample is treated with 15 - 20 g/l CaCO₃ F/M and 3 - 5 g/l CelbaF/M, the durability of mud cake increases from 30 seconds to 60 seconds and the moment decreases from 140 - 150 lb.in to 90 - 100 lb.in. Vietsovpetro has applied this to process DF for many wells with high efficiency.

4.4. To improve thermal stability

KGAC Plus M1 DF system being applied in Vietsovetro can withstand temperature up to 130°C. In order to drill wells with temperatures up to 150°C, the authors have found new products that are equivalent to MI SWACO’s chemical, such as Oxoscav 5000, PTS 200, Resinex II, Soltex, Driscall D..., which are used intensively and or replace some components in KGAC Plus M1 to form a new system that can withstand temperatures up to 150°C.

Test results of KGAC Plus M1* system in Table 5 show that:

- DF parameters before and after heating at 150°C/16 hours meet technical requirements of the high-temperature wells up to 150°C.
- There is no sticky phenomenon due to thermal destruction of lubricant; torque parameter remains unchanged.

4.5. Field test results of KGAC Plus M1*

4.5.1. Parameters of DF KGAC Plus M1* in field test

Table 6 shows that DF parameters in the field test are within design ranges and stability.

4.5.2. Field test results

Drilling parameters in section 2,846 - 4,627 m:

- Average drilling rate: $1,781/71,6 = 24.9$ (m/hours);
- Average drilling rate per day: $1,781/7 = 254.4$ m

After reaching TD at 4,627 m, tripping and logging were performed without problem.

DF parameters were stable within design ranges; pH value and K⁺ ion content remained unchanged after long logging period.

Adding Tube Kleen along with lubricant did not cause any increase in DF viscosity or blockage of the shaker screens. However, after a long logging operation, blockage of the shaker screens occurred.

There was no bit- and BHA-balling (Figures 17 and 18).

DF system KGAC Plus M1* using polyamine-based inhibitor (Viethib-258) has been improved in shale inhibition ability; pH and rheology values are stable within technical ranges for drilling Vietsovetro’s wells.

Tube Kleen chemical has effect of anti-sticking on bit and stabilizer, improving mechanical drilling rate through lower Miocene thick shale layer.

Wellbore was stable after 60 hours of logging operation at hole temperature of 112°C. This means that Viethib-258 effectively inhibits clay swelling and helps to stabilize the action of polymers under well conditions. Thereby, dilution rate and consumption of chemicals were reduced compared to the KGAC Plus M1 DF system.

Therefore, the addition of new chemicals to the KGAC Plus M1 system has resulted in a new DF system, the KGAC Plus M1*. Laboratory experiments and field test results of KGAC Plus M1* system with innovative solutions as described above have confirmed the effectiveness of the new DF system. Specifically, clay inhibition ability, anti-accretion and anti-bit-balling effect, thermal stability and wellbore stability have all been improved.

5. Applicability

After being successfully researched and applied in many wells, KGAC Plus M1 DF system has been approved for widespread use in Vietsovetro’s wells. All three newly developed systems, KGAC, KGAC Plus, and KGAC Plus M1, meet all economic and technical criteria while ensuring safety for humans and the ecological environment.

Since 2019, these DF systems have been



Figure 17. No bit-balling while drilling.



Figure 18. Clean stabilizer.

widely applied in Vietsovpetro's wells, not only replacing the need to hire external DF services but also providing DF services to other partners.

6. Conclusions

Technical efficiency and applicability of the 4 high-performance DF systems KGAC, KGAC Plus and KGAC Plus M1 and KGAC Plus M1*: All 4 new DF systems are equivalent to or superior in some aspects to current high-quality advanced fluid systems, ensuring good drilling through highly active clay formations and complex geologic conditions. At the same time, all 4 DF systems are suitable for Vietsovpetro's technical conditions and ensure safety for the ecological environment. Depending on stratigraphic and geological conditions, selecting the right DF system helps save costs while still meeting the technical requirements of the well.

Economic and social efficiency: The application of the abovementioned 4 DF systems has achieved high economic efficiency, contributing to solve current problems and difficulties in the context of falling oil prices. Furthermore, Vietsovpetro has trained a team of highly qualified DF specialists capable of executing DF packages for oil and gas wells without hiring external DF services. Especially, it is possible to use materials and chemicals available on the Vietnamese market and completely master the technology to drill complex wells.

References

- [1] Viện Dầu khí Việt Nam, "Báo cáo đánh giá độc tính sinh thái của hệ dung dịch KGAC và KGAC-Plus", 2017.
- [2] Xí nghiệp Khoan và Sửa giếng, "Hướng dẫn điều chế và xử lý dung dịch khoan", 2009.
- [3] Xí nghiệp Khoan và Sửa giếng, "Quy trình điều chế và xử lý hệ dung dịch KGAC", 2016.
- [4] Ngô Văn Tự, Hoàng Hồng Lĩnh, và Nguyễn Xuân Ngọ, "Các vấn đề nhằm làm ổn định thành giếng khi thi công các giếng khoan có độ xiên lớn tại mỏ Bạch Hổ", Hội nghị cơ học đá toàn quốc lần thứ III, trang 192 - 206.
- [5] А.И. Булатов, А.И. Пеньков, и Ю.М. Проселков, *Справочник по промывке скважин*. Москва "Недра", 1984.
- [6] Tổng công ty Dầu khí Việt Nam, "Hướng dẫn thực hiện các quy định về bảo vệ môi trường liên quan đến sử dụng và thải hóa chất, dung dịch khoan trong các hoạt động dầu khí ngoài khơi Việt Nam", 2005.
- [7] Vietsovpetro, "Báo cáo tổng hợp kết quả áp dụng hệ dung dịch KGAC, KGAC-Plus tại các giếng khoan của Vietsovpetro", 2014 - 2016.
- [8] Hoàng Hồng Lĩnh, Nguyễn Thành Trường, Bùi Văn Thơm và Nguyễn Xuân Quang, "Nghiên cứu áp dụng hệ dung dịch KGAC cho những giếng khoan dầu khí tại Vietsovpetro", Hội thi sáng tạo kỹ thuật toàn quốc lần thứ 13, 2014.
- [9] Hoàng Hồng Lĩnh, Nguyễn Thành Trường, Nguyễn Xuân Quang, Bùi Văn Thơm, Vũ Văn Hưng và Phạm Đình Lơ, "Nghiên cứu thí nghiệm và đề xuất áp dụng hệ dung dịch KGAC-Plus cho những thành hệ sét hoạt tính mạnh", Giải thưởng sáng tạo khoa học công nghệ Việt Nam (VIFOTEC), 2016.
- [10] MI SWACO "Ultradril - High performance water-base mud", 2015.
- [11] Ryen Caenn, H.C.H. Darley, and George R. Gray, *Composition and properties of drilling and completion fluids, 6th edition*. Gulf Professional Publishing, 2011.
- [12] Ngo Van Tu, Hoang Hong Linh, and etal., "Experiences of using non-clay polymer drilling fluids for highly deviated drilling in Vietsovpetro", *Proceedings of Conference on Vietnam Petroleum Institute 20 years development and prospects, Hanoi, 1998*, pp. 367 - 374.
- [13] Tạ Đình Vinh, "Dung dịch khoan cho các giếng khoan ngang", *Tạp chí Dầu khí*, Số 3, trang 21 - 25, 1995.
- [14] MI SWACO, "Drilling fluids manual", 1995.
- [15] MI SWACO, "Drilling fluids solutions", 2008.
16. Hoàng Hồng Lĩnh, Bùi Văn Thơm, Vũ Văn Hưng, Mai Duy Khánh và Phạm Đình Lơ, "Nghiên cứu, áp dụng hệ dung dịch KGAC Plus M1 tại các giếng khoan của Vietsovpetro", Hội thi sáng tạo kỹ thuật toàn quốc lần thứ 15, 2018 - 2019.

QUANTITATIVE ASSESSMENT OF A NOVEL METHOD FOR FLUID THERMODYNAMIC TEST SIMULATION IN MULTICOMPONENT SYSTEMS

Ta Quoc Dung^{1,2}, Pham Phuoc Tinh¹, Le The Ha³

¹Ho Chi Minh City University of Technology (HCMUT)

²Vietnam National University Ho Chi Minh City (VNUHCM)

³Vietnam Oil and Gas Group

Email: tqdung@hcmut.edu.vn

<https://doi.org/10.47800/PVSI.2024.06-08>

Summary

This paper presents a quantitative methodology for simulating fluid thermodynamic tests, including constant composition expansion (CCE), differential liberation (DL), and separator tests, within multicomponent systems. The approach combines equilibrium ratios, flash calculations, and the Peng-Robinson equation of state. Utilizing the PVTp (Pressure - Volume - Temperature) package regression procedure enables the calibration of OmegaA and OmegaB values, enhancing accuracy and minimizing error margins in fluid thermodynamic calculations compared to empirical data. Numerical results demonstrate the effectiveness of this method. Bubble point pressure values from observed, software-generated, and calculated data are 2344, 2339, and 2350.42 psia, respectively. Calculated fluid thermodynamic test results closely align with software predictions and exhibit acceptable error levels compared to the measured data. However, discrepancies in the solution gas - oil ratio during the DL test highlight the need for more comprehensive measured data to improve simulation accuracy and reduce error margins. The comparison between the proposed methodology and collected data confirms the effectiveness of integrating equilibrium ratios, flash calculations, and the Peng-Robinson equation of state for precise fluid thermodynamic calculations. This approach offers a quantitative framework for simulating fluid thermodynamic tests, providing insights while reducing reliance on costly laboratory experiments.

Key words: Fluid thermodynamic tests, CCE test, DL test, separator test, equilibrium ratio, flash calculation, Peng-Robinson EOS.

1. Introduction

In the realm of reservoir engineering, the composition of reservoir fluids varies widely, encompassing a diverse array of hydrocarbons and non-hydrocarbons, thereby introducing significant chemical complexity. To address this complexity and gain insights into the phase behavior of such intricate fluids, equations of state have emerged as valuable tools. These equations establish precise mathematical relationships between pressure, volume, and temperature, enabling the comprehensive modeling of volumetric characteristics, vapor - liquid equilibria, and thermal properties, both for pure substances and complex mixtures [1].

In the field of petroleum engineering, the application of equations of state is a common practice in the computation of various tests, including the constant composition expansion (CCE), differential liberation (DL), and separator tests [2]. These tests serve as indispensable tools for elucidating volumetric behavior, vapor - liquid equilibria, and thermal properties of reservoir fluids. Typically, conducting these tests in a laboratory necessitates the use of expensive PVT (pressure - volume - temperature) equipment and the expertise of skilled personnel [3, 5]. However, the application of an equation of state offers a compelling alternative by enabling the simulation of these tests based on specific hydrocarbon composition data, thus providing a cost-effective and efficient means to glean valuable insights [6].



Date of receipt: 8/1/2024.

Date of review and editing: 8/1 - 21/2/2024.

Date of approval: 21/2/2024.

2. Methodology

2.1. Laboratory thermodynamic test for multi-component hydrocarbon system

2.1.1. Principle of constant composition expansion test

Constant composition expansion experiments on gas condensates or crude oil are carried out to replicate the pressure - volume relationships of these hydrocarbon systems. The test is performed to determine:

- Saturation pressure (bubble point or dew point pressure).
- Single-phase fluid isothermal compressibility coefficients in excess of saturation pressure...

The ratio of the reference volume signifies the hydrocarbon system's volume in relation to the cell pressure. This critical parameter is known as the relative volume and can be expressed mathematically as follows [1]:

$$V_{rel} = \frac{V_t}{V_{sat}} \quad (1)$$

Where:

V_{rel} : Relative volume

V_t : Total hydrocarbon volume

V_{sat} : Volume at the saturation pressure

At saturation pressure, the relative volume is equal to 1. This test is also known as flash liberation, flash vaporization, or flash expansion.

It should be emphasized that no hydrocarbon material is taken from the cell; therefore, the composition of the overall hydrocarbon mixture in the cell stays constant.

The density of the oil may be determined above the bubble point pressure using the observed relative volume:

$$\rho = \frac{\rho_{sat}}{V_{rel}} \quad (2)$$

Where

ρ : Density at any pressure above the saturation pressure

ρ_{sat} : Density at the saturation pressure

V_{rel} : Relative volume

Smoothing is commonly required to adjust laboratory mistakes in estimating total hydrocarbon volume immediately below saturation pressure and at lower

pressures. To smooth the values of the relative volume, a dimensionless compressibility function, also known as the Y-function, is utilized. In its mathematical form, the function is only defined below the saturation pressure and represented by the expression:

$$Y = \frac{p_{sat} - p}{p(V_{rel})} \quad (3)$$

The Y-function, displayed on a Cartesian scale as a function of pressure, effectively smooths relative volume data below saturation pressure. Graphically, the Y-function typically appears as a straight line or exhibits slight curvature. The following steps outline the simple process for smoothing and correcting relative volume data [1]:

Step 1: Utilizing equation (3), compute the Y-function values for all pressures falling below the saturation pressure.

Step 2: On a Cartesian scale, construct a plot illustrating the relationship between the Y-function and pressure.

Step 3: Determine the coefficients for the best-fit line, expressed as:

$$Y = a + bp \quad (4)$$

Here, 'a' and 'b' correspond to the intercept and slope of the linear regression, respectively.

Step 4: Re-evaluate the relative volume at all pressures below the saturation point using the Expression (5):

$$V_{rel} = 1 + \frac{p_{sat} - p}{p(a + bp)} \quad (5)$$

Isothermal compressibility coefficients are used to solve numerous reservoir engineering problems, including transient fluid flow difficulties, and to determine the physical parameters of undersaturated crude oil.

The isothermal compressibility (c) of a material can be precisely described through the mathematical expression:

$$c = -\frac{1}{V} \left(\frac{\partial V}{\partial p} \right)_T \quad (6)$$

To calculate the isothermal compressibility coefficient (c_o) for the oil phase above the bubble point, you can use one of these equivalent equations:

$$c_o = -\frac{1}{V} \left(\frac{\partial V}{\partial p} \right)_T \quad (7)$$

$$c_o = -\frac{1}{B_o} \left(\frac{\partial B_o}{\partial p} \right)_T \quad (8)$$

$$c_o = - \frac{1}{\rho_o} \left(\frac{\partial \rho_o}{\partial p} \right)_T \quad (9)$$

$$c_o = - \frac{1}{B_o} \frac{\partial B_o}{\partial p} + \frac{B_g}{B_o} \frac{\partial R_s}{\partial p} \quad (10)$$

Where:

c_o : Isothermal compressibility

B_o : Oil formation volume factor

B_g : Gas formation volume factor

T: Temperature

p: Pressure

Equations (6) - (10) define oil compressibility, which may be expressed in terms of relative volume as:

$$c_o = - \frac{1}{V_{rel}} \frac{\partial V_{rel}}{\partial p} \quad (11)$$

The relative volume above the bubble point pressure is commonly displayed as a function of pressure. To evaluate c_o at any pressure p, all that is required is to draw a tangent line and determine the slope of the line, i.e. $\frac{\partial V_{rel}}{\partial p}$.

It should be noticed that it lists the compressibility coefficient at various pressure levels. These values are calculated by computing the changes in relative volume at the specified pressure intervals and assessing the relative volume at the lower pressure, or

$$c_o = \frac{-1}{[V_{rel}]_2} \frac{[V_{rel}]_1 - [V_{rel}]_2}{p_1 - p_2} \quad (12)$$

with the subscripts 1 and 2 demonstrating the values at the higher and lower pressure ranges, respectively.

2.1.2. Principle of Differential Liberation (DL) test

The solution gas liberated from an oil sample during a pressure drop is constantly removed from contact with the oil before achieving equilibrium with the liquid phase in the differential liberation process. The overall hydrocarbon system's composition varies during this sort of escape. The test produced the following experimental outcomes:

- Gas concentration in solution is a function of pressure.
- Oil volume shrinkage is a function of pressure.
- Properties of the evolved gas, such as the composition of the liberated gas, the gas compressibility factor, and the gas-specific gravity.

- The remaining oil's density is a function of pressure.

The differential liberation test is thought to better represent the separation process occurring in the reservoir and to model the flowing behavior of hydrocarbon systems above the critical gas saturation. When the saturation of the liberated gas reaches the critical value, it begins to flow, leaving behind the oil that initially housed it. This is due to the fact that gasses have better mobility than oils in general. As a result, this behavior is consistent with the differential liberation sequence [1].

2.1.3. Principle of separator test

Separator tests are performed to examine how the volumetric behavior of reservoir fluid changes as it flows through the separator (or separators) and into the stock tank. The resultant volumetric behavior is heavily impacted by the surface separation facilities' working parameters, such as pressures and temperatures. The main objective of conducting separator tests is to give the critical laboratory information required to determine the appropriate surface separation conditions that will enhance stock-tank oil output. Furthermore, when the test findings are properly integrated with the differential liberation test data, they give a method of getting the PVT parameters (B_o , R_s , and B_t) necessary for petroleum engineering calculations. Only the original oil at the bubble point is used in these separation tests [1].

2.2. Equilibrium ratios and flash calculation

2.2.1. Equilibrium ratio for ideal gas

In the context of multicomponent systems, the equilibrium ratio K_i is established as the ratio of a component's mole fraction in the gas phase (y_i) to its mole fraction in the liquid phase (x_i). This mathematical relationship is formally expressed as follows [2]:

$$K_i = \frac{y_i}{x_i} \quad (13)$$

For pressures below 100 psia, Raoult's and Dalton's laws provide a simple way to calculate equilibrium ratios. Raoult's law states that the partial pressure (P_i) of a component in a multicomponent system is the product of its mole fraction in the liquid phase (x_i) and its vapor pressure (P_{vi}).

$$P_i = x_i P_{vi} \quad (14)$$

Conversely, Dalton's law states that the partial pressure of a component is calculated by multiplying its mole

fraction in the gas phase (y_i) by the total pressure of the system (P):

$$p_i = y_i p \tag{15}$$

Where 'p' represents the total system pressure in psi.

At a state of equilibrium, in accordance with the aforementioned principles, the partial pressure exerted by a component in the gas phase is required to be equal to the partial pressure exerted by the same component in the liquid phase. Combining the equations that characterise these two fundamental laws yields the expression:

$$x_i p_{vi} = y_i p \tag{16}$$

Upon rearranging this relationship and incorporating the concept of the equilibrium ratio, the equation can be reformulated as follows:

$$\frac{y_i}{x_i} = \frac{p_{vi}}{p} = K_i \tag{17}$$

For ideal solutions, the equilibrium ratio depends only on system pressure (p) and temperature (T) regardless of the overall composition of the hydrocarbon mixture since the vapor pressure of a component is solely temperature-dependent.

The total number of moles in the system is defined as:

$$n = n_L + n_V \tag{18}$$

Where 'n' represents the total number of moles in the system, 'n_L' is the total number of moles in the liquid phase, and 'n_V' denotes the total number of moles in the vapor phase.

Consequently, a material balance on the *i*th component can be expressed as:

$$z_i n = x_i n_L + y_i n_V \tag{19}$$

Where: z_i : Mole fraction of component in the entire hydrocarbon mixture

Furthermore, by utilizing the concept of mole fraction, we can articulate the equation as:

$$\begin{aligned} \sum_i x_i &= 1 \\ \sum_i y_i &= 1 \\ \sum_i z_i &= 1 \end{aligned} \tag{20}$$

All phase-equilibria calculations may be performed based on 1 mol of the hydrocarbon mixture, i.e., $n = 1$. This assumption is reduced to

$$n_L + n_V = 1 \tag{21}$$

$$x_i n_L + y_i n_V = z_i \tag{22}$$

Combining equations (21) and (22) to exclude y_i results in

$$x_i n_L + (x_i K_i) n_V = z_i \tag{23}$$

When we solve for x_i we get

$$x_i = \frac{z_i}{n_L + K_i n_V} \tag{24}$$

It is also possible to solve it for y_i by combining to delete x_i :

$$y_i = \frac{z_i K_i}{n_L + K_i n_V} = x_i K_i \tag{25}$$

When all of the equations are combined, the result is

$$\sum_i x_i = \sum_i \frac{z_i}{n_L + K_i n_V} = 1 \tag{26}$$

and

$$\sum_i y_i = \sum_i \frac{z_i K_i}{n_L + K_i n_V} = 1 \tag{27}$$

Since

$$\sum_i y_i - \sum_i x_i = 0 \tag{28}$$

therefore

$$\sum_i \frac{z_i K_i}{n_L + K_i n_V} - \sum_i \frac{z_i}{n_L + K_i n_V} = 0 \tag{29}$$

or

$$\sum_i \frac{z_i (K_i - 1)}{n_L + K_i n_V} = 0 \tag{30}$$

When is replaced with $(1 - n_V)$, the result is

$$f(n_V) = \sum_i \frac{z_i (K_i - 1)}{n_V (K_i - 1) + 1} = 0 \tag{31}$$

This compilation of equations furnishes the essential phase relationships necessary for conducting volumetric and compositional assessments of hydrocarbon systems. Such calculations, as denoted in the scientific literature, are commonly referred to as "flash calculations" [2].

2.2.2. Equilibrium ratio for real gas

The equilibrium ratios, as discussed in Section 2.2.1, which describe the distribution of each component between the liquid and gas phases in terms of vapor pressure and system pressure, have been found to be insufficient. This deficiency arises from certain critical assumptions, namely:

- The ideal gas assumption characterizes the vapor phase according to Dalton's law.
- The ideal solution assumption characterizes the liquid phase as stipulated by Raoult's law.

At elevated pressures, these assumptions break

down, leading to imprecise equilibrium ratio calculations. In a realistic solution, these ratios are no longer exclusively dependent on pressure and temperature but are also influenced by the composition of the hydrocarbon mixture. This concept can be quantified as follows:

$$K_i = K(P, T, z_i)$$

Various methods have been proposed for determining equilibrium ratios in hydrocarbon mixtures. These correlations span a spectrum, from fundamental mathematical expressions to complex equations involving multiple composition-dependent variables.

Notably, Wilson (1968) devised a concise thermodynamic formulation for computing K values, articulated as follows [2]:

$$K_i = \frac{p_{ci}}{p} \exp [5.37(1 + \omega_i) (1 - \frac{T_{ci}}{T})] \quad (32)$$

Where:

P_{ci} : Critical pressure of component i

T_{ci} : Critical temperature of component i

ω_i : Acentric factor of component i

When applied under low pressure conditions, this equation yields more accurate equilibrium ratio values.

2.2.3. Flash calculation

All reservoir and process engineering calculations include flash calculations. They are required to determine the amount (in moles) of hydrocarbon liquid and gas coexisting in a reservoir or vessel at a specific pressure and temperature. These computations are also necessary to determine the composition of the present hydrocarbon stages. Flash calculations are used to calculate the moles of the gas phase, n_v , moles of the liquid phase, n_L , liquid phase composition, x_i , and gas phase composition, y_i , given the total composition of a hydrocarbon system at a certain pressure and temperature [2].

The following stages outline the computational methods for finding n_L , n_v , y_i , and x_i of a hydrocarbon mixture with a known overall composition of z_i and defined by a set of equilibrium ratios, K_i .

The first step involves using the Newton-Raphson iterative approach to determine n_v following these iterative procedures [2]:

Beginning with an arbitrary value assumption for n_v , for instance, $n_v = 0.5$, the following relation is used to calculate an improved assumed value [2]:

$$n_v = \frac{A}{A + B} \quad (33)$$

with

$$A = \sum_i [z_i(K_i - 1)]$$

$$B = \sum_i [z_i (\frac{1}{K_i} - 1)]$$

When contemplating the correctness of the equilibrium ratios, these equations hold the potential to yield an initial estimation for n_v . It is imperative to emphasize that the ascribed value for n_v must adhere to the constraints $0 < n_v < 1$.

In accordance with the adopted, preliminary n_v value, the function $f(n_v)$ is defined:

$$f(n_v) = \sum_i \frac{z_i(K_i - 1)}{n_v(K_i - 1) + 1} = 0$$

When the magnitude of the function $f(n_v)$ falls below a predefined threshold, typically set at values like 10^{-6} , the initially assumed value of n_v serves as the sought-after solution.

However, in cases where the absolute value of $f(n_v)$ surpasses the predetermined tolerance, an updated value, denoted as $(n_v)_{new}$, is determined via the subsequent expression:

$$(n_v)_{new} = n_v - \frac{f(n_v)}{f'(n_v)} \quad (34)$$

using the derivative $f'(n_v)$ defined by

$$f'(n_v) = - \sum_i \left\{ \frac{z_i(K_i - 1)^2}{[n_v(K_i - 1) + 1]^2} \right\} \quad (35)$$

And $(n_v)_{new}$ is the new n_v value that will be utilized in the following iteration. This operation is continued with each new value of n_v until convergence is reached, i.e.

$$|f(n_v)| \leq \epsilon$$

Or

$$|(n_v)_{new} - n_v| \leq \epsilon$$

Where:

ϵ : Preset error tolerance

When convergence is reached, n_L , x_i , y_i are derived.

2.3. Peng-Robinson equation of state & its applications

2.3.1. Fundamental of Peng-Robinson equation of state

Peng and Robinson are engaged in an extensive research endeavor aimed at evaluating the applicability

of the Soave-Redlich-Kwong (SRK) equation of state in forecasting the characteristics of naturally transpiring hydrocarbon systems. Their investigations have illuminated the necessity for enhancing the equation of state's capability to anticipate various fluid properties, with a specific emphasis on liquid densities, particularly within the critical region. In pursuit of this objective, Peng and Robinson posited the subsequent formula as an initial framework for the development of an enhanced predictive model [1]:

$$p = \frac{RT}{V-b} - \frac{a\alpha}{V(V+b) + b(V-b)} \quad (36)$$

The traditional critical point conditions are enforced, and the parameters a and b are calculated:

$$a = 0.45724 \frac{R^2 T_c^2}{P_c} \quad (37)$$

$$b = 0.07780 \frac{RT_c}{P_c} \quad (38)$$

Peng and Robinson utilized Soave's approach to calculate the temperature-dependent parameter α :

$$\alpha = \left[1 + m \left(1 - \sqrt{\frac{T}{T_c}} \right) \right]^2 \quad (39)$$

at

$$m = 0.3796 + 1.54226\omega - 0.2699\omega^2 \quad (40)$$

The following adjusted equation for the m value is also offered for heavier components with acentric values $\omega > 0.49$:

$$m = 0.379642 + 1.48503\omega - 0.1644\omega^2 + 0.016667\omega^3 \quad (41)$$

It will provide the compressibility factor form Z if it is rearranged:

$$Z^3 - (B-1)Z^2 + (A-3B^2-2B)Z - (AB-B^2-B^3) = 0 \quad (42)$$

Using the thermodynamic connection, the following formula for the fugacity of a pure component can be obtained by:

$$\ln\left(\frac{f}{p}\right) = \ln(\phi) = Z - 1 - \ln(Z-B) - \left(\frac{A}{2\sqrt{2}B}\right) \ln\left(\frac{Z+(1+\sqrt{2})B}{Z+(1-\sqrt{2})B}\right) \quad (43)$$

The following formula shows the fugacity coefficient of component i in a hydrocarbon liquid mixture:

$$\ln(\phi_i^L) = \frac{b_i(Z_L-1)}{b_m} - \ln(Z_L-B) - \left(\frac{A}{2\sqrt{2}B}\right) \left[\frac{2\psi_i}{(a\alpha)_m} - \frac{b_i}{b_m} \right] \ln\left(\frac{Z_L+(1+\sqrt{2})B}{Z_L+(1-\sqrt{2})B}\right) \quad (44)$$

Where b_m , B, A, ψ_i and $(a\alpha)_m$ are the previously established mixing parameters.

Any component's fugacity coefficient in the gas phase is computed by

$$\ln(\phi_i^V) = \frac{b_i(Z_V-1)}{b_m} - \ln(Z_V-B) - \left(\frac{A}{2\sqrt{2}B}\right) \left[\frac{2\psi_i}{(a\alpha)_m} - \frac{b_i}{b_m} \right] \ln\left(\frac{Z_V+(1+\sqrt{2})B}{Z_V+(1-\sqrt{2})B}\right) \quad (45)$$

Alternatively, the fugacity coefficient for any gas phase component is computed by substituting the liquid phase composition (x_i) with the gas phase composition (y_i) in the composition-dependent terms of the equation [1].

2.3.2. Applying the equation of state to determine equilibrium ratio

Upon satisfaction of all the specified conditions, the obtained solution is considered successful. In case that these criteria are not met, the sequence of steps denoted as steps 1 to 6 must be iteratively executed until the equilibrium ratios are found and confirmed. The process for ascertaining equilibrium ratios through the utilization of the equation of state is succinctly encapsulated in Figure 1.

2.3.3. Applications of the equation of state to calculate constant composition expansion (CCE) test

Step 1: Apply equation (24) in Section 2.2.1 to calculate x_i, y_i, n_L, n_V, K

Step 2: Determine the mixing parameters $(a\alpha)_m$ and b_m for the gas and liquid phases, resulting in:

- For the gas phase:

$$(a\alpha)_m = \sum_i \sum_j [y_i y_j \sqrt{a_i a_j \alpha_i \alpha_j} (1 - k_{ij})] \quad (46)$$

$$b_m = \sum_i (y_i b_i)$$

- For the liquid phase:

$$(a\alpha)_m = \sum_i \sum_j [x_i x_j \sqrt{a_i a_j \alpha_i \alpha_j} (1 - k_{ij})] \quad (47)$$

$$b_m = \sum_i (x_i b_i)$$

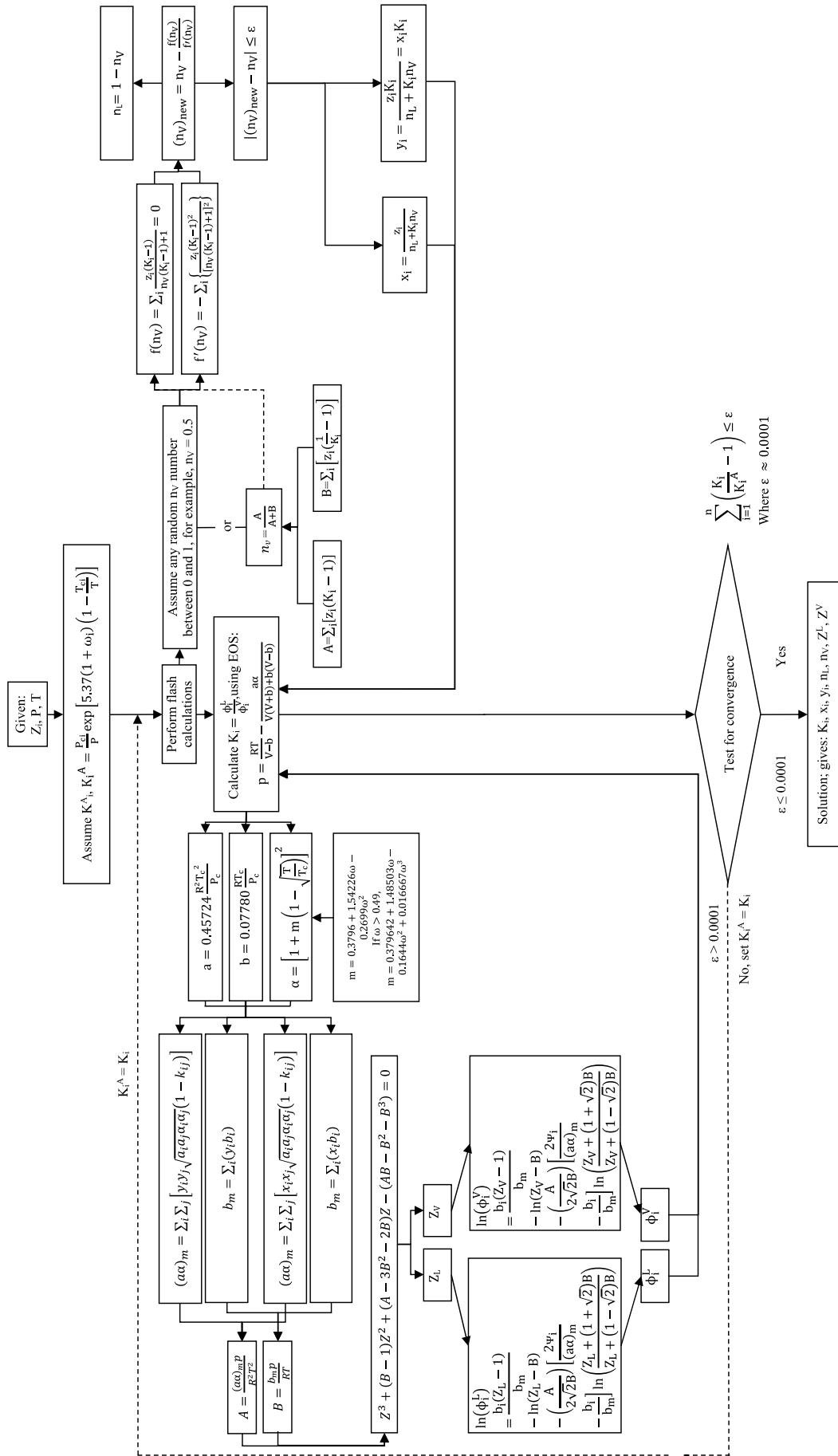


Figure 1. Flow diagram for determining equilibrium ratio using EOS [2].

Step 3: Calculate the coefficients A and B, for the gas/liquid phase, to give:

$$A = \frac{(a\alpha)_m p}{R^2 T^2} \quad (48)$$

$$B = \frac{b_m p}{RT} \quad (49)$$

Step 4: Determine the compressibility factor of the gas and liquid phases to yield:

$$Z^3 + (B - 1)Z^2 + (A - 3B^2 - 2B)Z - (AB - B^2 - B^3) = 0 \quad (50)$$

- For the gas phase: Z_v

- For the liquid phase: Z_L

Step 5: Calculate the adjusted densities and specific gravities of both phases ($\rho_v, \rho_L, \gamma_v, \gamma_L$)

$$\rho = \frac{pM_a}{RTZ} \quad (51)$$

$$\gamma_v = \frac{\rho_v}{\rho_{air}} \quad (52)$$

$$\gamma_L = \frac{\rho_L}{\rho_{water}} \quad (53)$$

Step 6: Apply equation (1) to equation (12) in Section 2.1.1 to calculate V_g, V_L, V_o, c_o

Step 7: Calculate the relative total volume

The isothermal compressibility coefficient of a single-phase fluid is commonly calculated using the equation above the saturation pressure.

$$c_o = - \frac{1}{V_{rel}} \left(\frac{\partial V_{rel}}{\partial p} \right)_T \quad (54)$$

In addition to the previously obtained experimental data, the gas compressibility factor, Z, is found for gas- condensate systems.

Below saturation pressure, the two-phase volume, V_t , is represented as a percentage of the volume at saturation pressure.

$$\text{Relative total volume} = \frac{V_t}{V_{sat}} \quad (55)$$

With V_t is total hydrocarbon volume.

Because no hydrocarbon material is eliminated from the cell, the composition of the overall hydrocarbon mixture in the cell remains constant [1].

2.3.4. Applications of the equation of state to calculate differential liberation test [1]

Step 1: Calculate relative oil volume factor (B_o):

$$B_o = \frac{V_L}{V_{sc}} \quad (56)$$

at

$$V_L = \frac{n_L Z_L RT}{p} \quad (57)$$

Step 2: Calculate solution GOR (R_s):

$$R_s = \frac{V_{gsc}}{V_{stosc}} \quad (58)$$

Step 3: Calculate gas volume factor (B_g)

$$B_g = \frac{V_g}{V_{gsc}} \quad (59)$$

Step 4: Calculate two phase volume factors (B_t)

$$B_t = B_o + R_p B_g \quad (60)$$

2.3.5. Applications of the equation of state to calculate separator test

Step 1: Determine the amount of oil filled by one pound of crude at the reservoir pressure and temperature, which is designated V_o . Remembering and applying the equation that determines the number of moles:

$$n = \frac{m}{M_a} = \frac{\rho_o V_o}{M_a} = 1 \quad (61)$$

V_o is then derived by:

$$V_o = \frac{M_a}{\rho_o} \quad (62)$$

Step 2: Calculate the equilibrium ratios for the initial stream composition (z_i) entering the first separator and the separator's operating conditions, such as pressure and temperature.

Step 3: Utilizing the equilibrium ratios obtained in step 2 and assuming an initial feed of 1 mol entering the first separator, perform flash calculations to ascertain the gas and liquid compositions and quantities (in moles) leaving the initial separator. The quantities of gas and liquid exiting the first separation stage are referred to as $(n_v)_1$ and $(n_L)_1$, respectively.

$$[n_v]_1 = (n)(n_v)_1 = (1)(n_v)_1 \quad (63)$$

$$[n_L]_1 = (n)(n_L)_1 = (1)(n_L)_1 \quad (64)$$

Step 4: Calculate the equilibrium ratios for the liquid leaving the first separator, using its composition ($z_i = x_i$) as the input, at the operating pressure and temperature of the second separator.

Step 5: Begin with 1 mol of initial feed, conduct flash calculations to determine the gas and liquid compositions and quantities leaving the second separation stage. These

calculations yield the precise number of moles for both gas and liquid phases.

$$[n_{v2}]_a = [n_{L1}]_a(n_v)_2 = (1)(n_L)_1(n_v)_2 \quad (65)$$

$$[n_{L2}]_a = [n_{L1}]_a(n_L)_2 = (1)(n_L)_1(n_L)_2 \quad (66)$$

Step 6: Repeat the preceding technique for each separation stage, including stock tank storage, and note the computed moles and compositions. The total number of moles of gas produced by all steps is then computed as follows:

$$(n_v)_t = \sum_{i=1}^n (n_{va})_i = (n_v)_1 + (n_L)_1(n_v)_2 + (n_L)_1(n_L)_2(n_v)_3 + \dots + (n_L)_1 \dots (n_L)_{n-1}(n_v)_n \quad (67)$$

The above expression can be expressed more succinctly:

$$(n_v)_t = (n_v)_1 + \sum_{i=2}^n [(n_v)_i \prod_{j=1}^{i-1} (n_L)_j] \quad (68)$$

Total moles of liquid left in the stock tank can alternatively be determined as follows:

$$(n_L)_{st} = n_{L1} n_{L2} \dots n_{Ln} \quad (69)$$

or

$$(n_L)_{st} = \prod_{i=1}^n (n_L)_i \quad (70)$$

Step 7: Determine the volume (in scf) of all liberated solution gas from:

$$V_g = 379.4(n_v)_t \quad (71)$$

Step 8: Calculate the amount of stock tank oil occupied by $(n_L)_{st}$ moles of liquid using the following formula:

$$(V_o)_{st} = \frac{(n_L)_{st}(M_a)_{st}}{(\rho_o)_{st}} \quad (72)$$

Step 9: Using the following formulas, calculate the specific gravity and API gravity of the stock tank oil:

$$\gamma_o = \frac{(\rho_o)_{st}}{62.4} \quad (73)$$

$$^\circ API = \frac{141.5}{\gamma_o} - 131.5 \quad (74)$$

Step 10: Determine the overall gas - oil ratio (also known as the gas solubility R_s):

$$GOR = \frac{V_g}{(V_o)_{st}/5.615} = \frac{(5.615)(379.4)(n_v)_t}{(n_L)_{st}(M)_{st}/(\rho_o)_{st}} \quad (75)$$

$$GOR = \frac{2130.331(n_v)_t(\rho_o)_{st}}{(n_L)_{st}(M)_{st}}$$

Step 11: Using the relationship, calculate the oil formation volume factor:

$$B_o = \frac{V_o}{(V_o)_{st}} \quad (76)$$

Combining equation (62) and equation (72) with the above expression gives:

$$B_o = \frac{M_a(\rho_o)_{st}}{\rho_o(n_L)_{st}(M_a)_{st}} \quad (77)$$

The separator pressure may be optimized by calculating the API gravity, GOR, and B_o at various assumed pressures as described above. The optimal pressure correlates to the highest API gravity and the lowest gas - oil ratio and oil formation volume factor [1].

3. Result and discussion

3.1. Overview of X oil field

The X oil field is situated within Block 01-X2, situated approximately 162 km off the northeastern coast of Ba Ria - Vung Tau province. This region is characterized by the development of several oil fields. Covering approximately 20.6 km² and residing at a water depth of approximately 43 m, the X oil field is operated under the product sharing agreement established between PVN and its partners. The oil field X was discovered in March 1996 when the exploration well A-1X was drilled for this purpose. Subsequently, three additional appraisal wells were drilled within the field to ascertain the in-situ reserves and the feasibility of reservoir exploitation within the terrigenous and basement sedimentary strata [5].

Recent well tests conducted at the A-4X well within the basement strata indicated a consistently favorable and robust oil flow at peak capacity. Commencing on April 17, 2011, the drilling of the A-4X has led to ongoing evaluations focused on on-site reserve estimation and recovery, marking a significant development in the field's operational progress.

3.2. Summary the data of the oil well XX-3Y

The methodology of employing lumping schemes has been adopted to condense the range of components, effectively reducing them from the C_{36+} group to the C_{12+} category. This strategic simplification of the component count is instrumental in streamlining the computational procedures, where the molecular weight of the C_{12+} group is 299.79 g/mol. Within this paradigm, distinct clusters of pure components are each substituted by a singular pseudo-component. These pseudo-components facilitate the application of mixing rules for the precise

Table 1. Compositional data of the XX-3Y

Component	Mole fraction	Component	Mole fraction	Component	Mole fraction
N ₂	0	C ₁₀	3.31	C ₂₄	0.51
CO ₂	0.34	C ₁₁	3.05	C ₂₅	0.55
H ₂ S	0	C ₁₂	3.32	C ₂₆	0.51
C ₁	33.82	C ₁₃	3.23	C ₂₇	0.44
C ₂	4.67	C ₁₄	2.87	C ₂₈	0.3
C ₃	4.89	C ₁₅	3.72	C ₂₉	0.27
iC ₄	1.25	C ₁₆	2.47	C ₃₀	0.31
nC ₄	2.45	C ₁₇	2.02	C ₃₁	0.29
iC ₅	0.96	C ₁₈	2.2	C ₃₂	0.29
nC ₅	1.08	C ₁₉	1.68	C ₃₃	0.06
C ₆	1.42	C ₂₀	1.28	C ₃₄	0.04
C ₇	2.23	C ₂₁	1.06	C ₃₅	0.18
C ₈	3.37	C ₂₂	0.92	C ₃₆₊	5.07
C ₉	2.97	C ₂₃	0.58		
MW C ₃₆₊ = 652.73 g/mol, γ = 0.872					

Table 2. Reservoir conditions of the XX-3Y

Reservoir pressure (psia)	4,495
Reservoir temperature (°F)	225.9

Table 3. Sample study at reservoir temperature of the XX-3Y

Bubble point pressure (psia)	2,344
------------------------------	-------

Table 4. Constant composition expansion at 225.9°F of the XX-3Y

CCE test	Pressure (psia)	Relative volume (V _r = V _r /V _b)	Liquid density (kg/m ³)
p _b	2,344	1	701
	2,600	0.997	703
	2,800	0.995	705
	3,000	0.993	706
	3,300	0.99	708
	3,500	0.988	710
	3,700	0.986	711
	3,900	0.985	712
	4,100	0.983	714
	4,300	0.981	715
	p _i	4,495	0.979

Table 5. Separator test of the XX-3Y

Separator test	Temperature (°F)	Pressure (psia)	GOR (scf/bbl)	Liq. Den (kg/m ³)	Oil FVF (B _o) (bbl/stb)
Stage 1	158	200	395	823	1,316
Tank	60	15	46	862	1

determination of essential EOS parameters, including critical pressure (p_c), critical temperature (T_c), and acentric factor (ω). These modified constants are subsequently assigned to the newly formed lumped pseudo-components, effectively enhancing the efficiency of the overall modeling process.

3.3. Regression & simulation of fluid thermodynamic tests workflow

3.3.1. Regression workflow by PVTp software

Step1: Choose a database from the PVTp option list including hydrocarbons, non-hydrocarbons, and pseudo components.

Table 6. Differential liberation at 225.9°F- liquid properties of the XX-3Y

DL test	Pressure (psia)	Oil FVF - B _o (bbl/stb)	Solution gas GOR R _s (scf/bbl)	Calculated liquid density (kg/m ³)
p_i	4,495	1,357	512	716
	4,300	1,359	512	715
	4,100	1,362	512	714
	3,900	1,364	512	712
	3,700	1,367	512	711
	3,500	1,369	512	710
	3,300	1,372	512	708
	3,000	1,376	512	706
	2,800	1,379	512	705
	2,600	1,382	512	703
p_b	2,344	1,386	512	701
	2,200	1,373	483	703
	1,900	1,348	424	707
	1,700	1,331	385	710
	1,500	1,314	346	714
	1,200	1,289	288	720
	1,000	1,272	249	725
	800	1,254	209	730
	500	1,223	146	742
	15	1,078	0	811

Step 2: Configure the value input and output units.

Step 3: Normalize total molar by entering components data (molar percent, molecular weight), reference data (reservoir temperature, reference depth/pressure).

Step 4: Enter specific gravity, choose the correlation method for boiling temperature, T_c, P_c, V_c, Omega. Also, compute the values of the pseudo components.

Step 5: Select the pure and pseudo component coefficients and compute the binary interaction coefficients.

Step 6: Choose a phase envelope test point, calculate the phase envelope, and plot the Phase diagram.

Step 7: Manual temperature and pressure range, and calculation CCE test.

Step 8: Manual range calculation (temperature and pressure), calculate DL test.

Step 9: Manual range calculation (temperature and pressure), calculate separator test.

Step 10: Enter lab data (P_{sat}, CCE, SEP, DL test).

Step 11: Setup for regression process by choosing mode, data and model

Option 3 is selected at Data Match Model: Individual OmegaA, OmegaB, and Pseudo T_{cs}, P_{cs}, AFs. Every component will have an eigenvalue of Omega A and B. Furthermore, the T_{cs}, P_{cs} and AF aggregated as well as the pseudo component will be provided for regression.

Step 12: Setup matching process - change OmegaA, OmegaB all components, change T_c, P_c, AF of pseudo components; change binary interaction coefficients of all pseudo components; and setup separator correction.

Step 13: Regression.

Step 14: Collect results and error details after regression.

Step 15: Repeat step 7 to step 9 to calculate the value of CCE, DL, separator test after matching process.

3.32. Simulation of fluid thermodynamic tests workflow

The initial phase of this procedure involves the input of essential parameters concerning both pure components and their corresponding pseudo components. Following this, under a specific set of pressure and temperature conditions, equilibrium ratios for individual components are approximated via correlations designed for real gasses. Subsequently, a flash calculation is executed,

yielding critical information such as the compressibility factor and fugacity coefficient for both the liquid and gas phases. Leveraging this data, the equilibrium ratios are then precisely computed, capitalizing on the fugacity coefficient.

The process advances with a pivotal assessment of the convergence between the calculated equilibrium ratios and their assumed counterparts. If the convergence criteria are satisfied, the values for equilibrium ratios (K_i), liquid phase compositions (x_i), gas phase compositions (y_i), mole quantities for the liquid phase (n_{li}), mole quantities for the vapor phase (n_{vi}), liquid phase compressibility factor (Z_{Li}), and vapor phase compressibility factor (Z_{Vi}) are finalized as the solution. However, in instances where the convergence is not achieved, a new set of equilibrium ratios is assumed, based on the calculated equilibrium ratios from the prior iteration, and the entire calculation process is iteratively repeated until convergence is established.

This methodology, once successfully executed, paves the way for comprehensive simulations of fluid thermodynamic tests. Specifically, the application of the Peng-Robinson equation of state (EOS) is deployed to calculate critical component equivalent (CCE), differentially liberated (DL), and separator test parameters, spanning from Section 2.3.3 to 2.3.5.

3.4. Results & discussions

3.4.1. Regression results by PVTp software

The outcomes pertaining to relative volume, liquid density, gas - oil ratio, solution gas - oil ratio, and oil formation volume factor for the critical component equivalent (CCE), differentially liberated (DL), and separator tests are succinctly synthesized within Tables 7 - 13.

Within the framework of the critical component equivalent (CCE) examination, the relative volume undergoes evaluation across the pressure range from p_i to p_b . The empirical observations manifest an interval of relative volumes lying between 0.979 and 1. Meanwhile, the outcomes derived from the PVTp software exhibit a spectrum spanning from 0.975136 to 0.999939. An analysis of the data shows a cumulative disparity of 0.027189, encompassing the differential between the laboratory-derived measurements and the software-generated results.

The separator test is executed in two stages. In the initial stage, conducted at 158°F and 200 psia, the gas - oil ratio from laboratory data stands at 395 scf/bbl, while the corresponding output from the PVTp software gives a notably contrasting value of 358.005 scf/bbl. Furthermore,

Table 7. Relative volume result at CCE test

CCE test	Temp.	Pressure (psia)	Relative volume ($V_r = V_r/V_b$)		
			Measured value	Software value	Error
p_i	225.9	4,495	0.979	0.975136	0.003864
	225.9	4,300	0.981	0.977008	0.003992
	225.9	4,100	0.983	0.978993	0.004007
	225.9	3,900	0.985	0.981047	0.003953
	225.9	3,700	0.986	0.983174	0.002826
	225.9	3,500	0.988	0.985379	0.002621
	225.9	3,300	0.99	0.987667	0.002333
	225.9	3,000	0.993	0.991267	0.001733
	225.9	2,800	0.995	0.993788	0.001212
p_b	225.9	2,600	0.997	0.996413	0.000587
	225.9	2,344	1	0.999939	6.1E-05
Error					0.027189

Table 8. Gas oil ratio result at separator test

Separator test	Temperature (°F)	Pressure (psia)	GOR (scf/bbl)		
			Measured value	Software value	Error
Stage 1	158	200	395	358.005	36.995
Tank	60	15	46	36.4963	9.5037
Error					46.4987

Table 9. Liquid density result at CCE test

CCE test	Temperature	Pressure (psia)	Liquid density (kg/m ³)		
			Measured value	Software value	Error
p_i	225.9	4,495	716	758.775	42.775
	225.9	4,300	715	757.321	42.321
	225.9	4,100	714	755.786	41.786
	225.9	3,900	712	754.203	42.203
	225.9	3,700	711	752.572	41.572
	225.9	3,500	710	750.888	40.888
	225.9	3,300	708	749.148	41.148
	225.9	3,000	706	746.428	40.428
	225.9	2,800	705	744.534	39.534
	225.9	2,600	703	742.573	39.573
p_b	225.9	2,344	701	739.954	38.954
Error					451.182

Table 10. Liquid density result at separator test

Separator test	Temperature (°F)	Pressure (psia)	Liquid density (kg/m ³)		
			Measured value	Software value	Error
Stage 1	158	200	823	815.358	7,642
Tank	60	15	862	843.585	18,415
Error					26,057

Table 11. Oil formation volume factor result at separator test

Separator test	Temperature (°F)	Pressure (psia)	Oil FVF (B _o) (bbl/stb)		
			Measured value	Software value	Error
Stage 1	158	200	1.316	1.04432	0.27168
Tank	60	15	1	1	0
Error					0.27168

Table 12. Oil formation volume factor result at DL test

DL test	Temperature (°F)	Pressure (psia)	Oil FVF B _o (bbl/stb)		
			Measured value	Software value	Error
p_i	225.9	4,495	1.357	1.19734	0.15966
	225.9	4,300	1.359	1.19964	0.15936
	225.9	4,100	1.362	1.20208	0.15992
	225.9	3,900	1.364	1.2046	0.1594
	225.9	3,700	1.367	1.20721	0.15979
	225.9	3,500	1.369	1.20992	0.15908
	225.9	3,300	1.372	1.21273	0.15927
	225.9	3,000	1.376	1.21715	0.15885
	225.9	2,800	1.379	1.22024	0.15876
	225.9	2,600	1.382	1.22347	0.15853
p_b	225.9	2,344	1.386	1.2278	0.1582
	225.9	2,200	1.373	1.21714	0.15586
	225.9	1,900	1.348	1.19469	0.15331
	225.9	1,700	1.331	1.18017	0.15083
	225.9	1,500	1.314	1.16594	0.14806
	225.9	1,200	1.289	1.14493	0.14407
	225.9	1,000	1.272	1.13116	0.14084
	225.9	800	1.254	1.11737	0.13663
	225.9	500	1.223	1.09571	0.12729
	225.9	15	1.078	1.04504	0.03296
Error					2.94067

Table 13. Liquid density result at DL test

DL test	Temperature (°F)	Pressure (psia)	Calculated liquid density (kg/m ³)		
			Measured value	Software value	Error
p_i	225.9	4,495	716	758.775	42.775
	225.9	4,300	715	757.321	42.321
	225.9	4,100	714	755.786	41.786
	225.9	3,900	712	754.204	42.204
	225.9	3,700	711	752.572	41.572
	225.9	3,500	710	750.888	40.888
	225.9	3,300	708	749.148	41.148
	225.9	3,000	706	746.428	40.428
	225.9	2,800	705	744.534	39.534
	225.9	2,600	703	742.573	39.573
p_b	225.9	2,344	701	739.954	38.954
	225.9	2,200	703	743.351	40.351
	225.9	1,900	707	750.773	43.773
	225.9	1,700	710	755.741	45.741
	225.9	1,500	714	760.736	46.736
	225.9	1,200	720	768.322	48.322
	225.9	1,000	725	773.434	48.434
	225.9	800	730	778.636	48.636
	225.9	500	742	786.862	44.862
	225.9	15	811	818.17	7.17
Error					825.208

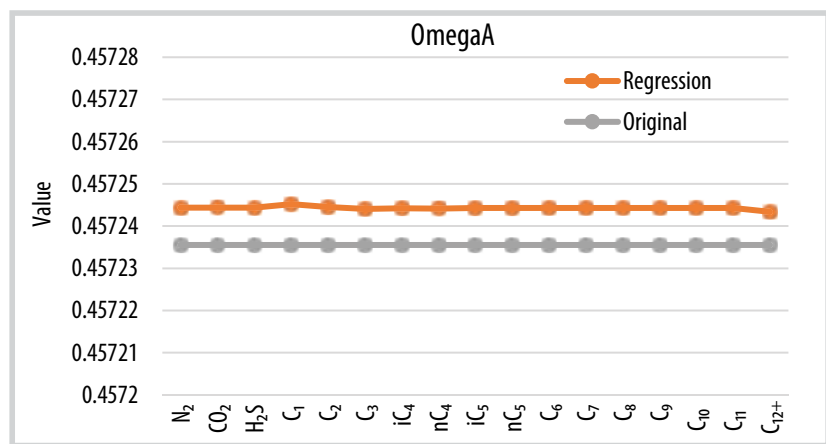


Figure 2. Regressed OmegaA by PVTp software versus original data.

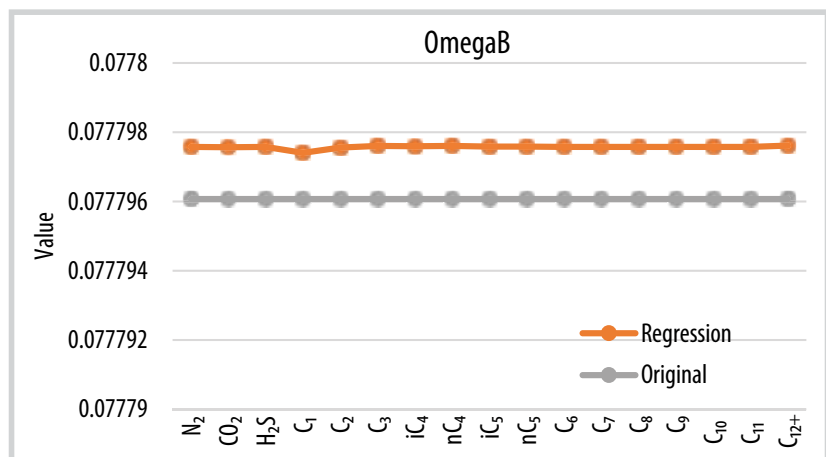


Figure 3. Regressed OmegaB by PVTp software versus original data.

during the subsequent stage under standard conditions, the gas - oil ratio is determined to be 46 scf/bbl based on laboratory findings, in stark contrast to the software-derived value of 36.4963 scf/bbl.

The liquid density values are ascertained across the pressure range from p_i to p_b . The experimental measurements indicate a range between 716 kg/m³ and 701 kg/m³, while the corresponding values generated by the PVTp software fall within the range of 758.775 kg/m³ to 739.954 kg/m³. It is noteworthy that there exists a substantial disparity of 451.182 between the laboratory data and the software results.

Liquid density from lab data is 823 kg/m³ at stage 1 (158°F, 200 psia), contrasted to PVTp software result of 815.358 kg/m³. Furthermore, the liquid density value from lab data and software findings at the standard condition stage is 862 kg/m³ and 843.585 kg/m³, respectively.

Oil FVF from lab data is 1.316 bbl/stb at stage 1 (158°F, 200 psia) compared to PVTp software result of 1.04432 bbl/stb. Furthermore, in the standard condition stage, the oil FVF value from lab data and software results are both equal to 1 bbl/stb.

In the DL test, the measured oil FVF increases from 1.357 bbl/stb at p_i to a peak of 1.386 bbl/stb at p_b . Then it decreases to 1.078 bbl/stb at 15 psia. Similarly, the software result rises from 1.19734 bbl/stb to 1.2278 bbl/stb, and drops to 1.078 bbl/stb.

The observed liquid density in the DL test drops from 716 kg/m³ at p_i to 701 kg/m³ at p_b , then climbs to 811 kg/m³ at 15 psia. Similarly, the software result falls from 758.775 kg/m³ to 739.954 kg/m³ and then climbs to 818.17 kg/m³.

- The comparison between original value of OmegaA, OmegaB by Peng-Robinson EOS and PVTp software regression process is shown in Figures 2 and 3.

The original OmegaA of P-R EOS is a constant value, 0.457235515; while the regressed one by software fluctuates between 0.457245171 and 0.457243413 with an average of 0.457244293.

The regressed OmegaB by software fluctuates between 0.077797614 and 0.0777974054 with an average of 0.077797572, while the original Omega A of P-R EOS is a constant value at 0.0777960718.

3.4.2. Simulation of fluid thermodynamic tests results

In Figure 4, the calculated value, software result, and measured data of the oil formation volume factor have roughly the same trend, increasing from p_i to reach a peak at p_b , then decreasing from p_b to 4,495 psia, although the measured data is always higher than two other types of values with an average gap of 0.15. Moreover, the calculated value and software result are relatively equal, except that at standard condition, the computed

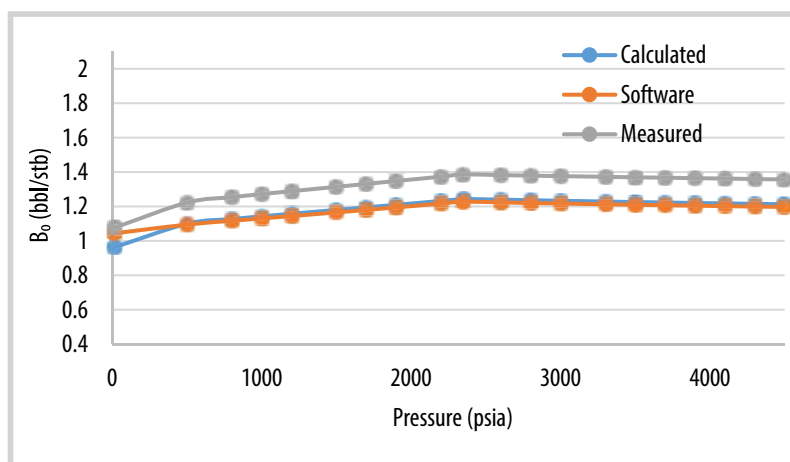


Figure 4. Oil formation volume factor versus pressure.

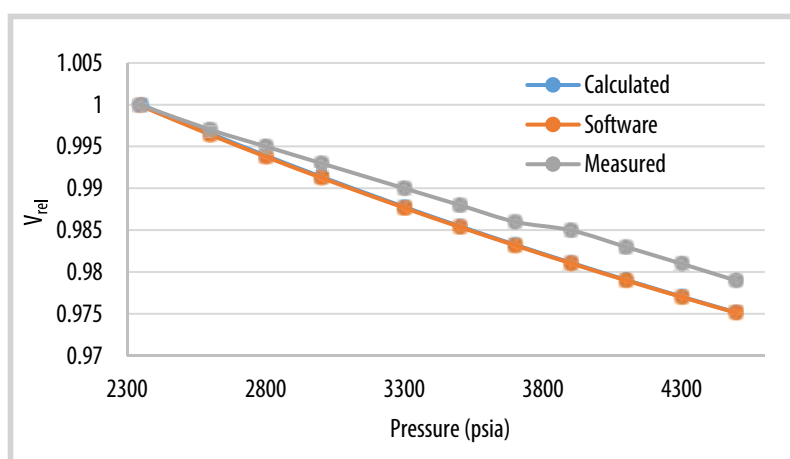


Figure 5. Relative volume versus pressure.

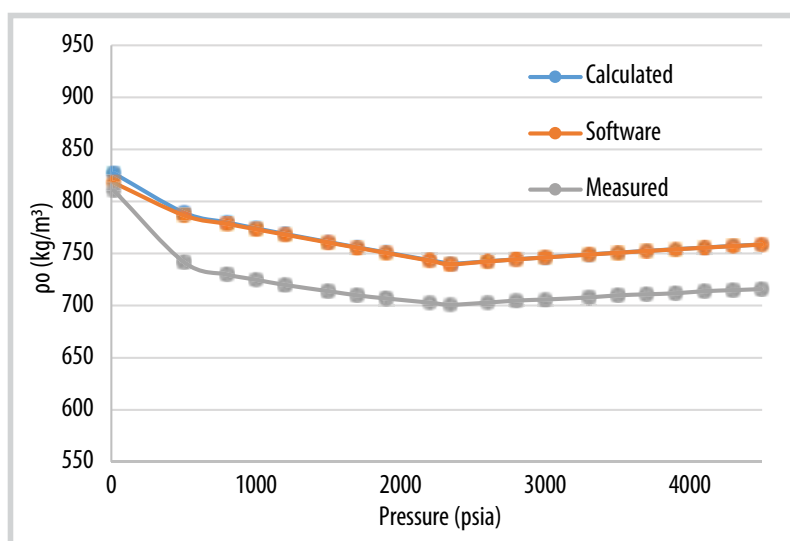


Figure 6. Oil density versus pressure.

value is 0.964166283 bbl/stb, the software result is 1.04504 bbl/stb, and the observed data is 1.078 bbl/stb.

In Figure 5, the value of relative volume is trending upward through the pressure range (from p_i to p_b). The calculated value and software

result of relative volume are nearly the same at each spot of the measured pressure scheme. For measured data, the value at p_{sat} is roughly 1, similar to the calculated and software results. After that, measured data is always higher than two other kinds of values until the end. At 4,495 psia, the calculated value is 0.97518753, compared to 0.975136 at the software result and 0.979 at the measured data.

Figure shows that the calculated value, software result, and measured data of the oil formation volume factor have essentially the same pattern, falling from p_i to p_b , then rising from p_b to 4,495 psia, despite the fact that the measured data value is always smaller than the two others with an average gap of 45. Moreover, the calculated value and software result is significantly matched, except that at the standard circumstance, the calculated value is 827.2420778 kg/m³, the software result is 818.17 kg/m³, and the observed data is 811 kg/m³.

4. Conclusion

In summary, this study has introduced a quantitative approach for simulating fluid thermodynamic tests, including CCE, DL, and separator tests, within multicomponent systems. This approach combines the utilization of equilibrium ratios, flash calculations, and the application of the Peng-Robinson equation of state. The calibration process, facilitated through the PVTp software regression procedure, allows the flexible determination of OmegaA and OmegaB values, thereby enhancing the precision of fluid thermodynamic test calculations and optimizing error margins in comparison to empirical data.

The efficacy of this proposed method has been substantiated through a set of numerical results. For instance, the bubble point pressure values extracted from observed data, software-generated values, and calculated outcomes stand at 2,344, 2,339, and 2,350.42 psia, respectively. In addition, the calculated results of various fluid thermodynamic tests, such as relative volume, oil formation volume factor, and liquid density, are close to those generated by the PVTp software and exhibit acceptable error levels compared to the measured data.

However, it is imperative to acknowledge that the DL test has revealed a substantial disparity in the solution gas - oil ratio. This incongruity emphasizes the necessity for more comprehensive measured data to enhance the simulation's accuracy and narrow the error gap.

The juxtaposition between the proposed methodology and the collected data underscores the suitability of integrating equilibrium ratios, flash calculations, and the Peng-Robinson equation of state as a dependable model for the precise calculation of equilibrium ratios and fluid thermodynamic tests within multicomponent systems. This approach provides a quantitative framework for simulating fluid thermodynamic tests, delivering valuable insights, and diminishing the dependence on costly laboratory experiments.

Acknowledgment

This research is funded by Vietnam National University HoChiMinh City (VNU-HCM) under grant number: DM2024-20-02.

References

- [1] Tarek Ahmed, *Reservoir engineering handbook*, 4th edition. Gulf Professional Publishing, 2010.
- [2] Tarek Ahmed, "Working guide to Vapor - Liquid phase equilibria calculations", *Reservoir Engineering Handbook*, 3rd edition. Gulf Professional Publishing, 2006, pp. 1096 - 1234.
- [3] Tarek Ahmed, *Equation of state and PVT analysis*. Gulf Publishing Company, 2007.
- [4] F. Esmailzadeh and F. Samadi, "Modification of Esmailzadeh - Roshanfekar equation of state to improve volumetric predictions of gas condensate reservoir", *Elsevier*, Volume 267, Issue 2, pp. 113 - 118, 2008. DOI: 10.1016/j.fluid.2008.02.017.
- [5] R. Wu and L. Rosenegger, "Comparison of PVT properties from equation of state analysis and PVT correlations for reservoir studies", *Journal of Canadian Petroleum Technology*, Volume 39, Issue 7, pp. 44 - 51, 2000.
- [6] Bharat S. Jhaveri and Gary K. Youngren, "Three-Parameter modification of the Peng-Robinson equation of state to improve volumetric predictions", *SPE Reservoir Engineers*, Volume 3, Issue 3, pp. 1033 - 1040, 1988. DOI: 10.2118/131118-PA.
- [7] Mourad Bengherbia and Djebbar Tiab, "Gas-Condensate well performance using compositional simulator: A case study", *SPE Gas Technology Symposium, Calgary, Alberta, Canada, 30 April - 2 May 2002*. DOI: 10.2118/75531-MS

[8] D. Ghorbani and R. Kharrat, "Fluid characterization of an Iranian carbonate oil reservoir using different PVT packages", *SPE Asia Pacific Oil and Gas Conference and Exhibition, Jakarta, Indonesia, 17 - 19 April 2001*.

[9] Tarek Ahmed, "On equation of state", *Latin American & Caribbean Petroleum Engineering Conference, Buenos Aires, Argentina, 15 - 18 April 2007*. DOI: 10.2118/107331-MS.

[10] Shu Pan, Asok Kumar Tharanivasan, Jiabao Jack Zhu, Kurt Schmidt, John Ratulowski, and Robert Fisher, "A robust workflow for reliably describing reservoir fluid PVT properties using equation of state models", *International*

Petroleum Technology Conference, Doha, Qatar, 6 - 9 December 2015. DOI: 10.2523/IPTC-18334-MS.

[11] Yau-Kun Li and Long X. Nghiem, "The development of a general phase envelope construction algorithm for reservoir fluid studies", *SPE Annual Technical Conference and Exhibition, New Orleans, LA, 26 - 29, September, 1982*. DOI: 10.2118/11198-MS.

[12] T.D.N. Giao, "Study on equation of state to build phase diagram", *Bachelor thesis in Petroleum Engineering*. The Faculty of Geology and Petroleum Engineering, Ho-chiminh city University of Technology, Vietnam National University, August 2021.

DEVELOPING SUPERHYDROPHOBIC/SUPEROLEOPHILIC POLYURETHANE SPONGE BASED ON Fe_3O_4 PARTICLES FOR OIL - WATER SEPARATION

Nguyen Thi Phuong Nhung, Phan Minh Quoc Binh, Vo Van Vu Thanh, Nguyen Van Kiet

Petrovietnam University

Email: nhungntp@pvu.edu.vn

<https://doi.org/10.47800/PVSI.2024.06-09>

Summary

Recently, the issue of oil and organic spills, driven by a growing human population, has become a significant concern globally, including in Vietnam. Researchers are increasingly focused on developing materials that can selectively absorb oils and organic solvents while repelling water. This project aimed to develop an oil-absorbing material by integrating stearic acid-modified Fe_3O_4 or Fe_3O_4 particles into a polyurethane (PU) foam base. The results demonstrated that the modified PU sponge exhibited superhydrophobic properties, with a water contact angle exceeding 150° , and superoleophilic characteristics, with an oil contact angle close to zero. With excellent oil selectivity, the modified PU sponge achieved diesel oil absorption capacity ranging from 44 to 53 times its weight, depending on the particle loading concentration.

Key words: Oil/water separation, superhydrophobic sponge, superoleophilic, stearic acid-modified Fe_3O_4 particles.

1. Introduction

Nowadays, the increasing demand for fossil fuels has led to the expansion of fossil fuel infrastructures, resulting in more oil spills and pollutant leaks. Consequently, the removal of oil, organic solvents, and gasoline from water has garnered significant attention over the years [1]. Various techniques have been employed to separate oil from water, including physical methods such as skimmers, booms, meshes, barriers, and absorbents; chemical methods using dispersants and solidifiers; and biological methods [2]. Although these traditional methods are easy to operate, they still have the disadvantages of low separation efficiency and low recycling rates in oily wastewater treatment. Therefore, the development of new oil - water separation materials with higher efficiency and higher recycling rates has become a hot trend in recent years [3, 4].

Inspired by the superhydrophobic/superoleophilic phenomena observed on lotus leaves, which have water contact angles greater than 150° and oil contact angles

less than 10° , many researchers have created artificial superhydrophobic/superoleophilic surfaces for a wide range of applications, such as anti-corrosion coatings [5], anti-wax treatments [6], self-cleaning mechanisms [7], anti-fog solutions [8], anti-adhesion technologies, and water - oil separation [9]. To create superhydrophobic surfaces, it is necessary to combine surface roughness or structure with decreased surface energy [10].

Regarding absorbents, it is noted that conventional absorbents can absorb both water and oil, not just oil. To enhance their specificity, scientists have proposed transforming traditional absorbents from superhydrophilic to superhydrophobic through chemical modification and structural introduction. These superhydrophobic oil sorbents are the most effective remediation method for large oil spills compared to dispersants and skimmer devices. Therefore, significant research efforts have been directed toward the fabrication of superhydrophobic/superoleophilic materials for the separation of oil water mixtures. In general, superhydrophobic/superoleophilic sponges are fabricated using a two-step procedure that increases the surface roughness and reduces the surface energy of the sponge surfaces. Firstly, the surface roughness can be increased by coating sponge surfaces



Date of receipt: 8/8/2024.

Date of review and editing: 8 - 22/8/2024.

Date of approval: 22/8/2024.

with micro/nano structures such as micro/nano particles (e.g., graphene, metal, metal oxides). In the 2nd step, the modified sponge with low surface energy materials is converted from superhydrophilic to superhydrophobic. Low surface energy materials can include fatty acids [11], organosilanes [12], polydimethylsiloxane [14], and graphene [15].

In this paper, we report a simple method to create a smart sponge with magnetic properties. It is easy to make in the laboratory using basic tools and inexpensive common chemicals.

2. Experiment

2.1. Materials

Stearic acid, high-density polyethylene, toluene, ethanol, acetone, H_2SO_4 , NaOH, $FeSO_4 \cdot 7H_2O$, $FeCl_3 \cdot 6H_2O$ and NaOH are supplied by Xilong company (China), diesel oil is from BSR company (Vietnam).

2.2. Preparation of superhydrophobic steel surface

2.2.1. Formation of Fe_3O_4 powder

800 ml of 0.1 M NaOH is slowly added to a mixture of 100 ml of 0.1 M Fe^{2+} and 200 ml of 0.1 M Fe^{3+} with vigorous stirring for 15 minutes. After centrifugal filtration, the Fe_3O_4 powders are rinsed with water and dried in the oven at 60°C.

2.2.2. Preparation of superhydrophobic Fe_3O_4 powder

2 g of Fe_3O_4 was added to 50 ml of ethanol containing 0.15 g of stearic acid. This mixture was continuously shaken for 3 hours. After the reaction, the particles were rinsed with ethanol 3 times, shaking for 5 minutes each time. Finally, the stearic acid-coated Fe_3O_4 particles (AS- Fe_3O_4) were obtained by centrifugal filtration and dried in the oven at 60°C. The mechanism of AS modification is shown in Figure 1. During the process, AS contains -COOH groups, which react with the surface -OH groups of the Fe_3O_4 particles (due to the presence of a trace layer of water surrounding the particles). This reaction leads to the attachment of -CH₃ groups onto the Fe_3O_4 particles.

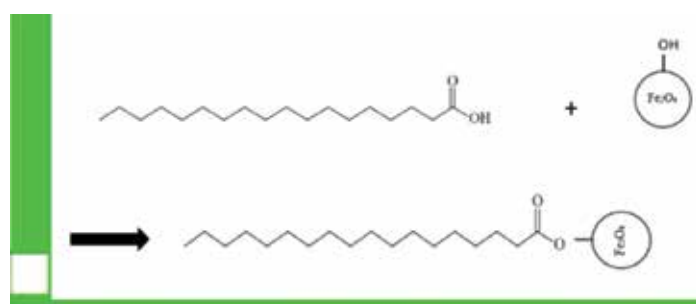


Figure 1. Mechanism of stearic acid modification on the Fe_3O_4 particle surface.

2.2.3. Preparation of superhydrophobic polyurethane sponge

Typically, a polyurethane (PU) sponge ($2 \times 2 \times 2$ cm³) was immersed in 15 ml of ethanol containing different concentrations ranging from 5 mg to 250 mg of Fe_3O_4 particles with or without chemical modification and shaken for 15 minutes. The Fe_3O_4 -coated PU sponge was dried before being coated with HDPE or PDMS according to the procedures below.

For HDPE coating: The Fe_3O_4 -coated sponge was immersed in 25 ml of toluene containing 2.5 g of high-density polyethylene (HDPE) for 5 minutes. Then, the modified PU sponge was dried in an oven at 50°C for 6 hours.

For PDMS coating: The Fe_3O_4 -coated sponge was immediately dipped in 25 ml of ethyl acetate containing 0.25 g of PDMS and 0.025 g of curing agent for 10 minutes, then dried in the hood for about 12 hours.

2.2.4. Materials characterisation

The morphology of Fe_3O_4 particles was characterised using a scanning electron microscopy (SEM, JEOL 7600F with EDS, Oxford Instruments). The FTIR methods were used to confirm the successful grafting of chemical modifications onto the Fe_3O_4 particle surface. The wetting properties of particles and PU surface were evaluated by measuring the static contact angle of water using an OCA-data physics instrument at three different positions on each surface, with a 5 μ L distilled water droplet. Specifically, the powder Fe_3O_4 particles will be deposited onto a glass slide. Then, a 5 μ L distilled water droplet will be placed on top, and the contact angle will be measured.

3. Results and discussion

3.1. Materials characterisation

Figure 2 illustrates the SEM images of pristine (Figure 2a) and chemically modified Fe_3O_4 particles with stearic acid (Figure 2b). In comparison to unmodified Fe_3O_4 particles, no thin chemical coating around the particles can be observed; the particles retain the same spin-like shape after modification. This indicates that the modification process did not

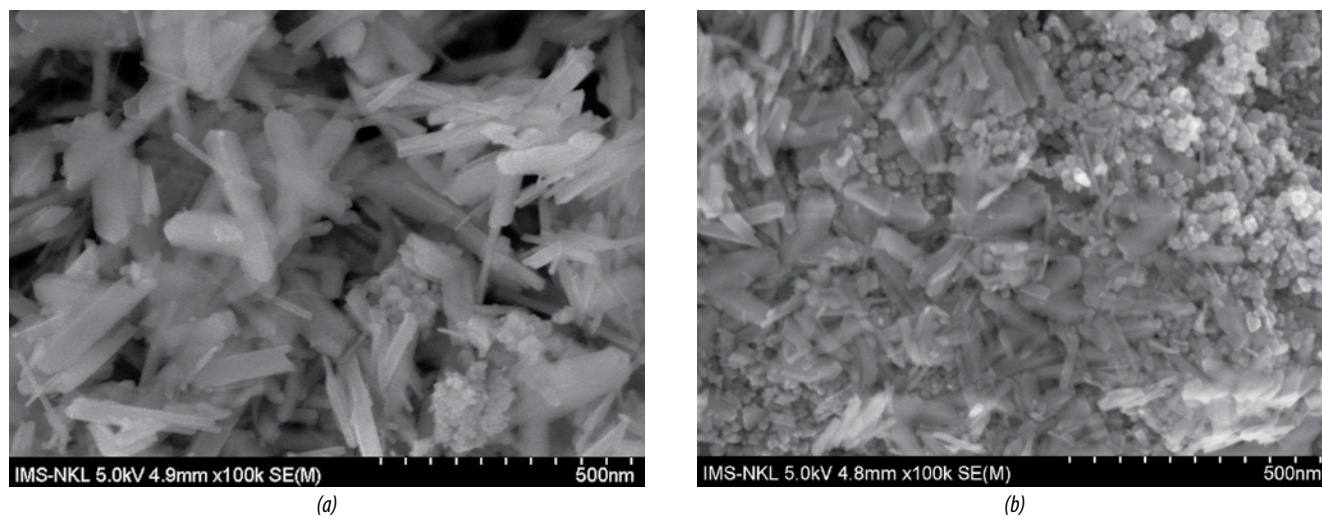


Figure 2. SEM images of pristine Fe_3O_4 (a) and (b) chemical modified- Fe_3O_4 particles with stearic acid. Insets are photos of corresponding water droplets.

significantly damage the morphology of the particles. The insets of Figure 2 are photos of corresponding water droplets, which confirm that the wettability of the Fe_3O_4 surface particles changed from superhydrophilic to hydrophobic properties

Stearic acid is known for its composition of a non-polar, hydrophobic alkane chain and a hydrophilic carboxyl group. When Fe_3O_4 particles are combined with stearic acid, the -OH groups on the Fe_3O_4 surface react with the -COOH group of the stearic acid. This reaction results in the formation of a hydrophobic layer, denoted as $-(\text{CH}_2)_n-\text{CH}_3$, on the Fe_3O_4 particle surface.

The FTIR spectra of unmodified Fe_3O_4 particles (shown by the gray line in Figure 3) reveal a strong absorption peak at $3,412\text{ cm}^{-1}$, indicating O-H stretching vibrations. This suggests that the surface of the pristine Fe_3O_4 particles contains numerous O-H groups, making them hydrophilic. A peak at 557 cm^{-1} , corresponding to the Fe-O skeleton, is also present and appears with lower intensity in the FTIR spectrum of Fe_3O_4 particles modified with stearic acid (blue line in Figure 3). In the modified spectrum, vibration absorption peaks at $1,794\text{ cm}^{-1}$, $1,769\text{ cm}^{-1}$, and $1,622\text{ cm}^{-1}$ are attributed to C=O bonds. Additionally, peaks at $1,447\text{ cm}^{-1}$ and $1,381\text{ cm}^{-1}$ correspond to C-H bonds of the - CH_3 group and peaks at $1,128\text{ cm}^{-1}$ and $1,048\text{ cm}^{-1}$ correspond to C-O bonds of the -COO group. This demonstrates that stearic acid can chemically bond to the surface of Fe_3O_4 , altering its properties [11, 16, 17].

After modification, Fe_3O_4 particles transform from superhydrophilic (contact angle $\sim 0^\circ$) to hydrophobic (contact angle $\sim 135^\circ$) as shown in Figure 4.

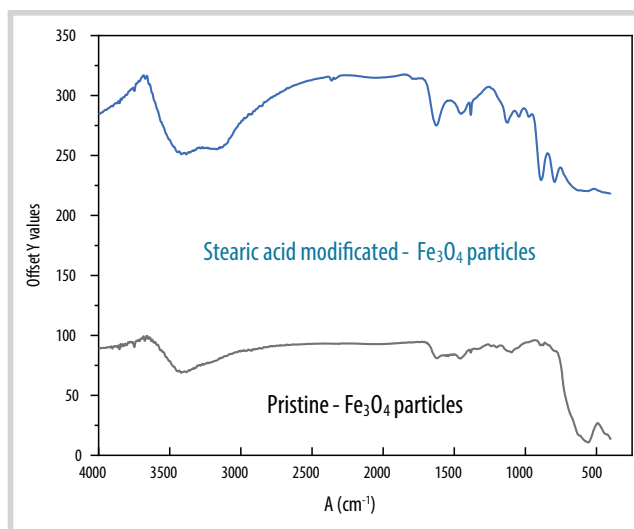


Figure 3. FTIR spectra of as-prepared Fe_3O_4 particles, stearic acid-modified Fe_3O_4 particles.

3.2. Wettability of modified sponge

In this section, the wettability of the sponge, both with and without modification, was characterised by contact angle measurement. The reason for introducing Fe_3O_4 particles into the PU sponge is to increase the robustness of the surface and integrate magnetic properties into the sponge. Figure 5 shows the water contact angle values on the pristine sponge modified with Fe_3O_4 particles (Figure 5a) and AS- Fe_3O_4 particles (Figure 5b), both of which were then coated with HDPE. It is noted that the PU sponge coated with Fe_3O_4 at different concentrations was hydrophobic, with a water contact angle of about $120^\circ \pm 2$ (Figure 5a), while the sponge coated with AS- Fe_3O_4 particles became more hydrophobic, with a water contact angle of about $125^\circ \pm 2$ at the same concentration. Moreover, adding HDPE coating to the PU sponge



Figure 4. Image of water droplet on Fe₃O₄ powder before (a) and after (b) modification.

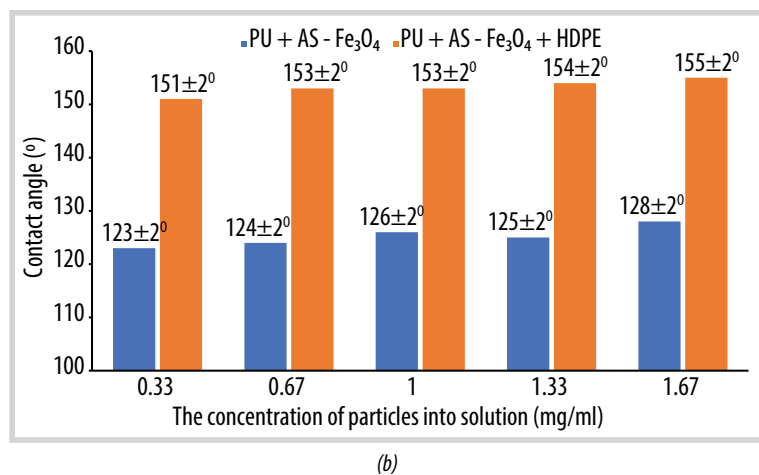
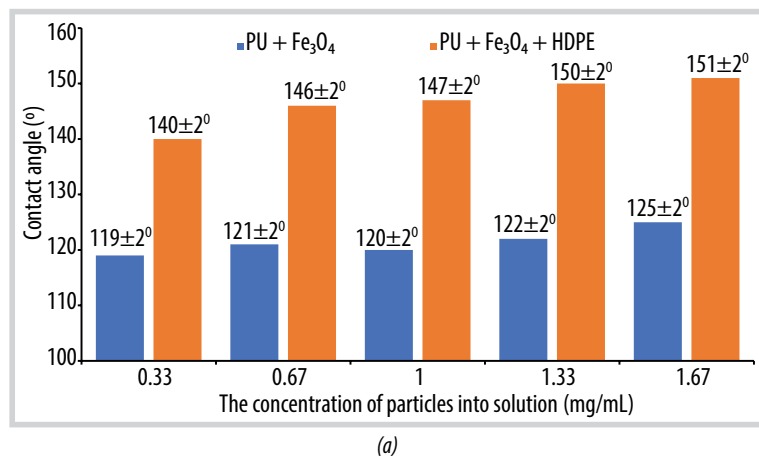


Figure 5. Water contact angle on the sponge with Fe₃O₄ coating (blue column) and HDPE coating (orange column) (a) and with AS-Fe₃O₄ coating (blue column) and HDPE coating (orange column) (b) vs the concentration particle solution (mg/ml).



Figure 6. Photograph of sponge used to test the hydrophobic and oleophilic behavior: (a) Sponge coated with modified HDPE-Fe₃O₄ coating (64%) vs. pristine sponge on the water surface; (b) Water droplet and diesel oil droplet on the sponge coated with modified HDPE-Fe₃O₄ coating (inset shows the corresponding water contact angle).

containing Fe₃O₄ particles or AS-Fe₃O₄ particles further increased its hydrophobicity.

In the case of the Fe₃O₄-coated PU sponge with HDPE, the surface became superhydrophobic with a contact angle of more than 150° when the concentration of particles was greater than 1.33 mg/ml. However, in the case of the PU sponge coated with AS-Fe₃O₄ and HDPE, the surface became superhydrophobic at lower particle concentrations (> 0.33 mg/ml).

3.3. Superhydrophobic and oleophilic sponge for oil separation

To compare the hydrophobic properties between the pristine sponge and the modified sponge, both samples were deposited on the water surface, as shown in Figure 5a. The results show that the sponge coated with modified Fe₃O₄ particles floats on the surface of water, whereas the pristine sponge completely submerges. This is because the sponge becomes superhydrophobic with a contact angle of more than 152° ± 2 degrees after being coated with modified Fe₃O₄ particles. On the other hand, when a diesel oil droplet is deposited on the superhydrophobic sponge, the diesel oil completely spreads with a contact angle close to zero (contact angle ~ 0°), as shown in Figure 6b. The result is opposite with water droplets, which stay on the surface of the sponge due to the superhydrophobic properties with a contact angle > 150°. Therefore, after coating with Fe₃O₄ particles or modified Fe₃O₄ particles, the sponge becomes both superhydrophobic and superoleophilic. This implies that the modified sponge exhibits high selectivity for oil/water separation.

The oil/water separation experiment using the magnetic PU sponge was performed as follows. As shown in Figure 7, manipulated by a magnet bar, the magnetic PU sponge approached the oil/water mixture (diesel oil) and selectively and rapidly absorbed the floating oil on the water surface, leaving only water behind.

To test the capability of the modified

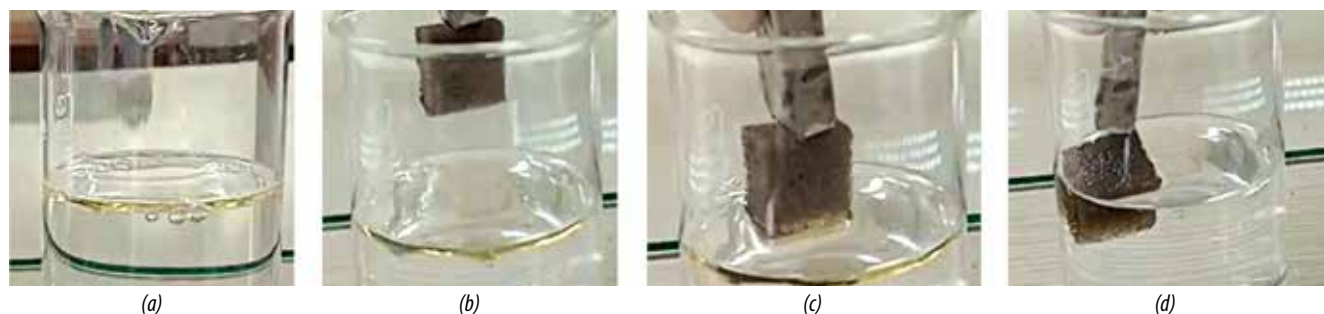


Figure 7. The sequence image of oil/water separation experiment under magnetic actuation.

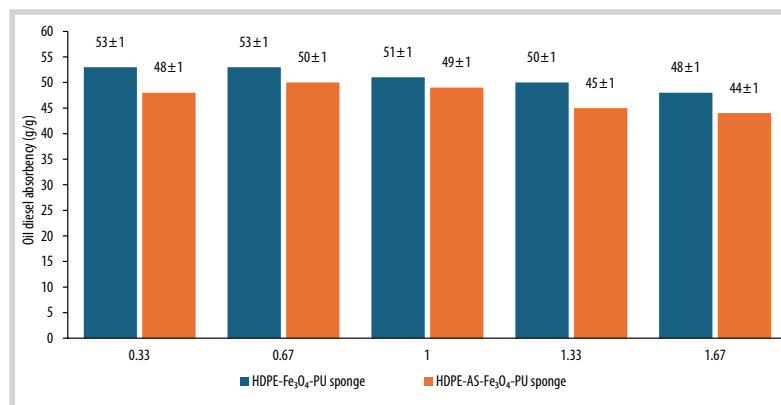


Figure 8. Oil mass absorption on modified PU sponge: with Fe₃O₄ particle and HDPE (HDPE-Fe₃O₄-PU sponge - blue column, with AS-Fe₃O₄ particles and HDPE sponge coating (HDPE-AS-Fe₃O₄-PU sponge - orange column).

sponge to absorb oil from the water surface, the sample was placed into a beaker containing oil. Then, the modified sponge was added. To calculate the absorption capacity of the sponge, the weight of the sponge before and after absorbing the oil was measured as m_0 and m_1 , respectively. The absorption capacity was calculated using the following equation [9], and the result of measurement is shown in Figure 8.

$$K = \frac{m_1 - m_0}{m_0} [9]$$

Figure 8 shows that at the same particle coating level, the modified PU sponge with pristine Fe₃O₄ particles and an HDPE coating (HDPE-Fe₃O₄-PU) exhibits slightly higher diesel oil absorption, averaging 51 g/g, compared to the sponge with AS-Fe₃O₄ particles and an HDPE coating (HDPE-AS-Fe₃O₄-PU), which averages 46 g/g. However, the oil selectivity of the HDPE-AS-Fe₃O₄-PU sponge is marginally better than that of the HDPE-Fe₃O₄-PU sponge, likely due to its increased hydrophobicity, as demonstrated in Figure 5. Moreover, this sponge can be reused up to 10 times without scattering or deforming. To reuse the product, the process is straightforward: simply extract the oil by squeezing, and the product is ready for subsequent use.

The mass of the HDPE-Fe₃O₄-PU sponge (2 x 2 cm) is about 0.2 g. After the first use as a diesel oil (DO, $d = 0.82$ g/ml) absorbent, the volume of absorbed DO oil is about 12.44 ml. Therefore, a sponge with dimensions of 41 x 46 cm could absorb approximately 5.3 l of oil for the

first use. In comparison, the Spilfyter Oil-Only Absorbent Pad, commonly used by most oil companies in Vietnam, can absorb 1.2 l of oil per use (once only). This research product shows great promise for oil absorption, likely due to its 3D structure, high oil absorption capacity, and high selectivity, with superior hydrophobic properties and a contact angle greater than 150°.

4. Conclusion

In summary, we fabricated a superhydrophobic PU sponge with magnetic properties through basic tools and inexpensive common chemicals. The smart PU sponge exhibited high absorption capacity and good oil selectivity. Therefore, this superhydrophobic and magnetic PU sponge has a high potential application in immiscible oil/water separation, such as in oil extraction or oil spill cleanup.

References

- [1] Ahmad Bayat, Seyed Foad Aghamiri, Ahmad Moheb, and Gholam Reza Vakili-Nezhaad, "Oil spill cleanup from sea water by sorbent materials", *Chemical Engineering & Technology*, Volume 28, Issue 12, pp. 1525 - 1528, 2005. DOI: 10.1002/ceat.200407083.
- [2] Abhinav Dhaka and Pradipta Chattopadhyay, "A review on physical remediation techniques for treatment of marine oil spills", *Journal of Environmental Management*, Volume 288, 2021. DOI: 10.1016/j.jenvman.2021.112428.
- [3] Chih-Feng Wang and Sheng-Jhih Lin, "Robust superhydrophobic/superoleophilic sponge for effective continuous absorption

and expulsion of oil pollutants from Water”, *ACS Applied Material & Interfaces*, Volume 5, Issue 18, pp. 8861 - 8864, 2013. DOI: 10.1021/am403266v.

[4] Sanjay S. Latthe, Rajaram S. Sutar, A.K. Bhosale, Kishor Kumar Sadasivuni, and Shanhu Liu, “Superhydrophobic surfaces for oil-water separation”, *Superhydrophobic Polymer Coatings*. Elsevier, 2019, pp. 339 - 356. DOI: 10.1016/B978-0-12-816671-0.00016-3.

[5] T. Iline-Vul, S. Bretler, S. Cohen, I. Perelshtein, N. Perkas, A. Gedanken, and S. Margel, “Engineering of superhydrophobic silica microparticles and thin coatings on polymeric films by ultrasound irradiation”, *Materialstoday Chemistry*, Volume 21, 2021. DOI: 10.1016/j.mtchem.2021.100520.

[6] Nguyen Thi Phuong Nhung, Nguyen Thi Ngoc Tien, Nguyen Hoang Luong, Tran Thu Hang, Nguyen Van Kiet, and Nguyen Phan Anh, “Micro/nanostructured ZnO-based superhydrophobic steel surface with enhanced corrosion protection”, *Petrovietnam Journal*, Volume 6, pp. 59 - 66, 2022. DOI: 10.47800/pvj.2022.06-07.

[7] Aziz Fihri, Enrico Bovero, Abdullah Al-Shahrani, Abdullah Al-Ghamdi, and Gasan Alabedi, “Recent progress in superhydrophobic coatings used for steel protection: A review”, *Colloids Surfaces A: Physicochemical and Engineering Aspects*, Volume 520, pp. 378 - 390, 2017. DOI: 10.1016/j.colsurfa.2016.12.057.

[8] Jan Zimmermann, Felix A. Reifler, Ulrich Schrade, Georg R.J. Artus, and Stefan Seeger, “Long term environmental durability of a superhydrophobic silicone nanofilament coating”, *Colloids Surfaces A Physicochemical and Engineering Aspects*, Volume 302, Issues 1 - 3, pp. 234 - 240, 2007. DOI: 10.1016/j.colsurfa.2007.02.033.

[9] Beibei Li, Xiaoyan Liu, Xinying Zhang, Wenbo Chai, Yining Ma, and Jingjing Tao, “Facile preparation of graphene-coated polyurethane sponge with superhydrophobic/superoleophilic properties”, *Journal of Polymer Research*, Volume 22, 2015. DOI: 10.1007/s10965-015-0832-1.

[10] Mengru Jin, Qianli Xing, and Zikang Chen, “A review: Natural superhydrophobic surfaces and applications”, *Journal Biomaterials and Nanobiotechnology*, Volume 11, Issue 2, pp. 110 - 149, 2020. DOI: 10.4236/jbmb.2020.112008.

[11] Wenkai Zhu, Yan Wu, and Yang Zhang, “Fabrication and characterization of superhydrophobicity

ZnO nanoparticles with two morphologies by using stearic acid”, *Materials Research Express*, Volume 6, Issue 11, 2019. DOI: 10.1088/2053-1591/ab4ec5.

[12] Shanhu Liu, Qingfeng Xu, Sanjay S. Latthe, Annaso B. Gurav, and Ruimin Xing, “Superhydrophobic/superoleophilic magnetic polyurethane sponge for oil/water separation”, *RSC Advances*, Volume 5, Issue 84, pp. 68293 - 68298, 2015. DOI: 10.1039/c5ra12301a.

[13] Xiaojia Gao, Xiufeng Wang, Xiaoping Ouyang, and Cuie Wen, “Flexible superhydrophobic and superoleophilic MoS₂ sponge for highly efficient oil-water separation”, *Scientific Reports*, Volume 6, pp. 1 - 8, 2016. DOI: 10.1038/srep27207.

[14] Teng Chen, Shuai Zhou, Zhenhua Hu, Xinkai Fu, Zhiyu Liu, Bolin Su, Hongri Wan, Xihua Du, and Zhaojian Gao, “A multifunctional superhydrophobic melamine sponge decorated with Fe₃O₄/Ag nanocomposites for high efficient oil-water separation and antibacterial application”, *Colloids Surfaces A Physicochemical and Engineering Aspects*, Volume 626, 2021. DOI: 10.1016/j.colsurfa.2021.127041.

[15] Hamed Hosseini Bay, Daisy Patino, Zafer Mutlu, Paige Romero, Mihrimah Ozkan, and Cengiz S. Ozkan, “Scalable multifunctional ultra-thin graphite sponge: Free-standing, superporous, superhydrophobic, oleophilic architecture with ferromagnetic properties for environmental cleaning”, *Scientific Reports*, Volume 6, pp. 1 - 9, 2016. DOI: 10.1038/srep21858.

[16] Jesús I. Tapia, Elizabeth Alvarado-Gómez, and Armando Encinas, “Non-expensive hydrophobic and magnetic melamine sponges for the removal of hydrocarbons and oils from water”, *Separation and Purification Technology*, Volume 222, pp. 221 - 229, 2019. DOI: 10.1016/j.seppur.2019.04.008.

[17] Tran Thi Viet Ha and Byeong-Kyu Lee, “Novel fabrication of a robust superhydrophobic PU@ZnO@Fe₃O₄@SA sponge and its application in oil-water separations”, *Scientific Reports*, Volume 7, Issue 1, pp. 1 - 12, 2017. DOI: 10.1038/s41598-017-17761-9.

GOVERNANCE IN ESG OF OIL AND GAS SECTOR

Nguyen Quang Huy, Dao Doan Duy, Nguyen Thi Thuy Tien

Vietnam Oil and Gas Group

Email: duydd@pvn.vn

<https://doi.org/10.47800/PVSI.2024.06-10>

Summary

ESG plays a vital role in modern business as it is a key for a company to build trust among stakeholders and access capital. On the one hand, investors look for companies having a good ESG practice to control and reduce potential risks. On the other hand, companies or investees should avoid “greenwashing” behaviors such as setting impractical targets in the name of sustainability, especially in high ESG risk sectors like oil and gas. For these reasons, governance (G) is the foundation of a company’s ESG, and it reflects the commitment of the top management level to achieving all ESG targets by managing risks, developing strategies and being transparent.

Key words: ESG, governance, strategy, risk, sustainability.

1. Introduction

ESG is the abbreviation of environmental, social and governance. It is a set of criteria demonstrating the performance of a company in these 3 pillars:

- Environmental: This refers to the impact of a company on the environment including natural resources usage, emissions, waste management, biodiversity and how they are mitigated.
- Social: This encompasses the human aspect, focusing on how the company treats its stakeholders including employees, customers and the communities where the company operates.
- Governance: This relates to the company’s structure, compliance with the law and how the company develops its strategy to control all ESG issues.

Together, ESG defines the sustainability of a company and is used by investors or stakeholders to assess the company’s value to make informed decisions.

1.1. The emergence of ESG

Beginning with the concept of Corporate Social Responsibility (CSR), it refers to the necessity for organizations to balance making profits with contributing to sustainable socio-economic development and

enhancing life quality in communities. Specifically, businesses should not focus solely on maximizing profits; rather, these profits can be leveraged to foster social well-being and protect the environment by engaging in responsible practices that go beyond legal requirements and core business targets [1].

There has been a notable shift from CSR to a more specific framework known as ESG (environmental, social, and governance). This evolution is driven by various factors used to create ratings and conduct non-financial assessments of companies. ESG has become widely recognized, particularly among corporations and investors in the capital markets [1]. Another pressure

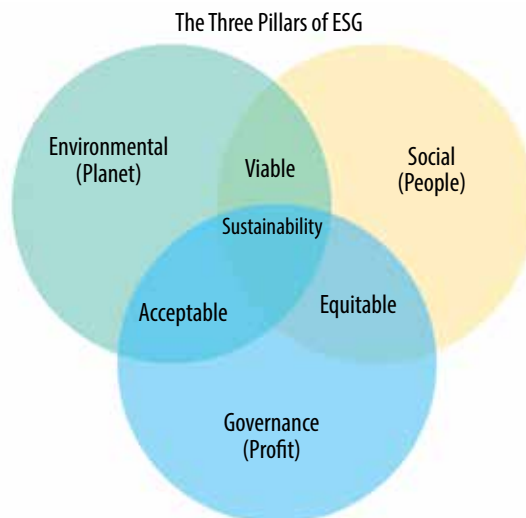


Figure 1. The three pillars of ESG [2].



Date of receipt: 1/11/2024.

Date of review and editing: 1 - 12/11/2024.

Date of approval: 12/11/2024.

forcing companies to practice ESG comes from climate change as this environmental topic grows ever bigger among panel discussions.

From the perspective of investors, ESG pertains to the risks of their investees, especially non-financial risks as crises can potentially arise from failures in human resource management, environmental protection or business ethics apart from monetary decisions. Companies having good ESG practices or at least transparency in ESG disclosures clearly look more reputable or trustworthy. Therefore, ESG helps bridge the gap between investors and investees and ensure the capital flows into sustainable businesses.

1.2. ESG to oil and gas sector

As climate change impacts become more visible, mitigating green house gas (GHG) emissions is required to limit temperature increase besides adaptation solutions. This places oil and gas sector at high-risk in terms of sustainability in general and the environment in particular due to the high carbon footprint of its value chain. According to IEA, 15% of total energy-related emissions originate from oil and gas. Furthermore, its indirect emissions are even more significant, driven by the enormous consumption of its products in power generation and transportation [3]. This results in the exclusion of new investment and the divestment of capital from oil and gas, hindering the development of new projects. In contrast, the capital flows into low-carbon energy projects such as renewables, promoting energy transition.

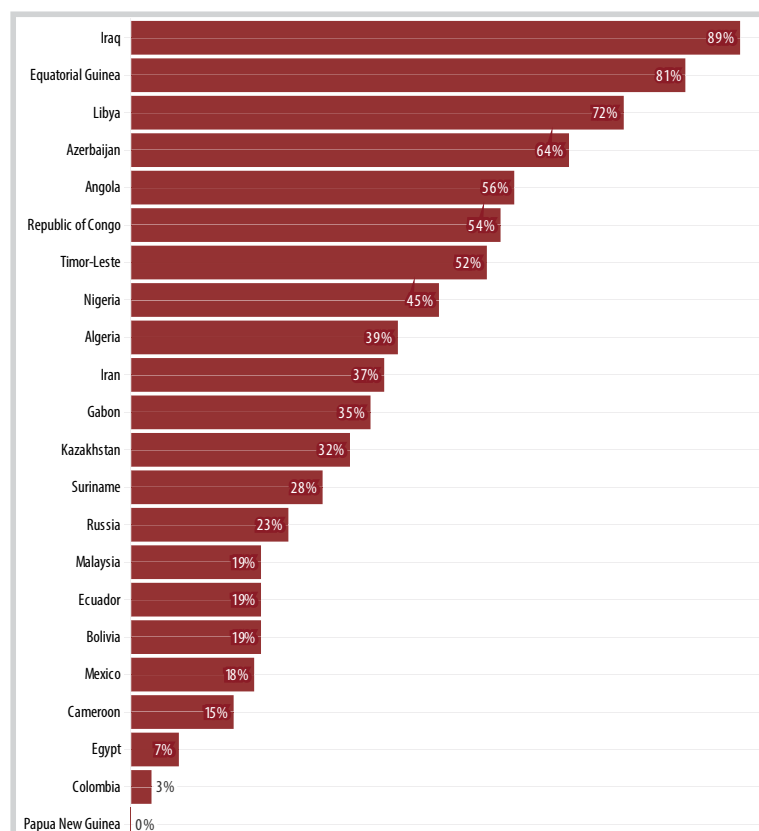


Figure 2. Oil and gas revenue as percentage of total government revenue [4].

In developing countries, national revenue depends heavily on the fluctuating prices of oil and gas but possesses fewer resources (technologies, money, human resources) than developed countries to proactively navigate the global energy transition [4]. Another important matter is the rapid economic growth of these nations. Their manufacturing-based economy and high population requires considerable energy consumption which is primarily generated from oil and gas besides coal. Ultimately, the development of the national oil and gas sector determines the development of the national economy and without capital inflows, stagnation is inevitable. As an adaptation, oil and gas companies take advantage of and promote ESG practices to access capital and maintain production.

2. ESG practices in oil and gas sector

Environmental risks share a substantial part in oil and gas by numerous aspects [5]:

- GHG emissions and climate adaptation, resilience and transition: Oil and gas value chain consists of exploration and production, transmission and transportation, refining and processing, petrochemicals, and distribution. These operations emit significant amounts of GHGs including methane, carbon dioxide and nitrous oxide, which contribute to global warming.
- Air emissions: The combustion of fuel along with chemical processing are the sources of air pollutants such as SOx, NOx, PM, VOCs and other hazardous air pollutants.
- Water and effluents: Oil and gas also uses and discharges a huge amount of water including produced water in oil and gas production, coolant water.
- Waste: Besides domestic and industrial waste, usage of chemicals in different processes generates hazardous waste.
- Biodiversity: Oil and gas resources can be found in Eco-Sensitive zone with various species.

The social aspect is another concern in the

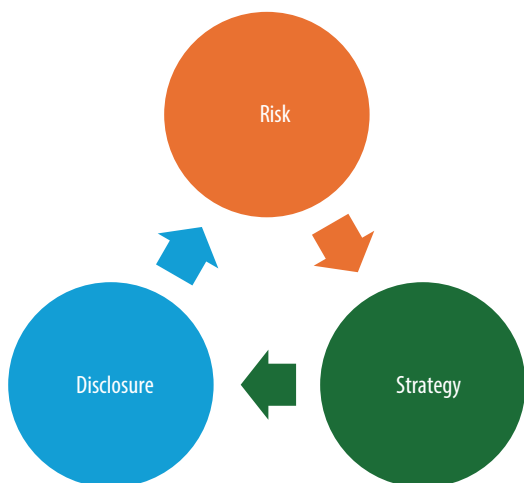


Figure 3. The three pillars of corporate governance.



Figure 4. Effective governance framework.

oil and gas sector due to its heavy industrial nature and harsh working conditions. Several social-related risks are:

- Occupational health and safety,
- Wages and employment practices,
- Local communities and resettlement,
- Incident management.

Finally, governance cannot be overlooked. From a different perspective, ESG is about risk, strategy and disclosure. Based on a risk assessment, a company can build its coping strategy and disclose it through a report to deliberate how it manages all ESG risks, thus gaining trust and attracting investments. To fulfill this objective, robust

governance is essential because it serves as a navigating tool for top management level to plan, implement and realize their vision eventually. Without proper governance, companies are likely to lose direction in ESG or worse, turn into greenwashing.

Regarding the governance aspect, stakeholders are concerned with the structure of sustainability, including governance body selection, communication mechanisms, evaluation, as well as company’s strategies, policies, and practices. Since oil and gas are valuable resources that contribute significantly to national revenue, many countries establish national oil companies to manage this sector. This, in turn, leads to other governance-related issues such as:

- Anti-competitive behavior,
- Anti-corruption,
- Payments to governments,
- Economic impacts,
- Public policy.

3. Role of governance in ESG implementation

Governance is the driving factor for environmental and social to be implemented. Strong governance plays a pivotal role in ensuring that ESG policies are woven into the core strategy of a company [6, 7].

Effective governance establishes clear leadership roles and responsibilities for ESG initiatives, assigning dedicated teams or executives to ensure that these priorities are addressed at the highest levels rather than being sidelined. This accountability fosters commitment and action across the organization.

Governance frameworks also align ESG objectives with the company’s broader strategy. By integrating ESG considerations into strategic planning, companies can identify sustainable growth opportunities, such as investments in renewable energy or improvements in operational efficiency. This alignment embeds ESG within the company’s mission rather than treating it as a separate objective.

Strong governance further incorporates robust risk management for ESG-related issues. By evaluating risks, such as regulatory changes and environmental impacts, companies can proactively address potential challenges and adapt their strategies to be both responsive and forward-looking.

Additionally, effective governance also promotes active engagement with stakeholders, including investors, employees, and communities. By understanding stakeholder expectations, companies can shape ESG policies that are both relevant and responsive, fostering trust and enabling more effective implementation.

Governance structures also include metrics and regular assessments to track ESG performance. By setting clear benchmarks and consistently evaluating results, companies ensure that their ESG initiatives remain effective and aligned with broader strategic goals. Transparent reporting further enhances credibility with stakeholders and reinforces accountability.

Lastly, strong governance integrates ESG values into the company culture. When leadership prioritizes ESG, it influences the entire organization, motivating employees to adopt sustainable practices. This cultural transformation is essential for the long-term success of ESG initiatives.

3.1. Sample governance structure for ESG implementation

An overview of the ESG governance structures at various energy companies, highlighting how they incorporate ESG principles into their organizational frameworks, is presented in Table 1.

Each of these companies has established clear roles and responsibilities within their governance structures

to ensure effective oversight and implementation of ESG initiatives. By establishing dedicated committees, involving executive leadership, and emphasizing transparency and accountability, with focus on sustainability, safety, and stakeholder engagement, they can better navigate the complexities of the oil and gas industry while promoting responsible practices.

3.2. The role of the Board of Directors

First and foremost, the foundation of ESG implementation lies in a company's commitment to responsible business practices, guided by ethical leadership from its boards and executives. When environmental and social considerations are not integrated into every stage of production - from product design to end-of-life management - companies risk transferring environmental and social risks to their suppliers, clients, consumers, stakeholders, and ultimately, to the planet. Therefore, a clear vision of the company for cultivating and sharing sustainable values across the value chain is essential. Only then can effective environmental and social initiatives be developed and realized, fostering sustainable growth for the company.

Therefore, the Board of Directors plays a central role in the successful implementation of ESG initiatives in oil and gas companies. Through strategic oversight, risk management, accountability, stakeholder engagement, cultural leadership, and promoting continuous

Table 1. An overview of the ESG governance structures at various energy companies

BP	BP has a dedicated Safety and Sustainability Committee that oversees ESG matters, ensuring that sustainability is integrated into the company's strategy. The Executive Vice President for Strategy, Sustainability & Ventures plays a key role in driving BP's sustainability agenda [8].
Shell	Shell has a Safety, Environment and Sustainability Committee (SESCO) that reviews the company's practices regarding safety and sustainability. The Strategy, Sustainability and Corporate Relations Director is part of Shell's Executive Committee, focusing on integrating sustainability into business operations [9].
Equinor	Equinor's Safety, Sustainability and Ethics Committee monitors ESG risks and performance, ensuring these issues are prioritized at the board level. This committee regularly discusses safety and sustainability issues, with the CEO responsible for day-to-day management of these areas [10].
Eni	Eni's governance includes a Sustainability and Scenarios Committee that advises the board on sustainability issues and climate transition strategies. The CEO implements the board's resolutions and oversees the internal control and risk management systems related to sustainability [11].
Petronas	Petronas establishes a robust sustainability governance including a Sustainability Executive Leadership Team (ELT) responsible for steering enterprise-wide sustainability activities, including strategy, performance, legal, and reputational impacts; the Board provides oversight on climate-related risks and opportunities, ensuring these are integrated into the company's long-term strategic direction; and the Sustainability Committee supports the ELT and ensures that sustainability priorities are embedded across the organization and in decision-making processes [12].
Pertamina	Pertamina's comprehensive sustainability governance structure includes a Sustainability Committee, chaired by the President Director & CEO, responsible for overseeing the implementation of sustainability initiatives and ensuring that ESG considerations are integrated into Pertamina's operations. The Board ensures that the company's ESG initiatives align with its overall business strategy and stakeholder expectations; and sub-holdings and subsidiaries implement sustainability initiatives at the operational level [13].

improvement, the Board of Directors can significantly advance their companies' sustainability efforts.

The Board is responsible for embedding ESG considerations into the company's strategy, prioritizing key issues relevant to the business, and ensuring these considerations remain central to decision-making. Equinor, for example, has integrated sustainability into its core business strategy, with the Board actively overseeing the incorporation of ESG factors into operational plans [14].

Risk management is another core responsibility. The Board oversees ESG-related risks, including environmental, regulatory, and social factors. For example, BP has established a dedicated Safety and Sustainability Committee that focuses on identifying and mitigating environmental and social risks, ensuring the company is well-prepared for potential challenges [15].

Accountability and transparency are also essential. The Board ensures the company is accountable for its ESG performance by setting clear sustainability goals and metrics and regularly reviewing progress. Shell, for instance, is committed to transparent ESG reporting, with the Board overseeing the accuracy and completeness of disclosures - a critical aspect of maintaining stakeholder trust [16].

Effective boards actively engage a diverse range of stakeholders, including local communities, investors, and NGOs. Eni, for instance, has implemented governance structures that promote dialogue with stakeholders, enabling the Board to understand community concerns and incorporate feedback into decision-making. Such engagement is crucial to maintaining a social license to operate [11].

The Board also plays a key role in shaping the company's culture regarding sustainability and ethics. By fostering a culture of responsibility and accountability, boards can encourage the organization to embrace ESG principles throughout its operations. Moreover, they are responsible for ensuring the company adapts to evolving ESG challenges and opportunities by regularly reviewing and updating ESG strategies based on new insights and stakeholder feedback. Equinor exemplifies this approach, continually refining its sustainability practices in response to changing market conditions and regulatory requirements [10].

3.3. The role of the internal control apparatus

Internal control systems are vital to the effective implementation of ESG initiatives in oil and gas companies.

These systems ensure accurate reporting, manage risks, maintain compliance, enhance stakeholder engagement, foster continuous improvement, and provide employee training, helping companies navigate the complexities of ESG management [17].

A critical function of internal controls is to ensure accurate ESG reporting by standardizing data collection, validation, and disclosure, which is essential for maintaining transparency and credibility with stakeholders.

Internal controls also facilitate proactive risk management by establishing processes to identify and address ESG-related risks, allowing companies to swiftly mitigate potential environmental and social impacts. These controls are also critical for regulatory compliance, ensuring companies' adherence to both local and international ESG-related regulations, including environmental laws, safety standards, and social responsibility guidelines. Strengthening internal controls helps companies navigate complex regulatory environments effectively, ensuring operations align with legal requirements and sustainability goals.

Internal controls enhance stakeholder engagement by establishing structured processes for communication and feedback, enabling companies to engage with local communities and NGOs meaningfully. Incorporating stakeholder concerns into decision-making helps maintain a company's social license to operate.

Additionally, these systems foster a culture of continuous improvement by enabling regular monitoring and evaluation of ESG initiatives. Through ongoing assessments, companies can identify gaps in their ESG strategies, implement corrective actions, and enhance ESG performance over time.

Finally, implementing robust internal controls include training employees on ESG principles and practices, ensuring that all staff understand their roles in meeting sustainability goals. This fosters a culture of responsibility and commitment to ESG throughout the organization.

3.4. The role of innovative digital transformation

Most oil and gas companies have large scales of assets, so they are highly vulnerable to the macro-economic changes, such as fluctuations in oil prices. Therefore, cost optimization, precise forecasting and rapid adaptation to change are crucial objectives. Given the complexity of oil and gas operations, digital transformation emerges as a key solution to overcome these challenges. Notable

applications of digital transformation in oil and gas include:

- Using a management platform to develop clear workflows and business models, aligning these with predefined KPIs across operations.
- Leveraging analytics tools to collect accurate, real-time data on business and operational activities, incorporating an AI-driven model to predict potential risks based on insights gathered.
- Strengthening data security by adopting various technologies, including multi-layered storage solutions and automated threat detection tools.

4. Case studies: Governance leading ESG success in oil and gas

Several energy companies have made significant strides in implementing effective governance structures to support their ESG initiatives. A few notable examples are presented in Table 2.

These companies exemplify how effective governance structures can drive the integration of ESG initiatives in the oil and gas sector. By establishing dedicated committees, setting ambitious targets, and committing to transparency, they not only address environmental

Table 2. Governance linked to specific ESG initiatives at several energy companies

Company	Specific ESG projects and initiatives
<p>BP [15, 18] has been proactive in integrating ESG principles into its governance framework. The company has established a dedicated board committee focused on sustainability. This committee oversees BP’s progress on ESG goals, ensuring accountability and transparency in their operations.</p>	<ul style="list-style-type: none"> • Net-zero ambition: BP aims to become a net-zero company by 2050 or sooner. They have set specific targets, such as reducing operational emissions by 50% by 2030 and investing between USD 6 - 8 billion annually in transition growth projects. • Methane measurement: BP is implementing methane measurement technologies at all major processing sites to drive a 50% reduction in methane intensity. This initiative is crucial for minimizing greenhouse gas emissions.
<p>Shell [9, 16] is recognized for its strong governance practices related to ESG. The company has implemented a comprehensive sustainability strategy that includes reducing carbon intensity and increasing investments in renewable energy. Shell’s Board actively engages in ESG discussions, and is committed to transparent reporting on their sustainability performance, which helps build trust with stakeholders.</p>	<ul style="list-style-type: none"> • Carbon capture technology: Shell is advancing its CANSOLV® carbon capture technology, which will be used in the world’s largest post-combustion carbon capture facility in Abu Dhabi, capturing 1.5 million tons of CO₂ annually. • Renewable energy investments: In 2023, Shell allocated a significant portion of its R&D budget (around USD 628 million) to decarbonization projects, including biofuels and hydrogen production from renewable sources.
<p>Equinor [10, 19] has integrated ESG considerations into its core business strategy. The company has a dedicated sustainability team that reports directly to the executive management and the Board. Equinor focuses on reducing its environmental footprint and has set clear targets for carbon reduction, demonstrating a strong commitment to sustainable practices.</p>	<ul style="list-style-type: none"> • Energy transition strategy: Equinor has committed to reducing net carbon intensity by 20% by 2030 and 40% by 2035. They are investing heavily in renewable energy projects, including offshore wind and solar. • Just transition plans: Equinor emphasizes a just energy transition, focusing on social and economic benefits for communities affected by energy shifts. They are actively engaging with stakeholders to ensure inclusive practices.
<p>Eni [11] has made significant efforts to align its governance structures with ESG principles. The company has established a sustainability committee within its Board to oversee ESG initiatives and ensure compliance with international standards. Eni is also committed to transparency, regularly publishing detailed reports on its sustainability performance.</p>	<ul style="list-style-type: none"> • Open innovation initiatives: Eni has adopted an open innovation approach, collaborating with startups and research institutions to accelerate the development of sustainable technologies. This includes projects focused on carbon capture and renewable energy. • Biorefining capacity expansion: Eni is increasing its biorefining capacity significantly, aiming to produce more sustainable fuels and reduce emissions in its operations.
<p>Petronas [12] has established a comprehensive ESG governance framework to drive its sustainability agenda. By linking ESG initiatives to its governance structure, Petronas ensures that sustainability is a core aspect of its operations, driving coordinated and effective ESG strategies with clear targets and accountability mechanisms in place.</p>	<ul style="list-style-type: none"> • Net-zero emissions by 2050: The ELT and Board oversee this target, which involves reducing emissions, improving efficiency, and investing in renewables. Some initiatives such as zero routine flaring and energy efficiency are integrated into operations. • Biodiversity and environment: The ELT and Sustainability Committee oversee strategies to protect biodiversity and implement responsible waste/water management.
<p>Pertamina [13] has launched several impactful ESG initiatives guided by its governance structure. The company has committed to reducing carbon emissions by 30% by 2030 and achieving net-zero emissions by 2060 and actively transitioning towards cleaner energy sources. This includes increasing investments in renewable energy projects and enhancing energy efficiency across its operations. Pertamina aims to align its energy mix with national and global sustainability goals.</p>	<ul style="list-style-type: none"> • Decarbonization: The ESG Committee and Board oversee the strategy to reduce carbon emissions by 30% by 2030 and achieve net-zero by 2060. This involves utilizing renewable energy and carbon capture technologies. • Energy transition: The ESG Committee ensures initiatives to increase investment in renewables and enhance energy efficiency.

and social challenges but also position themselves for long-term success in a rapidly evolving energy landscape. Beyond setting ambitious ESG goals, these companies actively implement innovative projects that promote sustainability and combat climate change. From carbon capture technologies to renewable energy investments, these initiatives reflect a commitment to integrating ESG principles into their core operations.

5. Role of investors and stakeholders in driving ESG governance

Investors are placing growing importance on strong governance frameworks to manage ESG risks, especially in the energy sector. This demand is reshaping corporate approaches to ESG by emphasizing transparency, stakeholder engagement, and long-term value creation, enabling companies to meet investor expectations while securing a competitive position in a rapidly evolving market.

With the rising focus on climate change and social responsibility, investors are more aware of the risks associated with poor ESG performance. Recognizing that weak governance can result in significant financial and reputational damage, they are pressing companies to adopt more rigorous governance frameworks to mitigate these risks effectively. Institutional investors, such as BlackRock, have also indicated a willingness to use their voting power to enforce ESG accountability. Recent statements suggest they are prepared to vote against management or board members if companies do not demonstrate progress on sustainability disclosures. This added pressure is driving oil and gas companies to strengthen their governance frameworks to address investor demands for accountability in ESG performance [20].

Investors increasingly seek a clear connection between a company's ESG efforts and its financial performance, demanding assurance that companies are not only compliant with regulations but also strategically prepared to succeed in a sustainable economy. This expectation is encouraging oil and gas companies to incorporate ESG into their core business strategies. Many investors now take a long-term view, recognizing that companies with robust ESG governance are often better positioned for sustainable growth and are willing to invest at a premium in those demonstrating solid governance practices and well-defined ESG commitments [21].

As regulations on sustainability evolve, investors expect companies to maintain governance mechanisms

to ensure compliance and transparency in ESG reporting. Investors are also advocating for stronger stakeholder engagement, urging companies to communicate actively with groups such as local communities and environmental organizations. Effective governance facilitates this engagement, allowing companies to address stakeholder concerns and incorporate feedback into their ESG strategies, thereby enhancing reputation and mitigating risks.

6. Recommendations

Integrating ESG into the core strategy of Vietnamese oil and gas companies like PetroVietnam is essential, as demonstrated by industry leaders like BP, Eni, Equinor, and Shell. Vietnamese oil and gas companies should:

- Set clear, measurable ESG goals that align with both national and global sustainability targets;
- Establish robust governance structures, such as an ESG Committee within the Board of Directors to ensure focused oversight of sustainability efforts and accountability for ESG performance similar to practices by those industry leaders;
- Engage stakeholders effectively by involving local communities, NGOs, and government bodies in decision-making processes to address concerns;
- Ensure transparency via regular sustainability reports, building trust with stakeholders and demonstrating accountability;
- Implement comprehensive risk management frameworks to better identify and address ESG-related risks more effectively.

6.1. Increase the role of governance in ESG

With governance at the core of ESG, the Board of Directors (BoD) plays a central role in ensuring the success of practice. First, the BoD must have a thorough understanding of critical ESG concerns and risks affecting both internal and external stakeholders. Gaining a perception of ESG current state requires reviewing ESG performances and benchmarking it to standards, best practices and regulations. Therefore, equipping the highest governance body or BoD with collective knowledge on sustainability is the foundational step in corporate governance practices.

Key responsibilities of BoD in governance aspects:

- Developing governance structures: A management-level committee led by a chief sustainability officer can

be organized. Its role is to oversee the management team or executive board, who is in charge of executing ESG strategy developed by the BoD. To operational level, an ESG committee can be established including staff specialized in ESG aspects such as legal, human resource, HSE, investor relations, public relations. Finally, an audit committee can be formed to bridge the management-level committee and ESG committee.

- Foster a culture of ethics and integrity: Gaining trust of stakeholders is the mission of ESG and can only be achieved through transparency. This includes developing codes of conduct raising ethical standards in all activities, whistleblowing mechanisms to ensure all complaints are addressed.

- Risk management and regulatory compliance: Adherence to applicable regulations as well as monitoring violations are compulsory. Additionally, other risks are also examined by engaging with stakeholders and conducting double materiality assessments.

- Driving corporate responsibility: By setting relevant, clear, measurable, time-bound goals and targets [22].

6.2. Integration of sustainability strategy into business model

Since ESG risks have become a critical aspect of risk management, ESG should be integrated into the development strategy of the company to solve each concern. Building a sustainability strategy is particularly important for sectors with high ESG risks like oil and gas.

Equinor is a typical example of building sustainability strategy. The company recognizes that climate change is the greatest challenge and net-zero journey can create new business opportunities. From that orientation, it develops an action plan focused on high value growth in renewables, optimized oil and gas portfolio and new market opportunities in low-carbon solutions [23].

6.3. Monitoring and reporting mechanism

Monitoring and controlling managers' decisions is required to ensure all activities bring environmental and social benefits to stakeholders. In this context, the team performing this task is tentatively called the audit committee. This team should be a sub-committee of the Board of Director, playing the connection role between BoD and Executive Board.

Its role includes supervising both the mandatory and voluntary ESG practice of the company. Besides,

this committee can advise BoD to set up ESG indicators aligned with the planned strategy [24].

6.4. Remuneration policies

In parallel with incorporating ESG into strategy and quantifying ESG indicators, remuneration policies should be built to create incentives. According to PwC, 45% of FTSE 100 companies now include ESG measures in executive pay, whilst 78% of board members and senior executives agree that strong ESG performance enhances organizational value and/or financial performance.

PwC suggests 4 approaches to develop remuneration policies tied to ESG performance [25]:

- Internal and external targets: Measured by activities leading to outcome, not the outcome itself.

- Individual KPIs and scorecards: Based on the achieved ESG metrics.

- Long-term incentive plan (LTIP) and annual bonus: Designed for goals requiring long-term implementation, such as climate targets.

- Underpins and scale targets: Not every metric can be quantified, thus, it needs qualitative assessment.

7. Conclusion

Practicing ESG is the key for companies in high-ESG-risk sectors like oil and gas to access capital markets. This is even more important in emerging economies, where national economy is contributed significantly by oil and gas. Successful ESG implementation begins with a robust governance system comprised of ESG structure, monitoring mechanism, KPI, and remuneration policies. Furthermore, the integration of ESG strategy into business model to form a sustainability strategy can promote companies to meet the demand of all stakeholders. In general, beyond superficial risks of oil and gas like climate resilience or energy transition, a shift in governance system is the most critical ESG topic that can foster the future of the sector.

References

[1] Magdalena Kaźmierczak, "A literature review on the difference between CSR and ESG", *Scientific Papers of Silesian University of Technology - Organization and Management Series*, Volume 162, pp. 275 - 289, 2022. DOI: 10.29119/1641-3466.2022.162.16.

[2] Eteams, "The three pillars of ESG: Shaping a

sustainable future for product design". [Online]. Available: <https://www.eteams.com.vn/article/the-three-pillars-of-esg-shaping-a-sustainable-future-for-product-design>.

[3] International Energy Agency, "Emissions from oil and gas operations in net zero transitions", *A world energy outlook special report on the oil and gas industry and COP28*, 2023.

[4] Devashree Saha, Ginette Walls, David Waskow, and Molly Bergen, "To shift away from oil and gas, developing countries need a 'Just transition' to protect workers and communities", 26/1/2023. [Online]. Available: <https://www.wri.org/insights/just-transition-developing-countries-shift-oil-gas/>.

[5] GRI, "GRI 11: Sector standard for oil and gas". [Online]. Available: <https://www.globalreporting.org/standards/standards-development/sector-standard-for-oil-and-gas/>.

[6] Stella Emeka-Okoli, Tochukwu Chinwuba Nwankwo, Christiana Adanma Otonnah, and Ekene Ezinwa Nwankwo, "Corporate governance and CSR for sustainability in oil and gas: Trends, challenges, and best practices: A review", *World Journal of Advanced Research and Reviews*, Volume 21, Issue 3, pp. 78 - 90, 2024. DOI: 10.30574/wjarr.2024.21.3.0662.

[7] CGEP, "Assessing ESG risks in national oil Companies: Transcending ESG ratings with a better understanding of governance". [Online]. Available: <https://www.energypolicy.columbia.edu/publications/assessing-esg-risks-in-national-oil-companies-transcending-esg-ratings-with-a-better-understanding-of-governance/>.

[8] BP, "Corporate governance". [Online]. Available: <https://www.bp.com/en/global/corporate/who-we-are/governance.html>.

[9] Shell, "ESG information hub". [Online]. Available: <https://www.shell.com/investors/environmental-social-and-governance.html>.

[10] Equinor, "Sustainability in Equinor". [Online]. Available: <https://www.equinor.com/sustainability>.

[11] Eni, "Governance". [Online]. Available: <https://report.eni.com/annual-report-2013/en/annual-report/operating-and-financial-review/governance.html>

[12] Petronas, "Petronas integrated report 2023", 2024.

[13] Pertamina, "Pertamina sustainability report 2023", 2024.

[14] Equinor, "Governance and transparency".

[Online]. Available: <https://www.equinor.com/sustainability/governance-and-transparency>.

[15] BP, "Our sustainability aims". [Online]. Available: <https://www.bp.com/en/global/corporate/sustainability/our-aims.html>.

[16] Shell, "Driving innovation". [Online]. Available: <https://reports.shell.com/sustainability-report/2023/achieving-net-zero-emissions/driving-innovation.html>.

[17] KPMG, "Strengthen internal controls to navigate ESG reporting". [Online]. Available: <https://kpmg.com/us/en/articles/2023/strengthen-internal-controls-navigate-esg-reporting.html>.

[18] BP, "Environment, social and governance". [Online]. Available: <https://www.bp.com/en/global/corporate/investors/esg.html>.

[19] Equinor, "Our climate ambitions". [Online]. Available: <https://www.equinor.com/sustainability/climate-ambitions>.

[20] Morgan Stanley, "4 ways investors can act on climate change". [Online]. Available: <https://advisor.morganstanley.com/keith.underwood/articles/investing/risks-and-opportunities-of-climate-change>.

[21] McKinsey, "Linking ESG initiatives to financial performance". [Online]. Available: <https://www.mckinsey.com/capabilities/strategy-and-corporate-finance/our-insights/investors-want-to-hear-from-companies-about-the-value-of-sustainability>.

[22] Jurgita Ashley, Thompson Hine LLP, and Randi Val Morrison, "ESG governance: Board and management roles & Responsibilities". [Online]. Available: <https://corpgov.law.harvard.edu/2021/11/10/esg-governance-board-and-management-roles-responsibilities/>.

[23] Equinor, "Equinor energy transition plan 2022", 2022.

[24] Hasan Mohamad Bamahros, Abdulsalam Alquhaif, Ameen Qasem, Wan Nordin Wan-Hussin, Murad Thomran, Shaker Dahan Al-Duais, Siti Norwahida Shukeri, and Hytham M. A. Khojally, "Corporate governance mechanisms and ESG reporting: Evidence from the Saudi stock market," *Sustainability*, Volume 14, Issue 10, 2022. DOI: 10.3390/su14106202.

[25] Phillippa O'Connor, Lawrence Harris, and Tom Gosling, "Linking executive pay to ESG goals". [Online]. Available: <https://www.pwc.com/gx/en/issues/esg/exec-pay-and-esg.html>.